STUDIES IN SPORT, PHYSICAL EDUCATION AND HEALTH
227

Ahti Rahikainen

Modeling Muscle Mechanics of Arm and Leg Movement

A new approach to Hill's equation

$$I \frac{d\dot{\varphi}}{dT} = \frac{P}{\dot{\varphi}} - C\dot{\varphi}$$

$$\dot{\varphi} = \sqrt{\frac{P}{C}\left(1 - e^{-\frac{2C}{I}T}\right)}$$

JYVÄSKYLÄN YLIOPISTO

STUDIES IN SPORT, PHYSICAL EDUCATION AND HEALTH 227

Ahti Rahikainen

Modeling Muscle Mechanics of Arm and Leg Movement

A new approach to Hill's equation

Esitetään Jyväskylän yliopiston liikuntatieteellisen tiedekunnan suostumuksella
julkisesti tarkastettavaksi yliopiston Liikunta-rakennuksen auditoriossa L302
syyskuun 4. päivänä 2015 kello 14.

Academic dissertation to be publicly discussed, by permission of
the Faculty of Sport and Health Sciences of the University of Jyväskylä,
in building Liikunta, auditorium L302, on September 4, 2015 at 2 o'clock pm.

UNIVERSITY OF JYVÄSKYLÄ

JYVÄSKYLÄ 2015

Modeling Muscle Mechanics of Arm and Leg Movement

A new approach to Hill's equation

STUDIES IN SPORT, PHYSICAL EDUCATION AND HEALTH 227

Ahti Rahikainen

Modeling Muscle Mechanics of Arm and Leg Movement

A new approach to Hill's equation

UNIVERSITY OF JYVÄSKYLÄ

JYVÄSKYLÄ 2015

Editors
Taija Juutinen
Department of Biology of Physical Activity, University of Jyväskylä
Pekka Olsbo, Timo Hautala
Publishing Unit, University Library of Jyväskylä

URN:ISBN:978-951-39-6271-5
ISBN 978-951-39-6271-5 (PDF)

ISBN 978-951-39-6270-8 (nid.)
ISSN 0356-1070

Jyväskylä University Printing House, Jyväskylä 2015

ABSTRACT

Rahikainen, Ahti
Modeling muscle mechanics of arm and leg movement – A new approach to Hill's equation
Jyväskylä: University of Jyväskylä, 2015, 63 p.
(Studies in Sport, Physical Education and Health
ISSN 0356-1070; 227)
ISBN 978-951-39-6270-8 (nid.)
ISBN 978-951-39-6271-5 (PDF)

The first purpose of this study was to develop a constant power model of arm rotations and to provide a new solution for Hill's force – velocity equation. Elbow and shoulder extensions/flexions with maximum velocity were recorded in the sagittal plane with a special camera system in which one film frame contained a series of subject images and the paths of the marker lights were seen as dashed light lines. Additional experiments were analyzed using the Vicon motion analysis system with 8 cameras, which enabled the use higher frame rates (300 Hz). The theoretically derived model of constant maximum power was fitted to the experimentally measured data. The moments of inertia of the arm sectors, needed for determining accurate values of friction coefficients of elbow and whole arm rotations, were calculated using the immersion technique. The experiments of the present study verified that the theoretically derived equation with constant maximum power was in agreement with the experimentally measured results. The results of the present study were compared with the mechanics of Hill's model and a further developed version of Hill's force–velocity relationship was derived: Hill's model was transformed into a constant maximum power model consisting of three different components of power. It was concluded that there are three different states of motion: 1) a state of low speed, maximal acceleration without external load, which applies to the hypothesis of constant moment, 2) a state of high speed, maximal power without external load, which applies to the hypothesis of constant power and 3) a state of maximal power with external load, which applies to Hill's equation. This is a new approach to Hill's equation.

The second model of the present study was based on the oscillatory movement of vertical jumping as the body center of mass moves first downwards and then upwards during ground contact. This path can be presented as a mathematical model of the leg movement. In the present study the model of leg movement without leg pushing force was constructed first and then the pushing force was added to the model. Equations (representing damped/strengthening and sine-formed oscillatory motion) were derived for the path of the body center of mass in jumping on one leg and on two legs and they fitted the experimental results. The equation of strengthening oscillatory motion also matched the measured paths of motion in counter movement jump (CMJ) starting from zero velocity and the pushing phase in shot put. It was hypothesized that the vertical displacement-time curve may become a strengthening oscillatory motion as exertion of leg force increases. In shot put the displacement of the body center of mass (CoM) was obtained from previously measured shot displacements. Velocities and forces acting at the CoM were calculated and the total ground reaction force was derived.

Keywords: Muscle mechanics, muscle power, force-velocity relationship, Hill's equation, arm movement, leg movement, jumping.

Author's address

Ahti Rahikainen
Department of Biology of Physical Activity
University of Jyväskylä, Jyväskylä, Finland
Email: ahrahik.zz@kolumbus.fi

Supervisors

University Researcher Mikko Virmavirta, PhD
Department of Biology of Physical Activity
University of Jyväskylä, Jyväskylä, Finland

Professor Janne Avela, PhD
Department of Biology of Physical Activity
University of Jyväskylä, Jyväskylä, Finland

Reviewers

Professor Aki Mikkola, PhD
Department of Mechanical Engineering
Lappeenranta University of Technology
Lappeenranta, Finland

Professor Zishun Liu, PhD
International Center for Applied Mechanics
Xi'an Jiaotong University
Xi'an, Shaanxi, P.R. China

Opponent

Professor Lauri Kettunen, PhD
Tampere University of Technology
Tampere, Finland

ACKNOWLEDGEMENTS

This doctoral thesis was carried out under the supervision of Dr. Mikko Virmavirta in the Department of Biology of Physical Activity, University of Jyväskylä. I would like to gratefully acknowledge all the people who in different ways made this work possible. Thanks are especially directed to the following persons:

- University Researcher Mikko Virmavirta, PhD, for supervising this work and for his technical assistance in writing the articles.
- Prof. Janne Avela, PhD, for co-authoring the articles.
- Pekka Luhtanen, PhD, for his expertise in the prior work of shot put.
- Prof. Matti Ranta, PhD and Prof. Rolf Stenberg, PhD, for examining the prior work of shot put and for their initiating contribution to this work.
- Preliminary examiners of this thesis Prof. Aki Mikkola, PhD, and Prof. Zishun Liu, PhD.
- Ritva Taipale, PhD, for checking the language of the text.

Jyväskylä, August 2015
Ahti Rahikainen

LIST OF ORIGINAL PAPERS

This thesis is mainly based upon the following original articles. In addition some data not presented in the articles are included.

I Rahikainen, A. and Virmavirta, M. 2014. Constant Power model in Arm Rotation – A New Approach to Hill's Equation. *World Journal of Mechanics*, 4, 90-97.

II Rahikainen, A., Avela, J. and Virmavirta, M. 2012. Study of Leg Movement in One- and Two Legged Hopping. *International Journal of Applied Mechanics*, 4 (1), 1250002 (16 pages).

III Rahikainen, A., Avela, J. and Virmavirta, M. 2012. Modeling the Force-Velocity Relationship in Arm Movement. *World Journal of Mechanics*, 2, 90-97.

IV Rahikainen A, Luhtanen P 2003. A study of the efficiency of the leg-pushing phase in shot put. *Russian Journal of Biomechanics* 7, (1), 65-79.

CONTENTS

1 INTRODUCTION

A good description of modeling was given by Nigg & Herzog (2006): "Modeling, the attempt to represent reality, is often used when the understanding of phenomena becomes difficult". It is known that the best way to obtain human movement data is to collect it from human subjects. However, human subjects are complex and randomly variable and they have often limitations related to e.g. fatigue, safety, and ethical questions (Whittlesey and Hamill 2014). Modeling has a wide range of different forms in biomechanics and different classifications have been used. Alexander (2003) presented physical, mathematical, and conceptual models from which the mathematical models have been the most prolific category in biomechanics. According to Alexander, mathematical models can be used to predict effects and find optimal patterns of behavior. The present study uses a set of equations to explain the behavior of human arm and leg movement and therefore it can be compared to mathematical modelling.

British Nobel laureate A.V. Hill introduced a muscle model consisting of contractile and elastic components. The force produced by the contractile component depends on its mechanical characteristics, which can be expressed, e.g. as a force-velocity relationship. In muscle mechanics this skeletal muscle force-velocity relationship is presented mathematically by the famous Hill's equation for a rectangular hyperbola (see Fig. 1) (Hill 1938 and 1970). This equation was based on laboratory measurements in which the activated muscle was released at a suitable speed in an isolated muscle condition. The obtained constant velocity was then plotted against the observed force. Force measured from skeletal muscle during maximum tension depends on several internal and external factors. In contrast to Hill's isolated muscle preparations, force (F) of the involved muscles create a moment ($M = r \times F$) about the joint. The length of the muscle's moment arm (r) depends on joint angle and it changes as the rotational movement proceeds about the joint axis. This rotation movement is the combined effect of the forces of several different muscles. Due to all of the above-mentioned factors, it is difficult to determine the contribution of each muscle on force production and to determine the torque about the joint. Therefore, the purpose of this study was to develop a new explicit calculation method to de-

termine the force – velocity relationship and test its function in experimental measurements. The methods of this study were based on the assumption that in muscle mechanics there exists a constant maximum power that the muscle is able to generate within a certain range of velocity. The principle of constant maximum power is the same as in Hill's equation except that the constant maximum power in the present study is a characteristic of a whole muscle group instead of separate muscle fibers as in Hill's equation. In this study a constant power model of arm movement was presented and its validity and accuracy of results were assessed. A new approach to Hill's equation was also presented. In the left side of Hill's equation $(F + a)(v + b) = b(F_0 + a)$ the constant a has the dimensions of force and b the dimensions of velocity, otherwise addition is impossible. Therefore, $(F + a)$ is force and $(v + b)$ is velocity, and force multiplied by velocity is power as can be seen in Figure 1. The term $(F + a)(v + b)$ represents muscles' total power including Fv, which is the power required to move an external load. The right side of the equation, $b(F_0 + a)$, includes only constants and in this regard, the equation can be considered as a constant power model. The constant power of Hill's equation presented in this paper is not the above mentioned power of Hill's original curve as it is usually considered in biomechanics, however, it is the sum of three different power components (see discussion and conclusions). The constant power model of this study acts during high speed movements with no external load, where Hill's equation does not seem to fit the experimental points (Hill 1970, p. 32, Fig. 3.2) very well. As an explanation for this mismatch, Hill himself mentioned that the "sharp rise at the end of the curve in the region of very low tension was due to the presence of a limited number of fibers of high intrinsic speed and no such equation could fit the observed points below $P/P_0 = 0.05$". The present model is based on the muscular system's ability to transfer chemical energy and, therefore, it is not necessary to know the contribution of the individual muscles involved.

In the shot put study Rahikainen and Luhtanen (2003) developed the theoretical equations for a human jump movement and fitted the curves to the measurements of shot putter's center of mass (CoM) during the ground contact. The present study revisited the above mentioned shot put study with some new calculations concerning the location of the body center of mass. In addition, the curves of damped and strengthening oscillatory movement were fitted into the measured jumps on one and two legs and Nigg's equation (2006) for decelerated motion was further developed and presented.

2 REVIEW OF LITERATURE

2.1 Force-velocity relationship of a skeletal muscle

Hill's force-velocity relationship of skeletal muscle (Fig. 1) (Hill 1938 and 1970) is one of the most essential equations of muscle mechanics and it has been an object of biomechanical studies for years (e.g. Herzog 1999, Herzog 2000, McIntosh and Holash 2000, Winter 2004). In muscle mechanics, this relationship is presented by Hill's equation $(F + a)(v + b) = b(F_0 + a)$, where F is current muscle force at current shortening velocity of contraction, a is constant force and b is constant velocity, F_0 is the maximum isometric muscle force, i.e. the maximum force that muscle can produce at a given constant length, and v is velocity. This equation was based on laboratory measurements with a Levin-Wyman ergometer in which the activated muscle was released at a suitable speed in an isolated muscle condition. The obtained constant velocity was then plotted against the observed tension. In Hill's equation the vectors of forces and velocities have the same direction and therefore it can be presented in a scalar form.

Force measured from skeletal muscle during maximum tension depends on several internal and external factors. Internal factors include e.g. anatomical structure of muscle (cross sectional area, pennation etc.), fiber type distribution (fast and slow twitch muscle fibers have different force-velocity equations), condition of the muscle (fatigued, trained), and muscle length. External factors include e.g. contraction type (isometric, concentric, and eccentric) and contraction velocity (rate of change of muscle length). Good reviews about the above mentioned factors have been published (e.g. Herzog 2000, Challis 2000 and Rassier 1999).

Validity of the force - velocity relationship for muscle contraction in the length region, $l \leqslant l_0$ was studied by Matsumoto (1967). In his paper Matsumoto has written: "Very few efforts have been made to study the profiles of the curves throughout the range of lengths over which shortening takes place. In examining the length region, $l \leq l_0$, for an isotonically contracting muscle, not only is the force - velocity relation valid for the initial reference length, $l \leq l_0$, but

also for any other length. The analysis in his report indicates that the constants a/F_0 and b/l_0 remain fixed throughout the length change of afterloaded isotonic shortening in the Rana pipiens Sartorius muscles". In Edman's study (1988) the force-velocity relation had two distinct regions (double-hyperbolic shape), each one located within the ranges 0-78 and 78-100 % of the measured isometric force (P_0), respectively. This deviates from the single Hill hyperbola in a low-velocity-high-force situation and probably better represents the concentric force-velocity relationship (Caldwell 2014). Edman found that an increase in sarcomere length from 1.85 to 2.60 μm did not affect Vmax but caused a steady decrease in curvature of the force-velocity relationship.

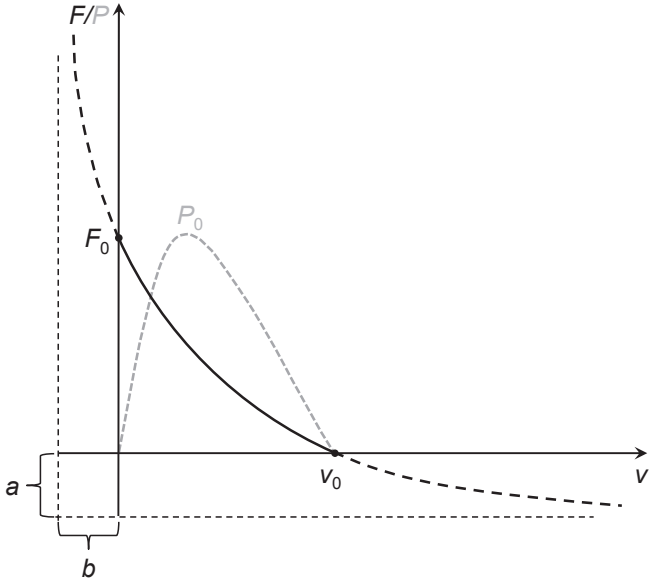

FIGURE 1 Hill's force-velocity relationship with corresponding power-velocity curve (dashed gray curve), where F_0 is maximum isometric force or force with zero velocity, v_0 is the highest possible velocity, a and b are constant force and constant velocity, respectively. Maximum power P_0 is typically found at about 30 % of v_0 (Herzog 2000). In rotational movement torque M corresponds to force F and angular velocity corresponds to velocity v in Hill's equation.

2.2 Modeling the human movement

Hundreds of models representing the neuromusculoskeletal system have been presented since Hill's (1938) classic non-linear, two-component model of muscle contraction. The relative merits of simple (e.g. Alexander 1989, 1990, 1992, 1995, 1997) and complex (e.g. Hatze 1980, 1981, 1983, 1984, 1985) mathematical models of the neuromusculoskeletal system were well discussed by Glazier & Da-

vids (2009). Hatze suggested that it is necessary to use a highly sophisticated mathematical model whereas Alexander preferred the generation of simpler models. Glazier and Davids (2009) wrote about model sophistication as follows: "Exactly how sophisticated a mathematical model has to be is a contentious issue for sport and exercise biomechanists. In the past, simple 2-dimensional (2-D) or planar models have been popular because of their mathematical convenience and computational simplicity. The advantage of using simple mathematical models is that they provide results that are more easily interpretable by clinical practitioners, coaches and athletes. Simple mathematical models, such as those outlined by Alexander (1995) for walking, running, jumping and throwing, have been used for providing basic mechanical insights and developing fundamental principles of human movement. Indeed, it has been argued that the most fundamental understanding often comes from the simplest of models and that establishing cause and effect is often easier with simpler models. More recently, however, more complex 3-dimensional (3-D) or spatial models have gained popularity as a result of advances in computer technology". Selbie and Caldwell (1996) used the muscle models with torque generators acting at the hip, knee and ankle joints in simulations of vertical jumping. Torque-velocity and torque-angle relationships without elastic characteristics were included in these rotational models. The possible discrepancies between the simple models (inverted double pendulum) and more complex, muscle actuated models in walking were examined by Pandy (2003). One good review of the kinds of models (conceptual, physical, and mathematical) that have been used in biomechanics has been presented by Alexander (2003). Non-linear dynamical methods used in neuroscience and complex data analysis are well reviewed by Ivancevic et al. (2009).

Optimization models have also increased the understanding of biomechanics of human movement. Optimization is problematic because we do not know whether or not humans actually produce movements based on one single performance criterion (Umberger and Caldwell 2014). Examples of these optimization models have been published by e.g. Bobbert et al. (1986), Pandy and Zajac (1991) and van Soest et al. (1993).

2.2.1 Arm movement

Several extensor and flexor muscles were used by Raikova (1996) in her model of the flexion – extension motion in the elbow joint. Furthermore, the force of a skeletal muscle is an accumulation of forces generated by active motor units belonging to this muscle (Raikova et al 2013). Raikova et al. (2005) mentioned that access to each motor unit (MU) is impossible, and the recruitment and force developing properties of all individual MUs cannot be known. In this paper (Raikova et al. 2005) the process of learning fast elbow flexion in the horizontal plane was simulated and the result was compared with experimentally measured data.

A model of non-linear equation of motion $m\ddot{x} + a\dot{x} + bx^3 = c\sin(dt)$ was presented by Gacesa et al. (2010). This is an elbow extension model in which the Hill-Huxley muscular force-length curve was used for developing the cubic elastic component bx^3. This elastic component is a combination of the active muscular curve (which is roughly quadratic) and passive tendon elastic curve (which is roughly exponential). The contractile component is a sine form force $c\sin(dt)$.

Recently Haufle et al. (2014) presented a Hill-type muscle model with the combined effect of a serial damping element (Günther et al. 2007) and eccentric force–velocity relationship. The model was applied to arm movements and the authors mentioned that this more realistic representation of the eccentric force–velocity relationship resulted in human-like elbow-joint flexion. One of the limitations mentioned was that the model cannot reproduce the shift of optimum muscle length to longer lengths, which has been observed in experiments at submaximal muscle activation.

One example of the application of modeling was done by Rahikainen and Luhtanen (2004) as they modeled the arm push of shot put performance. Figure 2 shows the speed of the shot and its mathematical modeling can be seen in Figure 3. Some limiting factors for the generation of the speed (e.g. arm pushing force and rotational technique) were discussed.

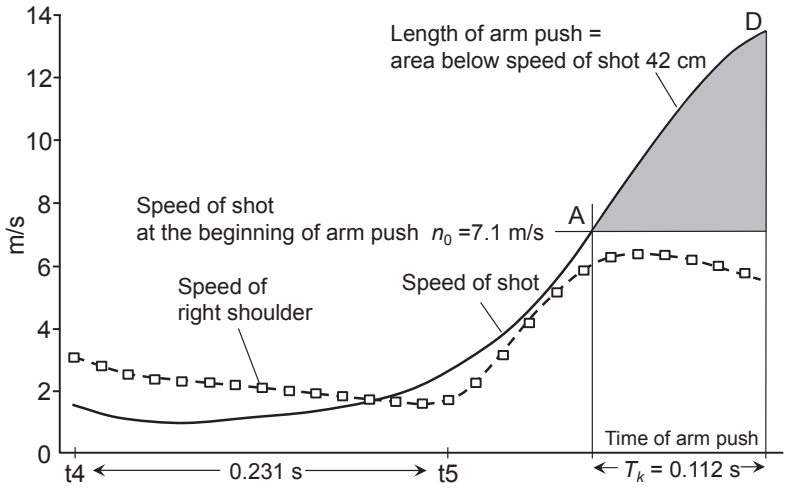

FIGURE 2 The measured speed of the shot in 20.90 m put with rotational technique. The contacts of the right leg (t4) and left leg (t5) are shown (modified from Rahikainen and Luhtanen 2004).

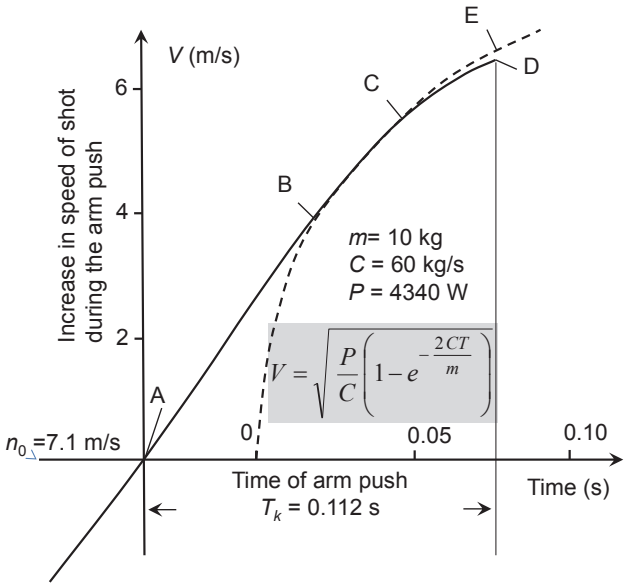

FIGURE 3 The measured (solid line) and theoretical (dashed line) speed of the shot in 20.90 m put with rotational technique providing the initial speed of the shot of 7.1 m/s (modified from Rahikainen and Luhtanen 2004).

2.2.2 Leg movement

Other analytical models of human locomotion and especially leg movement have been presented by e.g. Ackermann and van den Bogert (2010), Morio et al. (2009), Ni et al. (2003), Pop et al. (2003) and stiffness and damping at leg joints by Blum et at. (2009), Hobara et al. (2009, 2010), and Rapoport et al. (2003). Functional ability and reliability of these models have usually been evaluated by comparing the results obtained by the model (for instance ground reaction force – time function) with the actual movement measurements. Developing a theoretical model is difficult because the complicated actual movement must first be simplified into a model fitting mode and then the factors principally influencing the present movement must be chosen from the great number of factors acting in actual movement. One typical example of a leg movement model was presented by Nigg (2006). The model describes a runner as two masses, the runner's body mass with and without leg mass. In this model the internal force of the system acting between the body mass and the leg mass has been calculated by minimizing the power generated therein. The model yielded results which fitted relatively well the measured results. Another model presented by Nigg (2006) involved the mechanics of human heel. In this model the motion of subject's mass m is damped by the spring force kx and the damping force $r\dot{x}$. The equation of motion is then $m\ddot{x} + r\dot{x} + kx = 0$ and its solution is $x(t) = Ae^{-ct}$. In the decelerated motion the roots of the constant c are real. Constant force of the contractile element is also added to the system $m\ddot{x} + r\dot{x} + kx = F$ and then the solution for the equation of motion is $x(t) = Ae^{-ct} + F/k$.

The above mentioned principle was used by Rahikainen and Luhtanen (2003) as the oscillation equations were fitted to the measurements of a shot putter's center of mass (CoM) during the ground contact. In this study the displacement and velocity of the shot were actually measured and the path of the athlete's CoM was assumed to correspond to the shot movement (Fig. 4). Although the curve fittings worked fairly well they showed that for a more accurate analysis a model better suited for practical situations was needed. The idea of the study was first to develop a model of leg movement without pushing force and then from this model a more sophisticated version of leg movement using maximum muscular force was created. It was assumed that a model of leg movement without leg force fits the jump on one leg with appropriate accuracy. It was also assumed that the path of the CoM when jumping on one leg is a damped oscillatory movement. The model of leg movement with maximum leg pushing force was obtained by adding the leg pushing force to this basic model of jumping on one leg. The equation of motion for the model of jumping on one leg was $m\ddot{x} + \lambda\dot{x} + kx = mg$ where m is body mass, x vertical displacement of the CoM, $\lambda\dot{x}$ liquid friction and kx is the elastic force due to tendons and internal elasticity of muscles.

A solution for this differential equation was damped oscillatory movement $x(t) = Ae^{-\gamma t} \sin(\omega t) + g/\omega_0^2$ [Alonso and Finn, 1980], where x is vertical displacement, t is time and A, ω and γ are constants and g/ω_0^2 is constant effect of gravity. Thereafter the model of leg push in shot put was obtained by adding the pushing force to the equation of jumping on one leg. The equation of motion for leg pushing phase in shot put was $m\ddot{x} + \lambda\dot{x} + kx = -K + mg$ where K is leg pushing force. A solution for this differential equation was strengthening oscillatory movement $x(t) = Ae^{\gamma t} \sin(\omega t) + g/\omega_0^2$. The functionality of the above mentioned theories were tested by fitting the equations of damping and strengthening oscillation to the measured path of the CoM in shot put. The constants A, ω, γ, ω_0^2 were determined within curve fitting.

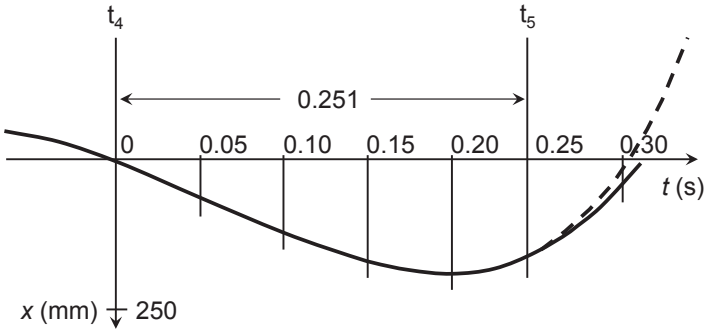

FIGURE 4 The measured path of the shot (broken line) and its mathematical fitting (solid line) of the 19.47 m put. The ground contact of the right leg (t_4) and the left leg (t_5) are shown (modified from Rahikainen and Luhtanen 2003).

3 PURPOSE OF THE STUDY

The present study follows the diagram of Popper's (2002) testing of hypothesis. One circle in the diagram of Figure 5 represents the progress of research (testing the hypotheses) as follows: 1. Equations of models of leg and arm movement were derived and test predictions were made. 2. Experiments were performed. 3. Equations of arm and leg movement were fitted to the experimental results and their compatibility was evaluated. 4. If the present equation of motion did not fit the measuring results, the hypothesis would be disproved. If the present equation of motion fitted the measuring results in some definite accuracy, the hypothesis would be confirmed. 5. By making an additional experiment (a new circle in the diagram) the hypothesis is further confirmed.

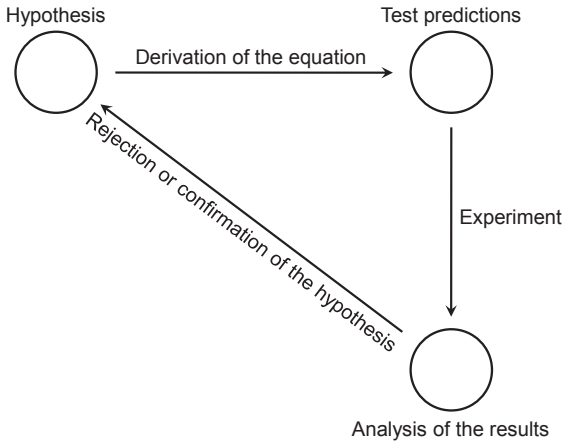

FIGURE 5 Diagram of the progress of testing the hypotheses of arm rotation and leg movement, Popper (2002).

Hill's force-velocity relationship is probably one of the most important models in muscle mechanics, but it has deficiencies that restrict its application for the actual muscular mechanics of human motion. In Hill's equation there is always

a force that is resisting motion and resulting in a constant velocity. Thus, Hill's equation cannot be applied, if there is no force resisting speed, but in which the motion is in a state of high acceleration. Also at the point of maximum speed, at the state of zero force, Hill's equation does not seem to fit the experimental points very well. One more deficiency in the models based on Hill's equation is that they do not take into account the effect of the elasticity of tendons and muscular tissues. The purpose of the present study was to create models of arm and leg motion in order to compensate for the deficiencies of Hill's equation. The model of leg motion is the function of body mass, elasticity of the leg's muscle tendons and tissues, and activation of leg's muscle forces. The model of arm rotation is as follows: First, start of rotation resulting in total tension of a muscle's elastic tendons and tissues; second, model of maximum constant moment at the state of low speed high acceleration; and third, model of constant maximum power at the state of high speed low acceleration. These theoretical models are then examined how they fit into measured values of arm rotations and one- and two legged jumping. The further purpose of the study was to determine how Hill's equation functions as a constant power model and to compare Hill's equation with the model developed in the present study.

3.1 Arm movement

According to the present theory and above mentioned facts, the movement proceeds as follows: 1) start of motion; 2) movement proceeds at a constant maximum rotational moment during the first part of the movement [Hypothesis 1]; 3) movement proceeds at a constant maximum muscular power during the second part of the movement [Hypothesis 2]; 4) stopping of motion. In order to test the research hypotheses, the following experiments were conducted: forearm rotation downwards (elbow extension) at maximum velocity, forearm rotation upwards (elbow flexion) at maximum velocity, whole arm rotation downwards at maximum velocity, whole arm rotation upwards at maximum velocity. The maximum power hypothesis was tested so that the theoretical angular velocity-time values from Equation (16) were fitted into the measured angular velocity-time curves of arm rotations. It was assumed that if the measured angular velocity-time values matched the theoretical values within a certain velocity range then the Hypothesis 2 would be fulfilled. The maximum rotational moment hypothesis was tested by Equation (10).

3.2 Leg movement

In this study it was hypothesized that the vertical movement of a subject's center of mass fulfills the equation of damped oscillatory motion $x = Ae^{-\gamma t}\sin(\omega)$ or

strengthening oscillatory motion $x = Ae^{\gamma t}\sin(\omega)$ with sufficient accuracy. According to the theory derived in the present study, the path of damped oscillatory motion represents the leg movement without muscular force. This is a theoretical situation that is not completely possible in practice. However, it was presumed that relatively low force exertion would yield the path of damped oscillatory motion. As the exerted force increased it was assumed that the curve of the path of motion would resemble amplified oscillatory motion. The third possibility was that the coefficient $\gamma = 0$ and the path of the CoM becomes sine-form motion $x = A\sin(\omega t)$. Within derivation of the differential equation of a subject's center of mass, the variables were simplified and it was therefore possible that the equations presented above would be not realized in the practical experiments. In order to find out the functional ability of the research hypotheses, actual experiments of jumps on one leg and on two legs were performed and analyzed. The jumps were performed using each subject's maximum force because the exertion of sufficient muscle force was required to make the oscillatory motion of the CoM large enough and this way the form of the path of motion could be examined with adequate accuracy. Thereby the following questions were examined: Is it possible to fit, with sufficient accuracy, the equation of damped oscillatory motion [Hypothesis 3] or the equation of strengthening amplified oscillatory motion [Hypothesis 4] or the equation of sine-form motion [Hypothesis 5] to the measured vertical displacement-time function of the center of gravity? It is good to notice that some factors were omitted in the derivation of paths of motion and therefore, following assumptions were made:

- It is presumed that kinetic friction is directly proportional to velocity.
- It is also presumed that elastic force is directly proportional to vertical displacement during the legs´ ground contact.
- Horizontal force acting on the CoM during the ground contact may have an effect on the vertical movement of the CoM.
- The force of leg push is a result of total torque, which is generated by muscular forces through a transmission system of bony framework. As the angle of the joint changes, the arm of torque also changes and it influences the torque and the pushing force.
- The muscular force generated by a muscle contraction has its own dynamics and is controlled by the nervous system.

Due to these factors it is not certain whether the above mentioned equations are realized within leg mechanics. However, the role of the above mentioned factors is most likely minimal and they do not affect the dynamic mechanics of leg motion to any significant extent. On the other hand the control of nervous system can enhance the mechanics of damped and strengthening equations, which represents the effective mode of motion. Therefore it is possible that damped and oscillation equations can be realized within mechanics of human motion to

such an extent that this question is worth being studied. The real state of motion can only be found by performing an adequate number of experiments. Functionality of the oscillation equations in the shot put performance was also re-examined with the data of the earlier studies.

4 METHODS

4.1 Measuring devices

All the movements were photographed with a special motion recording system described by Rahikainen (1990, 2003). This measuring method is a useful complement to the existing methods (Sheets et al., 2010). The principle of the system is to photograph the moving subject through a rotating disk that consists of one transparent and nine filter openings serving as shutter apertures (Fig. 6). As the camera aperture is open, several overlapping exposures are generated on one frame. The transparent opening exposes images of the moving subject while the filter openings produce dashed light lines of the paths of the marker lights attached to the moving subject. As a result one film frame contains a series of subject images and the paths of the marker lights are seen as dashed light lines. A typical photograph of the jump on two legs is presented in Figure 7. The rotational speed of the disk was 150 revolutions per minute (recorded by a special tachometer) exposing the subject images at 0.4 s intervals from each other and giving nine light-lines (0.04 s) between each subject image. Marker lights were attached at the knee, center of mass (CoM, estimated point on hip, justified in Fig. 8) and hand. In the jumps the marker-light attached to the knee indicated the instant of the ground contact (touchdown) locating six light lines or 0.24 seconds before the second subject image in Figure 7. The transition from the braking phase to the pushing phase of the contact could be estimated from the marker light pattern during the ground contact. The bright marker light (brighter than the others) is exposed at the same time with the subject image (transparent disk opening). At the instant of the ground contact the path of the CoM goes below the horizontal reference line and the theoretical model of leg movement was fitted to the light lines under this horizontal line. Additional recordings were made using the Vicon system with eight cameras. Figures 7 and 8 clearly demonstrate that the curve of the CoM resembles oscillatory movement.

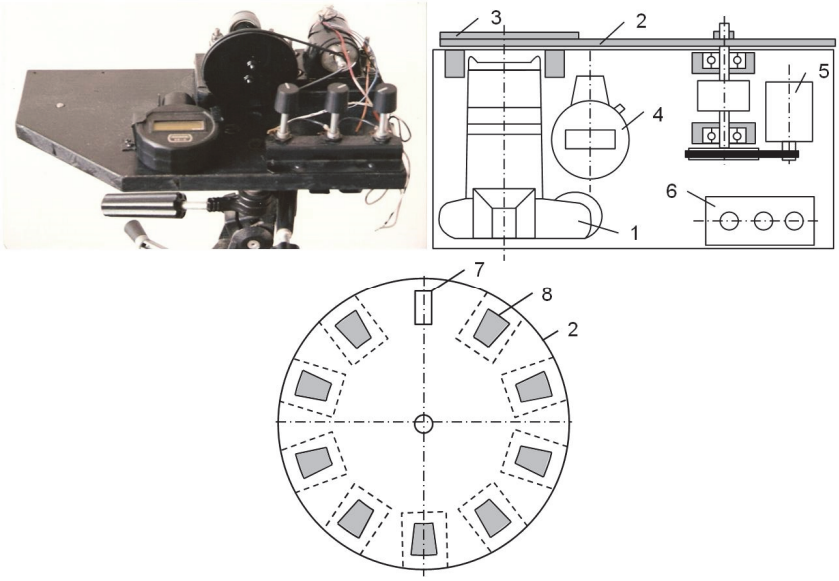

FIGURE 6 The photographing apparatus consists of the rotating disk (2) with one transparent opening (7) and nine filter openings (8) in front of the camera (1). Tachometer (4), electric motor (5) and adjusting knobs (6) for disk speed are seen as well.

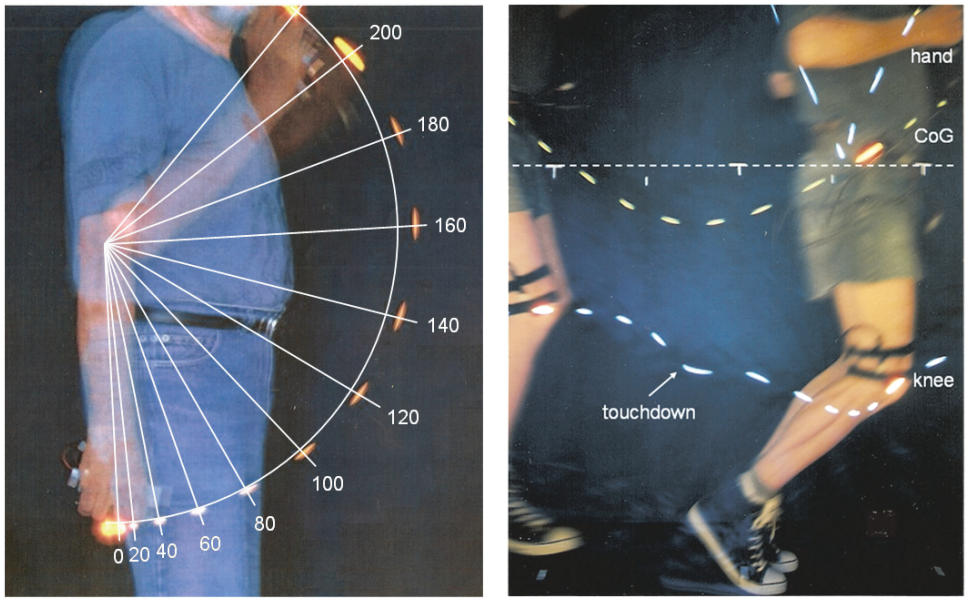

FIGURE 7 Examples of elbow flexion (rotation angles between two arm images are given in 20 ms increments) and jumping on two legs showing the paths of motion of the marker lights. It is noteworthy that the moment arm of the muscles involved in elbow flexion changes during the movement and, therefore, the muscles' contribution to power production changes as well.

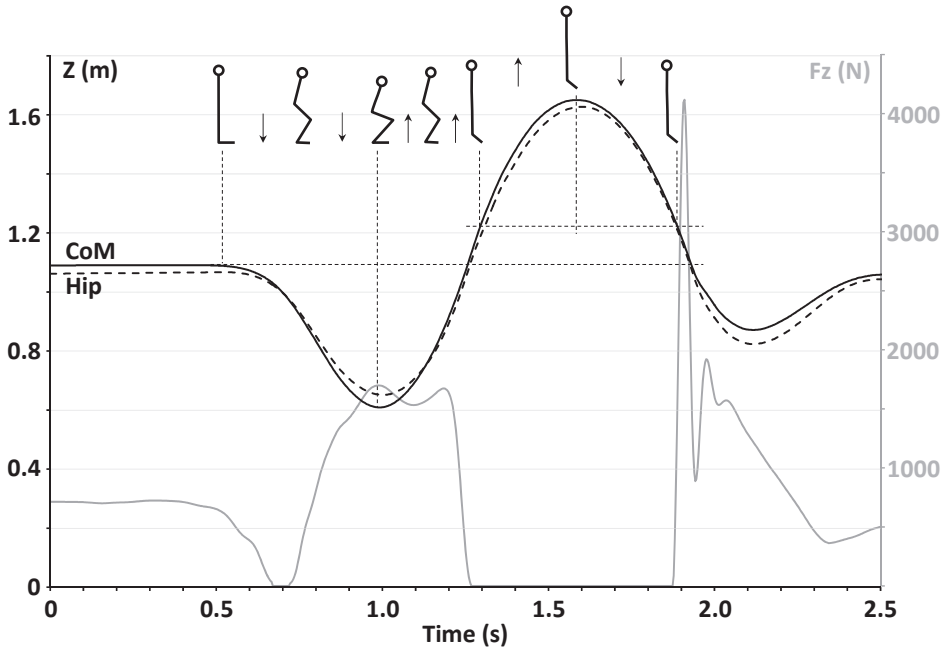

FIGURE 8 Typical example of the hip and CoM trajectories (Z) and vertical ground reaction force (Fz) measured during the counter movement jump (CMJ).

4.1.1 Measurement of arm rotation

In the present study, the measurements of arm rotations (subjects S1 and S2) were recorded by a special camera system Rahikainen (1990 and 2003). Figure 7 shows the principle of the system where angular velocity was calculated with the formula

$$\dot{\varphi} = \Delta S / R \, \Delta T \tag{1}$$

where R is arm length, ΔS is the distance between two successive measuring points and ΔT is the time increment. Additional elbow flexion and extensions were performed for one subject (S3) using the Vicon motion analysis system with 8 cameras. This system made it possible to use higher frame rates (300 Hz). Subjects were normal healthy male people representing different age and physical activity background (S1: 62 years, 1.80 m, 82 kg, S2: 35 years, 1.69 m, 73 kg, aikido training, weight lifting and S3: 25 years, 1.83 m, 70 kg, high jumping).

The angular velocity - time curves were drawn from the manually determined marker light positions on squared graph paper, where 1 mm corresponded to an angular velocity of 0.1 rad/s and time of 1 ms giving the accuracy of velocity curves. The theoretical and measured angular velocity curves coincided within the distances of 35 - 70 mm, which was enough for the verification of the constant power model in the arm rotation experiments. Slight oscillations at the beginning of the movement did not exist within the constant power phase and, therefore, the verification of the constant power model was possible

in all experiments. The accuracy of the Vicon recording system, verified by calculating the root-mean-square error for each camera, ranged from 0.06 to 0.17 mm during calibration.

4.1.2 Measurement of rotation arc

For convenience the arc ΔS_1 was measured as a straight line ΔS_2 (Fig. 9) and the error between these two values was estimated. The arc ΔS_1 can be calculated from the straight line ΔS_2 using the formula:

$$\Delta S_1 = R \arccos\left(1 - \frac{1}{2}\left(\frac{\Delta S_2}{R}\right)^2\right)$$

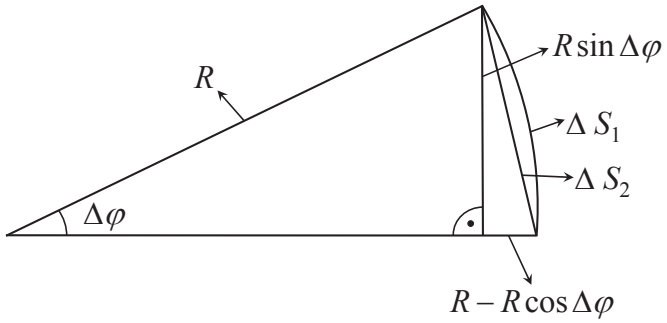

FIGURE 9 Measurement of the rotation arc. φ = angle of rotation, R = length of forearm, arc ΔS_1 = distance the marker light travels during the time interval Δt and ΔS_2 = the arc ΔS_1 measured as a straight line.

Formula derivation from the right-angled triangle in Figure 7

$$\Delta S_2^2 = R^2 \sin^2 \varphi + R^2 (1 - \cos \Delta\varphi)^2 \tag{2}$$

$$\left(\frac{\Delta S_2}{R}\right)^2 = \sin^2 \Delta\varphi + \cos^2 \Delta\varphi + 1 - 2\cos \Delta\varphi \tag{3}$$

$$\sin^2 \Delta\varphi + \cos^2 \Delta\varphi = 1 \tag{4}$$

$$\left(\frac{\Delta S_2}{R}\right)^2 = 2 - 2\cos \Delta\varphi \tag{5}$$

$$\cos \Delta\varphi = 1 - \frac{1}{2}\left(\frac{\Delta S_2}{R}\right)^2 \tag{6}$$

$$\Delta S_1 = R \arccos\left(1 - \frac{1}{2}\left(\frac{\Delta S_2}{R}\right)^2\right) \tag{7}$$

The maximum value measured from Figure 7 (corresponding time 140 ms) is $\Delta S/R = \Delta S_2/R = 0.356$. Substituting this value in the formula above the arc of rotation is obtained as ratio form $\Delta S_1/R = 0.358$. It can be seen that ΔS_2 fits with adequate accuracy to the distance ΔS_1.

4.1.3 Accuracy of time and distance measurements

The distance x_i that the marker light travels during one time interval was measured with the accuracy of half a millimeter. The accuracy of the time interval Δt corresponding to the successive distance measurements was obtained from the accuracy of the rotating speed of the exposure disc. The total error in the measurements was determined by drop experiments where a marker light attached to the battery was photographed in free fall. The accuracy was calculated as follows:

Equation of fall movement

$$\frac{\Delta x_n}{\Delta t} - \frac{\Delta x_0}{\Delta t} = g\, n\, \Delta t \tag{8}$$

where Δt is the time interval in measurements, Δx_0 is the distance which the marker light travels at the beginning of the drop, Δx_n is the distance which the marker light travels at the end of the drop, $n + 1$ is the number of measurements, $n\Delta t$ is the time from 0 to n-measurement, and g is gravitational acceleration. The time interval is calculated from Equation (8)

$$\Delta t = \sqrt{\frac{\Delta x_n - \Delta x_0}{g\, n}} \tag{9}$$

The accuracy of the measuring system was estimated by calculating the time intervals Δt from the formula above using a sufficient number of drop experiments. A higher accuracy was obtained by using a curve fitting for several (9) distance measurements in one frame. The final accuracy of the measurement system was calculated by comparing the time values from the formula (drop experiment) with the tachometer reading. In this study a measurement accuracy of ± 0.0005 seconds was achieved.

4.1.4 Coordinates of the path of jump motion

Figure 10 shows the background coordinate markers located at a distance of 0.25 m from each other. The lengths of the background coordinates at the plane of motion were calculated with the following equations:

$$\frac{S_1}{a} = \frac{S}{b} \qquad \Rightarrow \qquad S_1 = \frac{a}{b} S \tag{10}$$

$$\frac{S_1 + S_2}{a} = \frac{2S}{b} \quad \Rightarrow \quad S_1 = S_2, \tag{11}$$

where a is the distance of the camera from the plane of motion, b is the distance of the camera from the background coordinates, S is the length of the background coordinates, S_1 and S_2 are the lengths of the background coordinates at the plane of motion. Equation (11) shows that all background coordinates are the same length at the plane of motion.

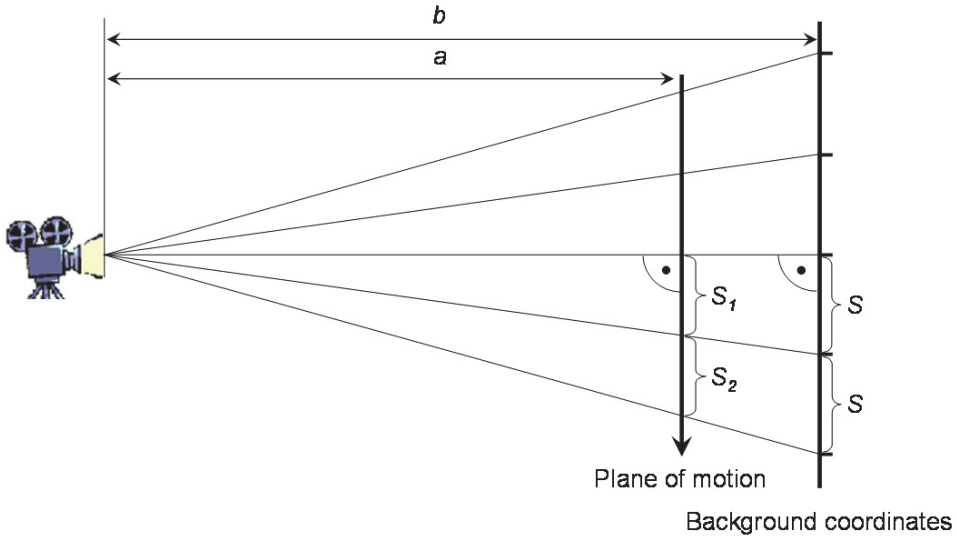

FIGURE 10 Calculation of the lengths of the background coordinates at the plane of motion.

4.2 Model of arm rotation

The model used in the present study was constructed according to Newton's II law and it was first used in linear motion (Rahikainen and Luhtanen 2004). The theory of arm rotation is as follows: At the beginning of the movement, angular velocity is naturally zero and it takes some time to generate force. In that phase of motion, elasticity of arm tendons has influence on the motion, thereafter the tendons are in a full state of tension, and they have no further dynamic effect. After that it can be assumed that a maximum muscle force takes action and within rotational motion, maximum rotational moment acts as well. At this phase of motion constant value glide friction acts. Because the muscular system is able to transfer only a certain quantity of chemical energy during the time of contraction, there must be a constant maximum power that the muscle is able to generate within a certain range of velocity. "A constant power theory" is possible only when the velocity is high enough. As the velocity increases the motion

reaches a point where the maximum power takes action and the acting rotational moment is less than the maximum moment. As a result power remains constant as the angular velocity increases and moment decreases. In that phase of motion, liquid friction, directly proportional to velocity, acts. The constant value glide friction decreases as forces at the joint decrease and it becomes indifferent. The model of arm rotation during constant power phase is constructed as follows: the rotational moment is the moment of inertia multiplied by angular acceleration that equals the moment generated by muscle force minus the moment generated by inner friction of the muscle. The effect of gravitational force is added afterwards (see paragraph 4.2.2).

$$I \frac{d\dot{\varphi}}{dT} = \frac{P}{\dot{\varphi}} - C\dot{\varphi} \tag{12}$$

where

Moment of inertia in arm rotation	I
Angular velocity	$\dot{\varphi}$
Power generated by arm muscles	P
Time	T
Moment generated by muscle force	$P/\dot{\varphi}$
Moment generated by inner friction of muscle	$C\ \dot{\varphi}$
Coefficient of friction	C

Inner friction of the muscle is liquid friction inside the muscle that is directly proportional to velocity. This liquid friction was initially adopted from Alonso and Finn (1980). It was initially assumed that movement proceeds at a constant maximum moment and the moment generated by the muscle force ($P/\dot{\varphi}$ in Eq. 12) is constant. It was also assumed that as velocity increases, movement proceeds at constant maximum power at a certain range of velocity and then the power P in Equation 12 is constant. In order to determine the validity of this hypothesis, Equation (12) was solved for angular velocity-time function and this equation was employed for determination of validity.

Solution

$$I \ \frac{\dot{\varphi}}{P - C\dot{\varphi}^2} d\dot{\varphi} = dT \tag{13}$$

$$-\frac{I}{2C} \int_0^{\dot{\varphi}} -2C\dot{\varphi} \ \frac{1}{P - C\dot{\varphi}^2} d\dot{\varphi} = \int_0^T dT \tag{14}$$

$$\ln\left(P - C\dot{\varphi}^2\right) - \ln\left(P\right) = -\frac{2C}{I} T \tag{15}$$

$$\ln\left(\frac{P - C\dot{\varphi}^2}{P}\right) = -\frac{2C}{I} T \tag{16}$$

$$1-\frac{C}{P}\dot{\varphi}^2 = e^{-\frac{2C}{I}T} \tag{17}$$

$$\dot{\varphi} = \sqrt{\frac{P}{C}\left(1-e^{-\frac{2C}{I}T}\right)} \tag{18}$$

4.2.1 Calculation of moment of inertia

The mass distribution of the subjects´ arm sectors differed from the average values of mass presented in the literature. Therefore, the mass distribution of the arm sectors were determined by sinking the arm sectors into water. The masses of the arm sectors were calculated by multiplying the overflowed water volume with the corresponding arm sector density. The length of each subject's whole arm was measured with the fist clenched, and the lengths of arm sectors (hand, forearm, and upper arm) were measured. According to Winter (2004) the arm sector densities (kg/l) were as follows: hand 1.16, forearm 1.13, upper arm 1.07.

Definition of moment of inertia:

$$I = \int r^2 dm \tag{19}$$

where *dm* is rotating mass and *r* is the distance of rotating mass from the rotational axis. Derivation of the moment of inertia about the end of arm sector assuming even mass distribution:

$$I_1 = \int_0^L r^2 dm = \int_0^L r^2 \frac{dm}{dr} dr = \frac{m}{L}\int_0^L r^2 dr = \frac{m\,L^2}{3} \tag{20}$$

where *m* is the mass of rotating arm, and *L* is the length of rotating arm. Derivation of the moment of inertia about the center of the arm sector assuming even mass distribution:

$$I_2 = \int_{-L/2}^{L/2} r^2 dm = \frac{m}{3L}\left(\frac{L^3}{2^3}+\frac{L^3}{2^3}\right) = \frac{m\,L^2}{12} \tag{21}$$

Because the distribution of mass in the arm sector is not even, the moment of inertia of an additional mass was calculated with the formula:

$$I_3 = m r^2 \tag{22}$$

where *m* is the additional mass of the arm sector and *r* is the estimated distance of the center of gravity of the additional mass from the rotation axis. Subjects' arm sector distances, lengths, and masses are presented in Table 1. These values are then substituted in the above mentioned Equations (19 - 22) to calculate the final moments of inertia of forearm and whole arm rotations about the elbow and shoulder joint (example for S1 summarized in Table 2).

TABLE 1 The estimated mass distribution of arm sectors. The forearm's additional mass is due to the muscles' mass distribution in the other end of the arm sector.

	Distance from elbow joint (m)			Distance from shoulder joint (m)			Length (m)			Mass (kg)		
Subject	**S1**	**S2**	**S3**	**S1**	**S2**	**S3**	**S1**	**S2**	**S3**	**S1**	**S2**	**S3**
Hand							0.11	0.11	0.12	0.58	0.52	0.58
- center of mass	0.34	0.32	0.34	0.64	0.60							
Forearm							0.28	0.26	0.27	1.00	0.90	1.00
-center of mass				0.44	0.41							
-additional mass	0.07	0.06	0.07	0.37	0.34					0.24	0.22	0.24
Upper arm							0.30	0.28	0.33	2.14	2.53	
Battery	0.37	0.35		0.67	0.63					0.26	0.29	0.29

Moment of inertia of forearm rotation

Forearm

Moment of inertia of major forearm mass about the elbow joint (m = 1.0 kg, L = 0.28 m):

$$I_{11} = \frac{m\,L^2}{3} = \frac{1.0 \cdot 0.28^2}{3} = 0.0261 \text{ kgm}^2$$

Moment of inertia of additional forearm mass about the elbow joint (m = 0.24 kg, r = 0.07 m):

$$I_{12} = mr^2 = 0.24 \cdot 0.07^2 = 0.0012 \text{ kgm}^2$$

Hand

Moment of inertia of the hand sector about the center of mass (m = 0.58 kg, L = 0.11 m):

$$I_{13} = \frac{m\,L^2}{12} = \frac{0.58 \cdot 0.11^2}{12} = 0.0006 \text{ kgm}^2$$

Moment of inertia of the hand sector about the elbow joint (m = 0.58 kg, r = 0.34 m):

$$I_{14} = mr^2 = 0.58 \cdot 0.34^2 = 0.0670 \text{ kgm}^2$$

Light marker battery

Moment of inertia of the battery about the elbow joint (m = 0.26 kg, r = 0.37 m):

$$I_{b1} = 0.26 \cdot 0.37^2 = 0.0356 \text{ kgm}^2$$

Total moment of inertia of forearm rotation about elbow joint

0.0261 + 0.0012 + 0.0006 + 0.0670 + 0.0356 = 0.131

Moment of inertia of whole arm rotation

Upper arm
Moment of inertia about the shoulder joint (m = 2.14 kg, L = 0.30 m):

$$I_{21} = \frac{m\,L^2}{3} = \frac{2.14 \cdot 0.30^2}{3} = 0.0642 \text{ kgm}^2$$

Forearm
Moment of inertia of the major forearm mass the about center of mass (m = 1.0 kg, L = 0.28 m):

$$I_{22} = \frac{m\,L^2}{12} = \frac{1.0 \cdot 0.28^2}{12} = 0.0065 \text{ kgm}^2$$

Moment of inertia about the shoulder joint (m = 1.0 kg, r = 0.44 m):

$$I_{23} = m r^2 = 1.0 \cdot 0.44^2 = 0.1936 \text{ kgm}^2$$

Moment of inertia of additional mass about the shoulder joint (m = 0.24 kg, r = 0.37 m):

$$I_{24} = m r^2 = 0.24 \cdot 0.37^2 = 0.0329 \text{ kgm}^2$$

Hand
Moment of inertia of the hand sector about the center of mass (m = 0.58, L = 0.11 m):

$$I_{25} = \frac{m\,L^2}{12} = \frac{0.58 \cdot 0.11^2}{12} = 0.0006 \text{ kgm}^2$$

Moment of inertia of the hand sector about the shoulder joint (m = 0.58 kg, r = 0.64 m):

$$I_{26} = m r^2 = 0.58 \cdot 0.64^2 = 0.2376 \text{ kgm}^2$$

Light marker battery
Moment of inertia of the battery about the shoulder joint (m = 0.26 kg, r = 0.67 m):

$$I_{b2} = 0.26 \cdot 0.67^2 = 0.1167 \text{ kgm}^2$$

Total moment of inertia at whole arm rotation about shoulder joint

$0.0642 + 0.0065 + 0.1936 + 0.0329 + 0.0006 + 0.2376 + 0.1167 = 0.652\ \text{kgm}^2$

According to the above mentioned calculations, the corresponding moments of inertia of forearm rotation and whole arm rotation for S2 were 0.110 and 0.551 kgm^2, respectively. As the total length of forearm and hand was the same for subjects S1 and S3, it was assumed that the moments of inertia of these segments were also the same and, therefore, the moment of inertia of forearm rotation about the elbow joint for S3 was 0.131 kgm^2. The measurements with Vicon camera system for S3 were done with reflective markers and the corresponding moment of inertia without the battery was 0.095 kgm^2.

TABLE 2 Summarized information for calculation of moment of inertia of forearm rotation (upper part) and whole arm rotation (lower part) for one subject. Moment of inertia is calculated about the elbow joint, center of mass (com) and shoulder joint.

Segment	m (kg)	L (m)	r (m)	about	moment of inertia	I (kgm^2)
Forearm	1.00	0.28		elbow	$I_{11} = \frac{mL^2}{3}$	0.0261
Forearm (additional mass)	0.24		0.07	elbow	$I_{12} = mr^2$	0.0012
Hand	0.58	0.11		com	$I_{13} = \frac{mL^2}{12}$	0.0006
Hand	0.58		0.34	elbow	$I_{14} = mr^2$	0.0670
Battery	0.26		0.37	elbow	$I_{b1} = mr^2$	0.0356
Total						**0.131**

Segment	m (kg)	L (m)	r (m)	about	moment of inertia	I (kgm^2)
Upper arm	2.14	0.30		shoulder	$I_{21} = \frac{mL^2}{3}$	0.0642
Forearm	1.00	0.28		com	$I_{22} = \frac{mL^2}{12}$	0.0065
Forearm	1.00		0.44	shoulder	$I_{23} = mr^2$	0.1936
Forearm (additional mass)	0.24		0.37	shoulder	$I_{24} = mr^2$	0.0329
Hand	0.58	0.11		com	$I_{25} = \frac{mL^2}{12}$	0.0006
Hand	0.58		0.64	shoulder	$I_{26} = mr^2$	0.2376
Battery	0.26		0.67	shoulder	$I_{b2} = mr^2$	0.1167
Total						**0.652**

4.2.2 Effect of gravitational force on the movement

The moment that is induced by gravity was omitted from the motion model. The power generated by this moment is, where mg is gravitational force of arm segments, r is distance of the center of gravity of segments from the rotation axis, and angular velocity of arm rotation. The theoretical angular velocity function, Equation (18), and the measured angular velocity function coincide within such a narrow velocity range that the power induced by gravity can be calculated as a constant factor. In this case it is included in the power *P* as follows: *P* of rotation downwards = power generated by muscular force + power generated by gravitational force and *P* of rotation upwards: *P* = power generated by muscular force – power generated by gravitational force.

4.2.3 Matched range of measured and theoretical angular velocity

Figure 11 shows the technique that was used to determine the matched range of measured and theoretical angular velocity curves. Friction coefficient values (C) and power values (*P*) were obtained by fitting the theoretical angular velocity curves to the measured ones. These two curves coincide only if certain *C* and *P* values are used in the fitting process. The measured angular velocity values are shown as points on the velocity curve and the theoretical angular velocity (Eq. 18) is shown as a dashed line. The matched range was found by using the following iteration procedure: based on previous experiments, the randomized initial values (see Fig. 11) within the matched range were selected for angular velocity at point 1 ($\dot{\varphi}$ =16.8 rad/s). A zero point on the time axis for the theoretical angular velocity was selected 0.050 s before point 1, which corresponds to 0.060 s on the time axis of the Figure. Thereafter, the direction of the iteration process was observed and after some iteration, the final theoretical angular velocity was drawn according to Equation 18 to match the measured velocity curve. The correct theoretical angular velocity was obtained with the zero point at 0.073 s on the time axis. The ratio of power and friction coefficient in Figure 11 is

$$\frac{P}{C} = \frac{\dot{\varphi}^2}{1 - e^{-\frac{2C}{I}T}} \tag{23}$$

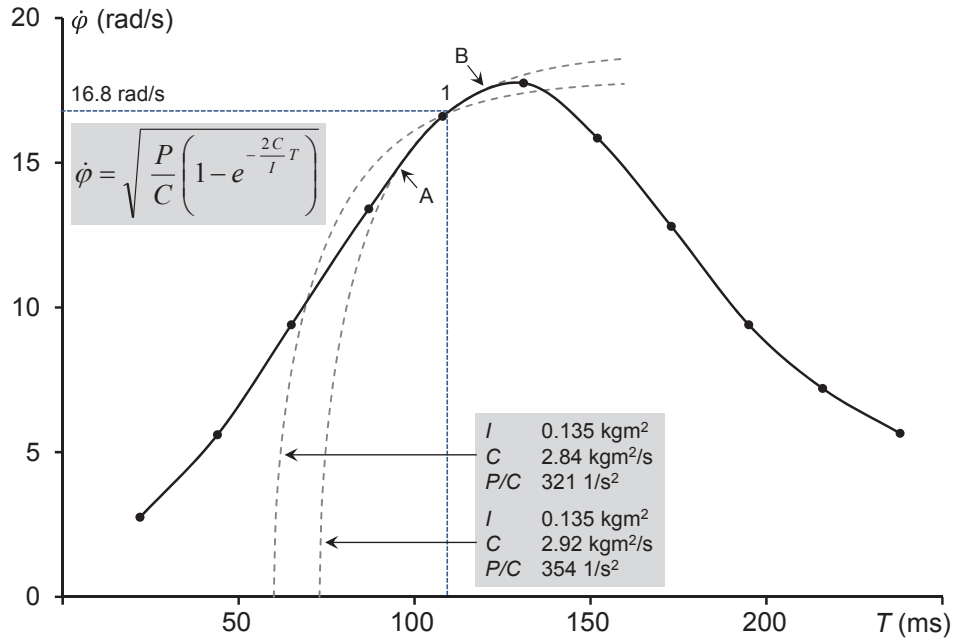

FIGURE 11 Example of the technique to find the matched range (A - B) of measured and theoretical angular velocity. The zero point of time for the theoretical angular velocity is at the intersection of the time-axis and the dashed line curve (see text for more information). The theoretical angular velocity curve (dashed line) coincides with the measured curve (solid line) between A and B.

The final theoretical angular velocity was drawn with the moment of inertia I = 0.135 kgm^2, friction coefficient value C = 2.92 kgm^2/s, and ratio of power and friction coefficient P/C = 354 1/s^2.

4.3 Model of leg movement

While jumping, the subject performs an oscillatory movement as the body center of mass moves first downwards and then upwards during the ground contact. This path can be presented as the mathematical model of leg movement. In the present study the model of leg movement without leg pushing force was constructed first and then the pushing force was added to that model. A model of leg movement without leg pushing force is not actually realized in practical circumstances. Leg pushing force must always be involved so that the system can be functional in reality. However, the model of leg movement without pushing force is important within the analysis of movement. It determines the natural oscillation time of the system as well as the resonance frequency.

4.3.1 Model of leg movement without pushing force

The following forces act at the subject's center of mass during the ground contact: 1. downwards, the force of gravity, 2. upwards, the force due to the elasticity of leg's tendons and the elastic structures of muscles, 3. against the motion, the force due to the kinetic friction, 4. upwards, the leg pushing force. Using these forces the equation of motion for the vertical movement of the subject's center of mass during the ground contact was derived as follows:

$$m\frac{d^2x}{dt^2} + \lambda\frac{dx}{dt} + kx = mg \tag{24}$$

where m is subject's moving mass, $\lambda\, dx/dt$ is liquid friction of muscle's internal structure, λ is linear viscous damping coefficient, kx is the elastic force of the muscles´ internal structure, mg is the force of gravity, k is the stiffness coefficient due to tendons and muscle structures (assumed to be constant), x is the vertical displacement of the center of gravity during the ground contact, and t is time. A schematic illustration for this model is presented in Figure 12. The equation of motion can be written as

$$\frac{d^2x}{dt^2} + 2\gamma\frac{dx}{dt} + \omega_0^2 x - g = 0 \tag{25}$$

where is $2\gamma = \lambda/m$ and $\omega_0{}^2 = k/m$ the natural angular velocity without damping. Solution of this equation suitable for jumping on one leg is

$$x = A e^{-\gamma t}\cos(\omega t + \delta) + \frac{g}{\omega_0^2} \tag{26}$$

For the integration constant δ is taken $\pi/2$ and the solution is

$$x = A e^{-\gamma t}\sin(\omega t) + \frac{g}{\omega_0^2} \tag{27}$$

where

$$\omega = \sqrt{\omega_0^2 - \gamma^2} \tag{28}$$

Equations 25 – 28 have been adopted from Alonso & Finn [1980], and have been applied into this model of leg movement in one and two legged jumping.

The time derivative of the path of motion Equation (27) is velocity

$$V = \frac{dx}{dt} = A e^{-\gamma t}\left[-\gamma\sin(\omega t) + \omega\cos(\omega t)\right] \tag{29}$$

The time derivative of the velocity in Equation (29) is acceleration, and multiplying it by the moving mass yields the force acting at the center of mass

$$\frac{d^2x}{dt^2} = A e^{-\gamma t}\left[\left(\gamma^2 - \omega^2\right)\sin(\omega t) - 2\gamma\omega\cos(\omega t)\right] \tag{30}$$

$$F = m\,A\,e^{-\gamma t}\left[\left(\gamma^2 - \omega^2\right)\sin(\omega t) - 2\gamma\,\omega\,\cos(\omega t)\right] \tag{31}$$

By substituting the path of motion Equation (27), velocity Equation (29) and acceleration Equation (30) into the differential equation (25) it can be seen that Equation (27) is the solution to Equation (25).

$$\frac{d^2x}{dt^2} + 2\gamma\frac{dx}{dt} + \omega_0^2 x - g = 0$$

$$A e^{-\gamma t}\left[\left(\gamma^2 - \omega^2\right)\sin(\omega t) - 2\gamma\,\omega\,\cos(\omega t)\right] + 2\gamma\,A e^{-\gamma t}\left[-\gamma\sin(\omega t) + \omega\cos(\omega t)\right]$$
$$+ \omega_0^2\left[A e^{-\gamma t}\sin(\omega t) + \frac{g}{\omega_0^2}\right] - g = 0$$

$$A e^{-\gamma t}\left[\left(\gamma^2 - \omega^2\right)\sin(\omega t) - 2\gamma\,\omega\,\cos(\omega t) - 2\gamma^2\sin(\omega t) + 2\gamma\,\omega\cos(\omega t) + \omega_0^2\sin(\omega t)\right] = 0$$
$$A e^{-\gamma t}\left[\gamma^2\sin(\omega t) - \omega^2\sin(\omega t) - 2\gamma^2\sin(\omega t) + \omega_0^2\sin(\omega t)\right] = 0$$
$$\gamma^2 - \omega^2 - 2\gamma^2 + \omega_0^2 = 0$$
$$\omega = \sqrt{\omega_0^2 - \gamma^2}$$

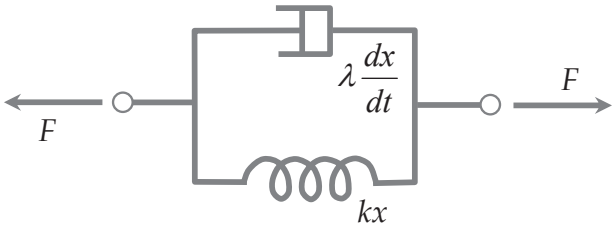

FIGURE 12 A model of the forces acting during the ground contact (without pushing force). The force *F* acts on the distal and proximal joints of the lower limbs (based on McMahon 1984).

4.3.2 The effect of the pushing force on the model

The model of actual leg movement was obtained by adding the leg's muscle force to the model of leg movement without pushing force (Fig. 13). The leg's muscle force is a determining factor within the oscillatory motion during ground contact. It can be assumed that the time of oscillation (period), the frequency and the angular velocity of the Equation of path of motion (Eq. 27) is determined by that force. The leg pushing force $F_j(t)$ was added to the basic model of leg movement Eq. (24).

$$m\frac{d^2x}{dt^2} + \lambda\frac{dx}{dt} + kx = mg - F_j(t) \tag{32}$$

By making substitutions $2\gamma = \lambda/m$ and $\omega_0^2 = k/m$ the equation can be written in the form

$$\frac{d^2x}{dt^2} + 2\gamma\frac{dx}{dt} + \omega_0^2 x - g + \frac{F_j(t)}{m} = 0 \tag{33}$$

A suitable solution for this differential equation fit for jumping movements is

$$x = Ae^{\gamma t}\sin(\omega t) + \frac{g}{\omega_0^2} \tag{34}$$

The time derivative of Eq. (34) is velocity

$$V = \frac{dx}{dt} = Ae^{\gamma t}\left[\gamma\sin(\omega t) + \omega\cos(\omega t)\right] \tag{35}$$

The time derivative of Equation (35) is acceleration, and multiplying it by the moving mass yields the force acting at the center of mass

$$\frac{d^2x}{dt^2} = Ae^{\gamma t}\left[\left(\gamma^2 - \omega^2\right)\sin(\omega t) + 2\gamma\omega\cos(\omega t)\right] \tag{36}$$

$$F = mAe^{\gamma t}\left[\left(\gamma^2 - \omega^2\right)\sin(\omega t) + 2\gamma\omega\cos(\omega t)\right] \tag{37}$$

By substituting Equation (34), (35) and (36) in the differential Equation (33), the leg pushing force is obtained

$$F_j(t) = -mAe^{\gamma t}\left[\left(3\gamma^2 - \omega^2 + \omega_0^2\right)\sin(\omega t) + 4\gamma\omega\cos(\omega t)\right] \tag{38}$$

If the coefficient $\gamma = 0$ the path of the center of gravity becomes sine-form motion

$$x = A\sin(\omega t). \tag{39}$$

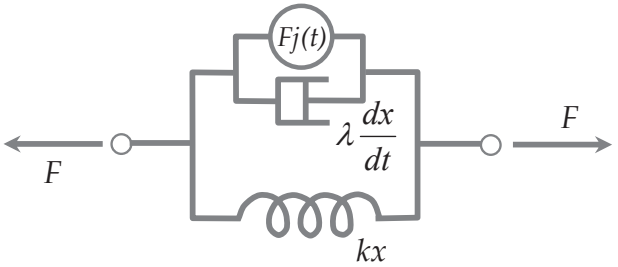

FIGURE 13 A model for the total leg forces acting during the ground contact. *F* is composed of the accelerating leg-pushing force *Fj*(*t*), elastic force of leg tendons *k* *x* and force of leg's internal friction λ d*x*/d*t* (based on McMahon 1984).

4.3.3 How to fit theoretical displacement curve into measured values

In Figure 14 there is a measured displacement curve of a jump on two legs, which is indicated by the dots of measured displacements. At the point of the

intersection of the measured displacement curve and time axis the time is t = 0.247 s. This time corresponds to the angle π in the fitting curve of the measured displacement curve. The angular velocity of the measured displacement curve is then $\omega = \pi/t = 3.1416/0.247 = 12.7$ 1/s. In order to find the curve fitting for this measured displacement curve, at first a sine wave shaped curve fitting was tested $x = A\sin(\omega t)$. This sine wave fitting has the same amplitude than the measured displacement curve A = 0.137 m. By drawing the theoretical sine wave curve on the measured dots of the displacement curve it can be seen that the theoretical sine wave fitting matches the measured displacement curve.

In Figure 14 damping $x = Ae^{-\gamma t}\sin(\omega t)$ and strengthening $x = Ae^{\gamma t}\sin(\omega t)$ oscillatory motions are also drawn. If the measured displacement curve does not fit to the sine wave curve, by comparing these curves it can be seen, is it damping or strengthening oscillatory motion or is it something else. Then the proper fitting for the measured displacement curve can be found by an iteration process. The fittings of the measured displacement curves are usually sine wave, damping or strengthening wave shaped. However, other forms of displacement curves are also possible. In the shot put study of Rahikainen and Luhtanen (2003) the form of the displacement curve in a longer put was $x = Ae^{\gamma t}\sin(\omega t) + g/\omega_0^2$ while in Figure 24 the beginning of the curve is different. In these cases curve fitting requires excess work.

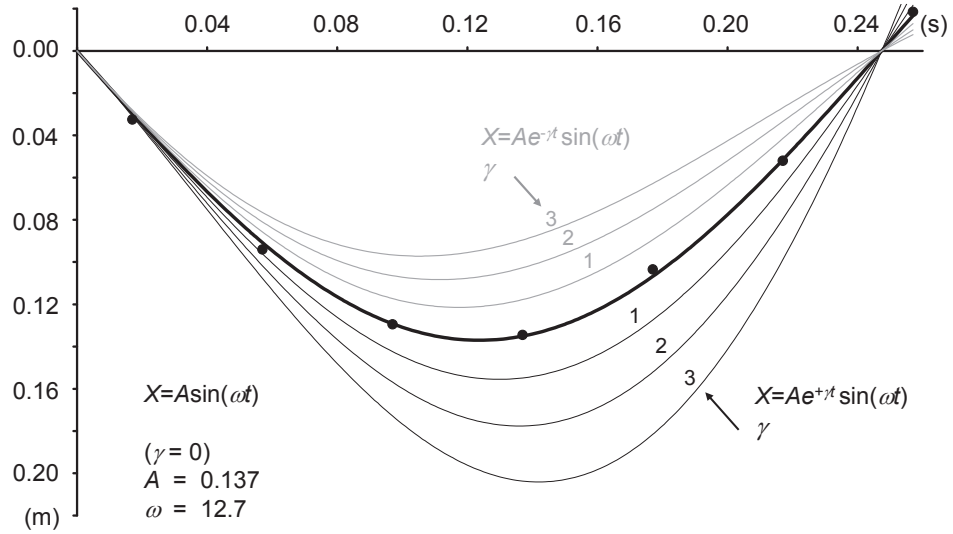

FIGURE 14 Experimental results of vertical displacement of center of mass in one jump on two legs with the corresponding curve fitting of Equation (39). Strengthening oscillatory motion (lower curves) and damped oscillatory motion (upper curves) are also shown. The zero-point indicates the beginning of the ground contact.

4.4 Leg movement in shot put

In the previous study of Rahikainen and Luhtanen (2003) the path of the athlete's CoM was assumed to correspond to the shot movement. This assumption is incorrect and therefore, in the present study, the corresponding movement of the CoM was set to only half of the movement of the shot by multiplying the previous equations by factor of ½. This was inferred from the measured ground reaction forces. Vertical displacement of the shot putter's CoM for the 20.90 m put (Rahikainen and Luhtanen 2003) was calculated from the Equation (34)

$$x = -\frac{1}{2} A e^{\gamma t} \sin(\omega t) + \frac{g}{\omega_0^2},$$

A=0.065 m, γ = 4 s^{-1}, ω = 14.2 s^{-1}, $\frac{g}{\omega_0^2}$ =0.045 m

and for the 19.47 m put (Fig. 4, zero time point shifted)

$$x = -\frac{1}{2} A e^{\gamma\left(t - 0.06\right)} \sin\left(\omega\left(t - 0.06\right)\right),$$

A=0.065 m, γ = 4 s^{-1}, ω = 10.0 s^{-1}.

Vertical velocity V of the shot putter's CoM in 20.90 and 19.47 m puts was calculated from Equation (35) and multiplied by -½, respectively

$$V = -\frac{1}{2} A e^{\gamma t} \left[\gamma \sin(\omega t) + \omega \cos(\omega t)\right],$$

A=0.065 m, γ = 4 s^{-1}, ω = 14.2 s^{-1}

$$V = -\frac{1}{2} A e^{\gamma\left(t - 0.06\right)} \left[\gamma \sin\left(\omega\left(t - 0.06\right)\right) + \omega \cos\left(\omega\left(t - 0.06\right)\right)\right],$$

A=0.065 m, γ = 4 s^{-1}, ω = 10.0 s^{-1}.

The force F acting on the shot putter's CoM in 20.90 and 19.47 m puts was calculated from Equation (37) and multiplied by -½, respectively. The moving mass m 124 kg was estimated from the shot putter's mass 131.6 kg

$$F = -\frac{1}{2} m A e^{\gamma t} \left[\left(\gamma^2 - \omega^2\right) \sin(\omega t) + 2\gamma\omega \cos(\omega t)\right]$$

A=0.065 m, γ = 4 s^{-1}, ω = 14.2 s^{-1}, m = 124 kg

$$F = -\frac{1}{2} m A e^{\gamma\left(t - 0.06\right)} \left[\left(\gamma^2 - \omega^2\right) \sin\left(\omega\left(t - 0.06\right)\right) + 2\gamma\omega \cos\left(\omega\left(t - 0.06\right)\right)\right]$$

A=0.065 m, γ = 4 s^{-1}, ω = 10.0 s^{-1}, m = 124 kg.

5 RESULTS

5.1 Arm movement

Arm rotation experiments recorded by the camera system of Rahikainen (1990) are presented in Figures 15 - 18 and experiments with the Vicon motion analysis system in Figure 19. The theoretical angular velocity curves in Figures 15 - 18 are marked with dashed lines and they coincide with the measured angular velocity curves (solid lines) between the points A – B, where movement proceeds at constant power. Initially, movement proceeds at constant acceleration, then liquid friction becomes effective and acceleration decreases just before the section A – B (constant power), which is finally followed by stopping of the movement. In general, the sections A – B were long enough to verify the existence of the constant power model. The measurements in Figure 19 with subject S3, made by the Vicon motion analysis system, did not have a clear section of constant acceleration at the beginning of the movement. High oscillation in that section turned it indefinite. In the elbow extension, the oscillation was weak and the usual constant acceleration section was distinguished at the movement initiation. It also seemed that the constant acceleration section in Figure 17 had a similar oscillation as in Figure 19. Measured values of one forearm extension (rotation downwards) can be seen in table 3.

The measured data in Figures 15 - 19 have been smoothed by the 6th order polynomial curve fitting. The used friction coefficient values C varied between 2.8 – 3.1 $\mathrm{kgm^2/s}$ in forearm rotations (elbow extension and flexion) and between 3.6 – 3.8 $\mathrm{kgm^2/s}$ in whole arm rotations (shoulder extension and flexion). The maximum angular velocities ranged from 13.7 rad/s (shoulder flexion) to 24.8 rad/s (elbow extension). The effect of the ratio of power and friction coefficient P/C on the progress of angular velocity is clearly seen in Figures 15 - 19. In Figure 15, the typical variation in consecutive trials of the same subject is seen. The effect of gravity can be seen in Figures 17 and 18 as the shoulder extension has larger angular velocity than the shoulder flexion.

TABLE 3 Measured values of the forearm rotation downwards. Angular velocity is calculated with Equation 1 and the angular acceleration according to Figure 20. A - B and C - D represent the estimated phases where the movement proceeds at constant acceleration and constant power, respectively.

T (ms)		$\Delta\varphi$ (rad)	$\Sigma\Delta\varphi$ (rad)	$\dot{\varphi}(rad/s)$	$\ddot{\varphi}(rad/s^2)$
20		0.055	0.06	2.75	114
40	A	0.110	0.17	5.50	155
60		0.170	0.35	8.52	155
80	B	0.231	0.59	11.54	155
	C				
100		0.291	0.89	14.56	128
120		0.319	1.22	15.93	72.5
140	D	0.329	1.56	16.48	12
160		0.319	1.89	15.93	-56

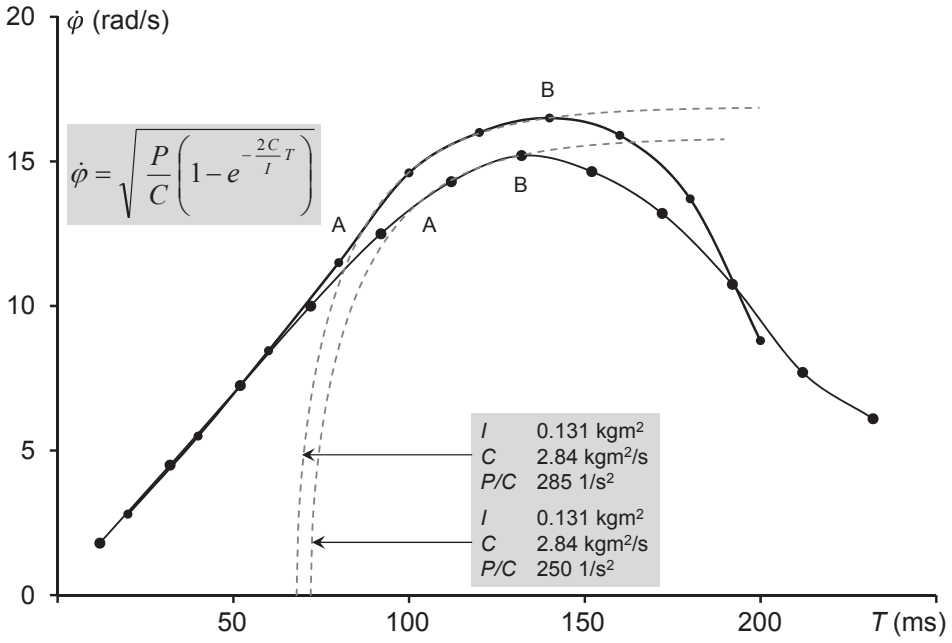

FIGURE 15 Two elbow extensions (subject S1). The theoretical angular velocity curve (dashed line) coincides with the measured curve (solid line) between A and B.

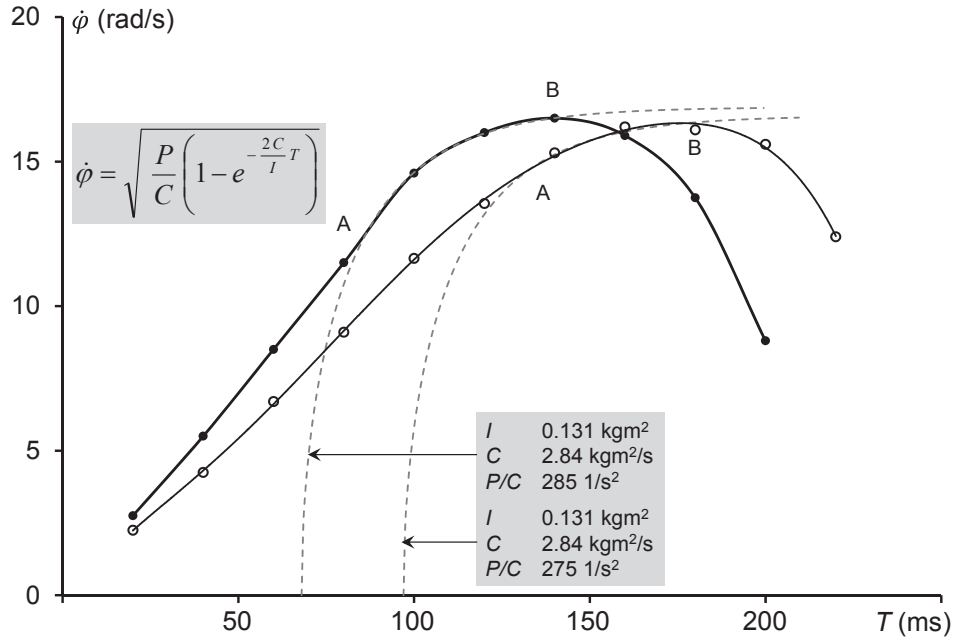

FIGURE 16 Elbow extension (filled circles) and elbow flexion (open circles) of subject S1. The theoretical angular velocity curve (dashed line) coincides with the measured curve (solid line) between A and B.

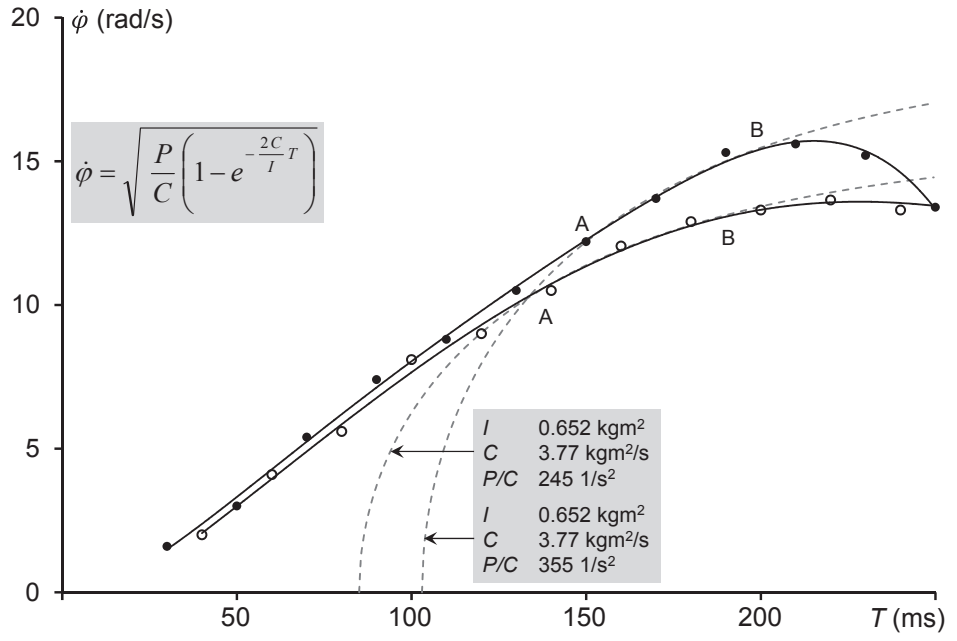

FIGURE 17 Shoulder extension (filled circles) and shoulder flexion (open circles) of subject S1. The theoretical angular velocity curve (dashed line) coincides with the measured curve (solid line) between A and B.

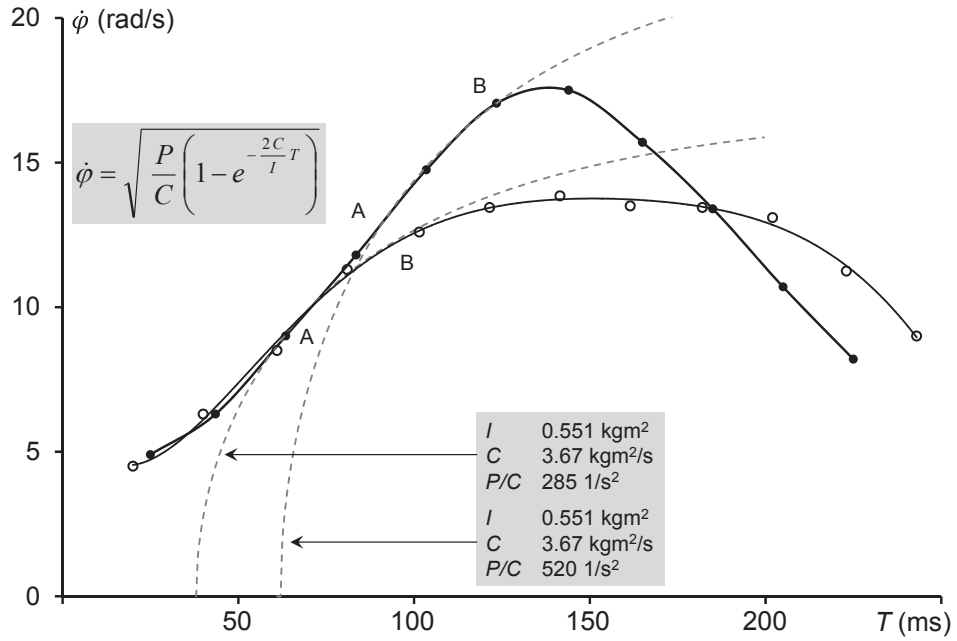

FIGURE 18 Shoulder extension (filled circles) and shoulder flexion (open circles) of subject S2. The theoretical angular velocity curve (dashed line) coincides with the measured curve (solid line) between A and B.

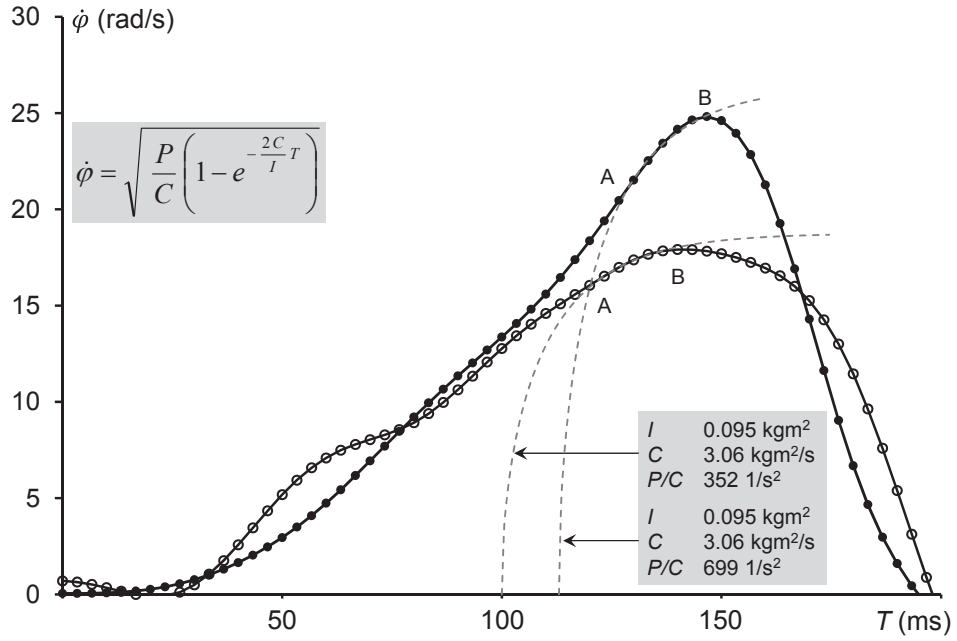

FIGURE 19 Elbow extension (filled circles) and elbow flexion (open circles) of subject S3. The theoretical angular velocity curve (dashed line) coincides with the measured curve (solid line) between A and B. The elbow joint angles for maximum angular velocity were 123° (extension) and 81° (flexion).

Validity and accuracy of results

In order to confirm the accuracy of results, power ***P*** was calculated by comparing two independent calculation methods. Equation 12

$$I\,\dot{\varphi}\,\frac{d\dot{\varphi}}{d\,T} = P - C\,\dot{\varphi}^2 \quad \Rightarrow \quad P = I\,\dot{\varphi}\,\frac{d\,\dot{\varphi}}{dT} + C\,\dot{\varphi} \tag{40}$$

yields one power value (***P*1**) and the other power value (***P*2**) comes from the curve fitting used in upper curves of Figure 15 and Figure 17 (***P*/*C***).

In forearm rotation downwards the angular acceleration at point T = 0.10 s, $\dot{\varphi}$ = 14.5 rad/s was calculated by using the tangent of the angular velocity curve (Fig. 20). The tangent point can be found because the tangent has only one point on the curve, otherwise there are two intersection points. The value of angular acceleration was calculated according to

$$\frac{d\dot{\varphi}}{d\,T} = 14.5/0.12\ \ 1/\mathrm{s}^2 = 121\ \ 1/\mathrm{s}^2$$

This value of angular velocity derivative can also be calculated using Equation (18). The time and angular velocity of this equation corresponding to the measured angular velocity curve time 0.10 s and velocity 14.5 rad/s was calculated with Equation (16) to be time 0.031s and velocity 14.5 rad/s. The derivative of Equation (18)

$$\dot{\varphi} = \sqrt{\frac{P}{C}\left(1 - e^{-\frac{2C}{I}T}\right)}\ , \qquad X_1 = 1 - e^{\frac{-2C}{I}T}\ , \ X_2 = \frac{-2C}{I}T$$

$$\frac{d\,\dot{\varphi}}{d\,T} = \frac{d\dot{\varphi}}{d\,X_1}\cdot\frac{d\,X_1}{d\,X_2}\cdot\frac{d\,X_2}{dT} = \frac{\sqrt{\frac{P\,C}{I^2}}\,e^{\frac{-2C}{I}T}}{\sqrt{1 - e^{\frac{-2C}{I}T}}} \tag{41}$$

Substituting in this equation T = 0.031 s, I = 0.131 kgm^2, C = 2.84 kgm^2/s and P = 809 W, the value of angular acceleration of 111 1/s^2 was obtained. Moment arm of gravitational force is so short at forearm rotation that the power generation of gravitational force has no significance. In whole arm rotation downwards and upwards the effect of gravitational force is within power P. The accuracy of results is presented in Table 4.

TABLE 4 Determination of accuracy of the results. The accuracy was obtained as a difference between the power values P_1 (from Eq. 40) and P_2 (from the curve fitting in upper curves of Fig. 15 and in Fig. 17).

	Forearm rotation	**Whole arm rotation**	
	down (Fig. 15)	**down (Fig. 17)**	**up (Fig. 17)**
Time (T)	0.100 s	0.160 s	0.144 s
Angular velocity $\left(\dot{\varphi}\right)$	14.5 rad/s	13.1 rad/s	11 rad/s
Angular acceleration $\left(\frac{d\dot{\varphi}}{dT}\right)$	14.5 / 0.12 1/s^2	13.1 / 0.168 1/s^2	11 / 0.17 1/s^2
Moment of inertia (I)	0.131 kgm^2	0.652 kgm^2	0.652 kgm^2
Power into acceleration $\left(I\dot{\varphi}\frac{d\dot{\varphi}}{dT}\right)$	229.5 W	666 W	464.1 W
Coefficient of friction (C)	2.84 kgm^2/s	3.77 kgm^2/s	3.77 kgm^2/s
Power into friction $\left(C\dot{\varphi}^2\right)$	597 W	647 W	456 W
Muscle Power (P_1)	**826 W**	**1312 W**	**920 W**
Power / Coefficient of friction (P/C)	285 1/s^2	355 1/s^2	245 1/s^2
Muscle Power (P_2)	**809 W**	**1338 W**	**924 W**
Error $\frac{P_1 - P_2}{0.5(P_1 + P_2)}100$	2.07 %	1.96 %	0.43 %

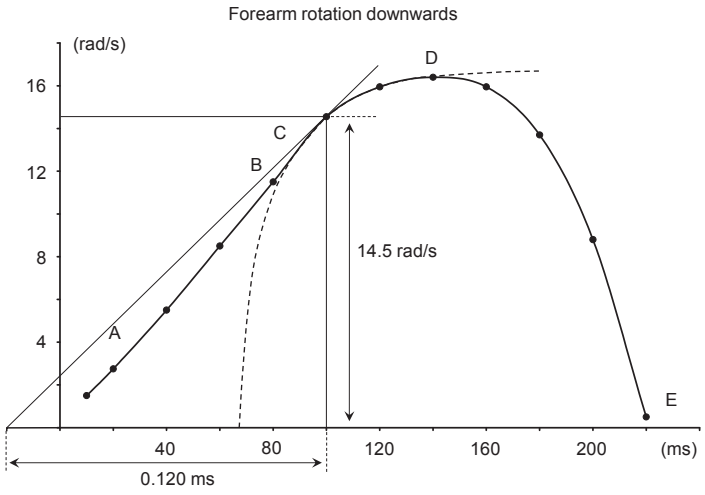

FIGURE 20 Calculation of angular acceleration at point (T = 0.10 s, $\dot{\varphi}$ = 14.5 rad/s), where the theoretical angular velocity curve (dashed line) coincides with the measured angular velocity curve (points) between C – D.

5.2 Leg movement in one- and two legged jumping

Table 5 presents the measured vertical displacement values of the body center of mass during the ground contact of four jumps performed by subject S1. Columns A and B show the results of two jumps on one leg and the corresponding curve fittings of the model are presented in Figure 22. Equation (27) has negative γ-values, which indicate that the paths are damped oscillatory motions [Hypothesis 3]. The constants of Equation (27) in the upper curve are: γ = 1.5 1/s, A = 0.0967 m and ω = 9.6 rad/s, and in the lower curve are: γ = 1.2 1/s, A = 0.126 m and ω = 9.6 rad/s. The angular frequency of both curves is the same ω = 9.6 rad/s and the γ-values are also very close to each other (γ = 1.2 - 1.5 1/s). It can be seen that immediately after the touchdown the theoretical values (based on the equation) differ slightly from the measured vertical displacement values.

Columns C and D in Table 5 present the results of the jumps on two legs and their curve fittings can be seen in Figures 14 and 23. In Figure 14 the fitting of Equation (39) to the measured values shows that the path of the center of gravity is a sine-formed motion [Hypothesis 5]. The constants of the curve are γ = 0, A = 0.137 m and ω = 12.7 rad/s. The difference between the measured and theoretical values observed at the beginning of the ground contact in the jump on one leg (Fig. 22) was not found in the jump on two legs (Figs 14 and 23). Mismatch between the equations, Equation (27), [Hypothesis 3] and Eq. (34), [Hypothesis 4] and the measured values, was also demonstrated with different γ-values in Figure 14. The jump on two legs (Fig. 23) fitted well with the measured values with Equation (27) negative γ-value of 0.6 1/s (A = 0.155 m and ω = 12.4 rad/s). In this case the path of the center of gravity is damped oscillatory motion [Hypothesis 3]. The angular frequency ω (12.4 rad/s) was very close to the jump in Figure 12 and thus they can be considered to be of same magnitude.

A jump on two legs (typical countermovement jump, CMJ) was performed by subject S3 (Figs. 8 and 24). The jump was analyzed by the Vicon motion analysis system with 8 cameras and 300 Hz frame rate. The result of the experiment was a strengthening oscillatory motion $x = Ae^{\gamma t}\sin(\omega t)$. The constants of equation were γ = 0.6 1/s, A =0.4 m, ω = 5.45 rad/s.

TABLE 5 Vertical displacement of the path of the CoM from the beginning of the ground contact in different jumps.

Jump on one leg			
A		**B**	
Time t (s)	Vertical Displacement x (m)	Time t (s)	Vertical Displacement x (m)
0.014	0.0145	0.017	0.0250
0.054	0.0475	0.057	0.0660
0.094	0.0675	0.097	0.0910
0.134	0.0765	0.137	0.1040
0.174	0.0740	0.177	0.1000
0.214	0.0635	0.217	0.0850
0.254	0.0430	0.257	0.0530
Jump on two legs			
C		**D**	
0.017	0.0325	0.018	0.0335
0.057	0.0940	0.058	0.0990
0.097	0.1295	0.098	0.1390
0.137	0.1345	0.138	0.1405
0.177	0.1035	0.178	0.1080
0.217	0.0520	0.218	0.0560
0.257	0.0185	0.258	0.0070

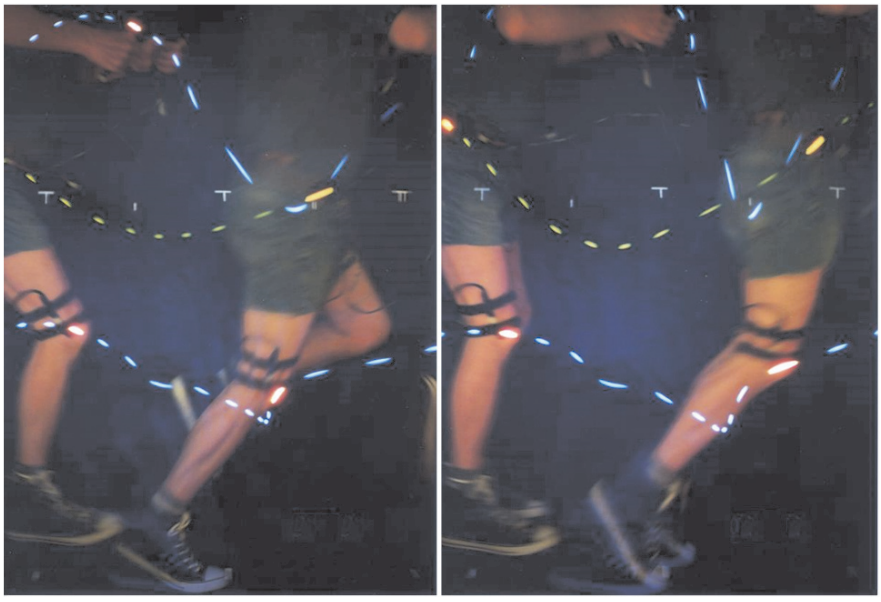

FIGURE 21 Experiments of the jumps on one leg (left) and on two legs (right).

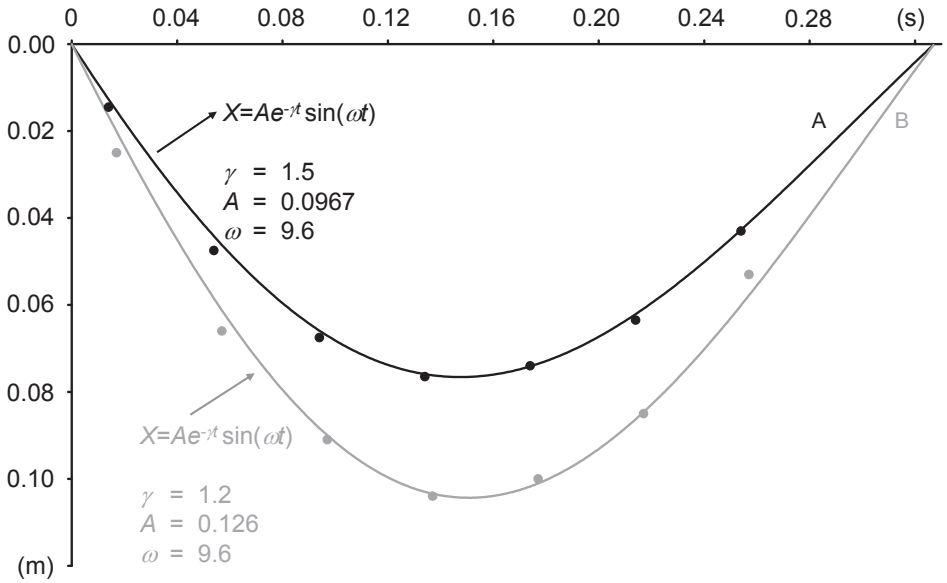

FIGURE 22 Experimental results (dots) of the vertical displacement (m) of the CoM in two jumps on one leg with the corresponding curve fittings (solid lines) of Equation (27) $x = A e^{-\gamma t} \sin(\omega t)$. Zero-point indicates the beginning of the ground contact.

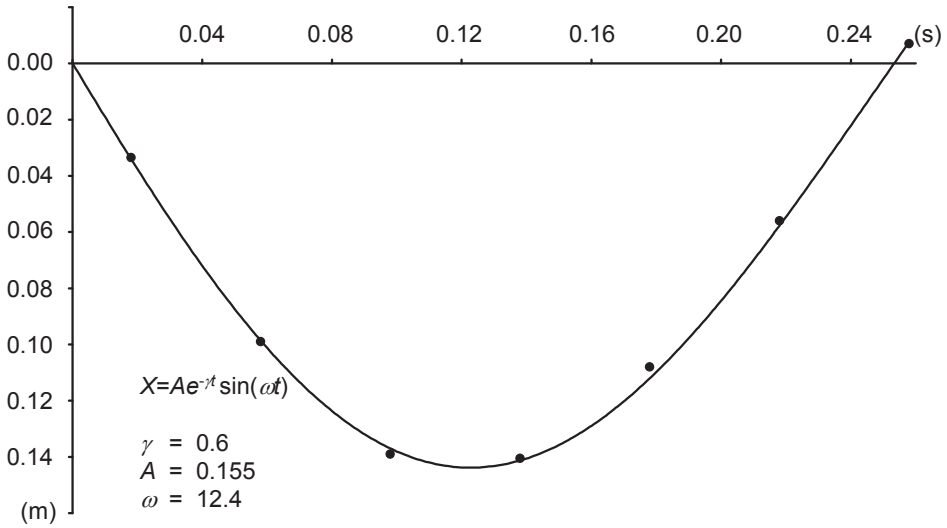

FIGURE 23 Experimental results (dots) of the vertical displacement of the CoM in jump on two legs with the corresponding curve fitting (solid line) of Equation (27) $x = A e^{-\gamma t} \sin(\omega t)$. Zero-point indicates the beginning of the ground contact.

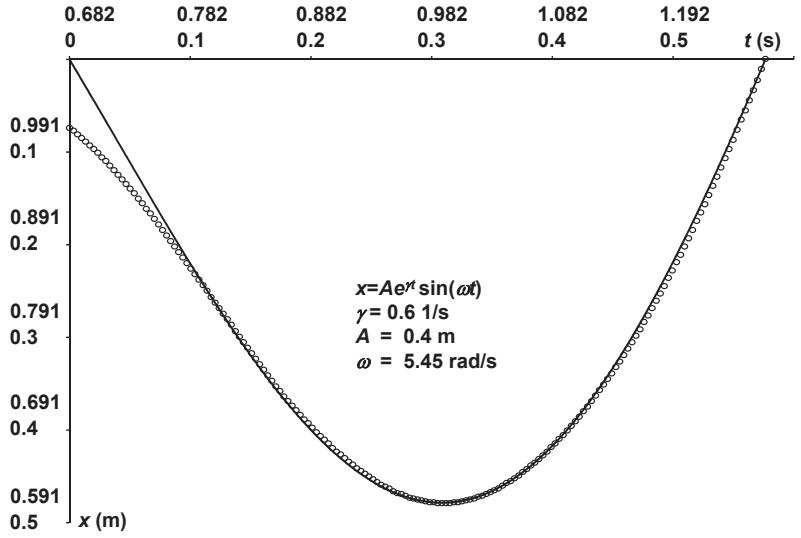

FIGURE 24 Experimental results (dots) of vertical displacement of the CoM in jump on two legs (CMJ) with the corresponding curve fitting of Equation (34) [Hypothesis 4]. The upper coordinates refer to Figure 8 and lower to Equation (34) $x = A e^{\gamma t} \sin(\omega t)$.

5.3 Leg movement in shot put

In Figures 25, 26, and 27 the displacements, velocities, and forces acting at the shot putters center of mass of 19.47 m put (dashed line) and 20.90 m put (solid line) are presented. The amplitude of the displacement curve of the 20.90 m put was larger than that of the 19.47 m put (Fig 25). The vertical velocity of 20.90 m put was 0.25 m/s higher than that of the 19.47 m put at the end of leg pushing phase (time 0.24 s, Fig. 26). The shot putter's mass was 131.6 kg and the moving mass was estimated to be 124 kg. In 20.90 m put the maximum force acting at the center of shot putter's mass was 1650 N and in the 19.47 m put 1250 N. Ground reaction force (GRF) can be calculated by adding the force acting at the center of shot putter's mass and the shot putter's gravitational force (1290 N). The values of the calculated maximum ground reaction forces are in good agreement with the measured GRFs of the same athlete in different occasion (Fig. 28).

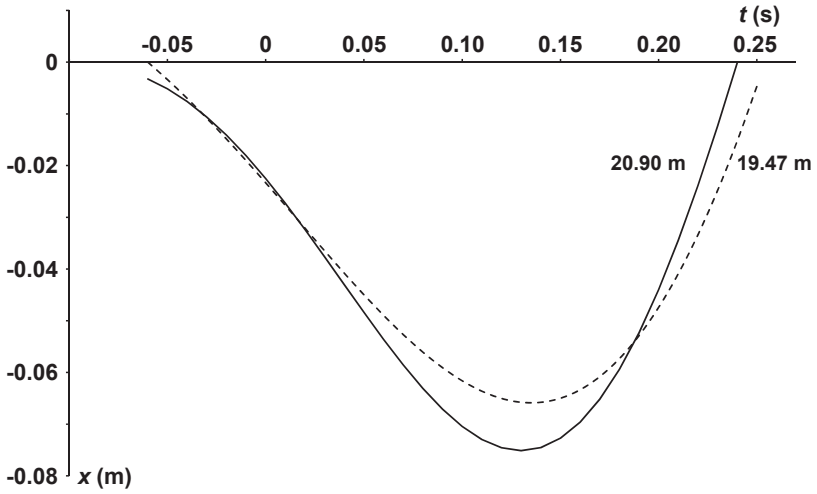

FIGURE 25 Vertical displacement of the shot putter's center of mass for two puts with different distance.

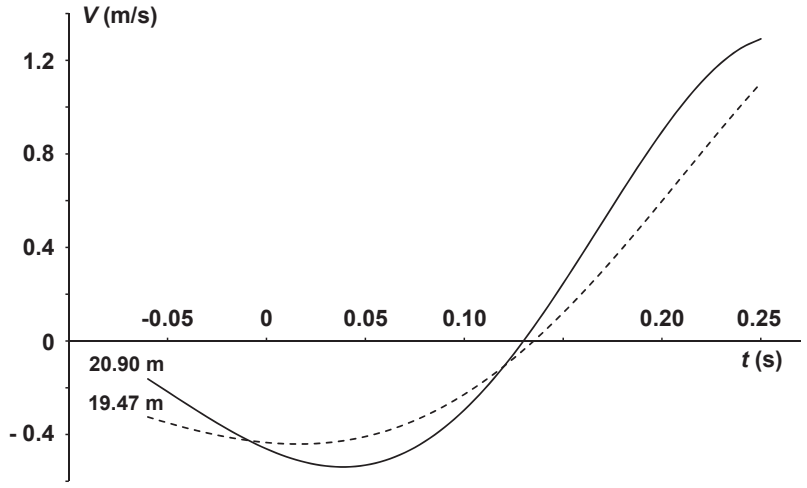

FIGURE 26 Vertical velocity of the shot putter's center of mass V calculated from Equation (35) for two puts with different distance.

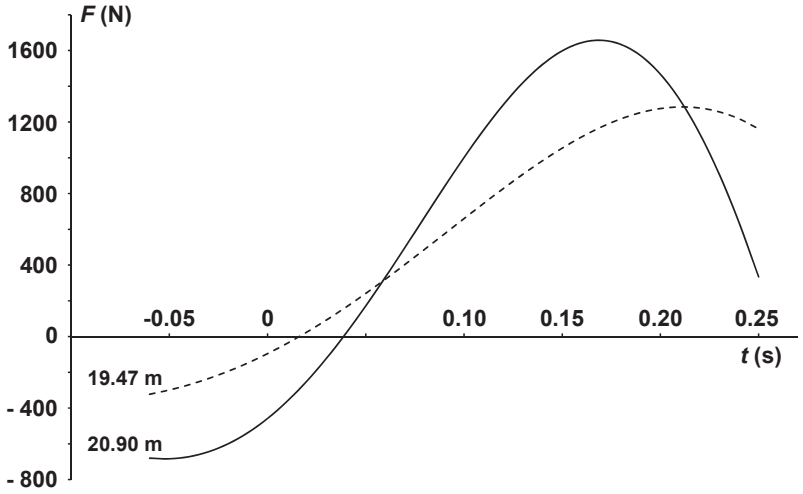

FIGURE 27 The force F acting on the shot putter's center of mass calculated from Equation (37) for two puts with different distance.

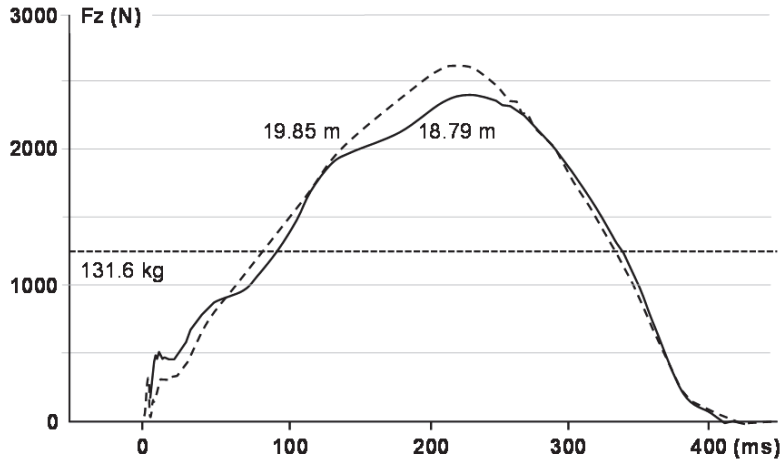

FIGURE 28 Measured ground reaction forces of two shot puts (19.85 and 18.79 m) of same athlete (unpublished data).

6 DISCUSSION

The original purpose of this thesis was to study how well the models of arm and leg movements match real experiments. In arm movement with maximum speed the hypothesis of constant power at the state of high speed [hypothesis 2] succeeded well, but the hypothesis of constant moment at the state of high rotational acceleration [hypothesis 1] was problematic. Leg movements in the present study had three hypotheses: damped oscillatory motion, strengthening oscillatory motion and sine form motion. In most experiments these hypotheses were fulfilled with adequate accuracy.

6.1 Arm movement

Within the present study ten elbow and shoulder rotations of three different subjects were analyzed and the constant power model for maximum velocity arm rotations was verified. Matched range of measured and theoretical angular velocity was not long, but enough to verify the existence of a constant power model. The range was short because the arm rotations were performed with maximum velocity. If there were a constant force resisting the arm rotation movement, speed of motion would be slower and the velocity – time curve of the measured arm rotation would continue the theoretical constant power curve (dashed lines, e.g. Fig 15) and it will level horizontally at the velocity of Hill's equation. In that case constant force in arm rotational movement corresponds to a constant velocity in the same manner as a force corresponds to velocity in Hill's equation

After the initiation of arm rotation, the movement proceeds at a state of low speed and high acceleration without external load. In this phase of movement it is assumed (hypothesis) that the movement proceeds at a constant maximum muscular moment. Measurements of the rotational movements show that the movement proceeds at constant angular acceleration. Therefore, we can

conclude that the torque accelerating the movement, or the right side of Equation (12), is constant.

$$I \frac{d\dot{\varphi}}{dT} = \frac{P}{\dot{\varphi}} - C\dot{\varphi}$$

Torque generated by the maximum muscular moment is $P/\dot{\varphi}$ and according to the hypothesis, it is constant. The moment generated by frictional force $-C\dot{\varphi}$ is not constant (because of the term of velocity) and, therefore, this hypothesis is not fulfilled. However, the finding "movement proceeds at constant acceleration" is interesting and should be studied more closely. In Equation (12) kinetic friction was assumed to be directly proportional to the velocity at the beginning of the movement. This is a new hypothesis, which is not necessarily true. It is possible that kinetic friction at small velocities is constant and at high velocities is directly proportional to velocity. This leads to a constant torque accelerating the movement at the beginning of movement. It is also possible that the constant acceleration phase of the movement is a matter of human ability to learn effective modes of motion than a direct cause of natural laws. It may be that the human nervous system is in control of the rotational moment accelerating arm rotational movement. One question of the present study was: How does Hill's equation function in the rotational movement of the arm? Experiments of the present study do not answer this question. To solve this question the experiments of arm rotations with a resisting constant force are needed.

After the phase of constant angular acceleration, the movement proceeds at a high speed and with low acceleration without external load. It is assumed that within this phase, the movement proceeds at a constant maximum muscular power. This hypothesis seems to be true between A and B in Figures 15-19. This is the most interesting finding of the present study and further development of Hill's equation provided another kind of model of constant power (see 6.2). The experiments of the present study verified that the conclusions of the theoretically derived equation with constant maximum power were in fact in agreement with experimentally measured results. As Hill's equation is also a constant power model it can be considered the same as the model of this study. Hill's force-velocity relationship was created by experiments in which the velocity of muscle contraction was measured against a specific constant force. The experiments of Hill's equation naturally started at zero velocity and continued in the same manner as the experiments of the present study through all the phases. Because of the external load, the experiments of Hill's equation did have slower velocities and, therefore, it was possible to reach maximum velocity within the measuring accuracy. The measurements of the present study were made without external load and none of them reached the maximum theoretical velocity of Equation (18).

6.2 Solution of Hill's force – velocity equation

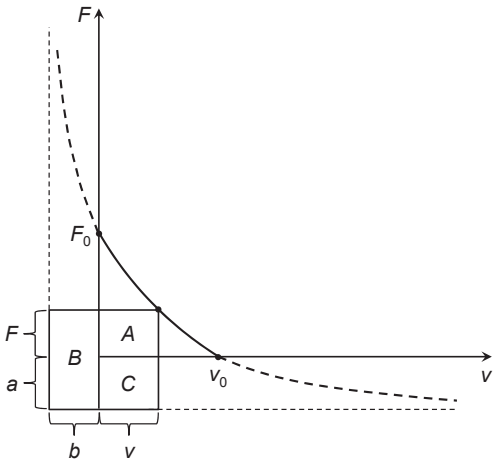

FIGURE 29 Hill's force-velocity relationship presented with asymptotes (dashed lines) and three rectangles of power. In traditional presentation of hyperbola a and b are negative, but here they refer to the positive constant terms of Hill' equation. Hill's equations, $(F + a)\ (v + b)$ = constant, implies that the area of rectangle $A + B + C$ is constant.

The results of Hill's experiments could be transformed into a hyperbola equation describing the force-velocity dependence of the movement. Figure 29 represents a further development of Hill's force-velocity relationship. The force – velocity axes are shown and also the asymptotes have been drawn as dashed lines. Hill's equation, $(F + a)\ (v + b)$ = constant, implies that the area of the rectangle $(F + a)\ (v + b)$ is constant. The total power of the muscle is comprised of three different components represented by rectangles A, B and C. The area of rectangle $A = F$ v represents the power needed from muscle against an external load (see the power curve in Fig. 1). If there is no external load, this power is consumed by acceleration. The area of rectangle $B = (F + a)\ b$ represents the power of muscle's internal loss of energy. This power creates a counter force against an external load. When the velocity is zero, this power B is highest and, therefore, it is not related to external movement. Thereafter, as velocity increases, this power initially decreases rapidly, and then power decreases more slowly at higher velocities. The area of rectangle $C = v\ a$ represents the power of friction due to the motion of the muscle – load system. Because power is force multiplied by velocity, the force of friction is a. This is not force directly proportional to velocity, generally known as liquid friction (which is the friction used in the present study), but constant force of friction, which is known as glide friction. Now we can see that there are three different states of motion: 1) the beginning of motion characterized by a state of low speed maximal acceleration without external load, then 2) as the motion continues a state of high speed,

maximal power without external load and 3) a state of maximal power with external load, which applies to Hill's equation. The maximum power is due to the fact that the transfer of energy within the muscle system must have a maximum rate and, therefore, muscles' power generation must also have a certain maximum rate. Within Hill's equation maximum power is due to the ability of muscles to lift loads, and within experiments of the present study, due to the high speed of motion.

Muscle mechanics of the present study is based on the experiments that were performed with maximum velocity and therefore the constant power phase became short. If there is a constant force resisting the motion, the motion becomes slower and it can be inferred that the time - velocity curve levels horizontally at the velocity of Hill's equation. Another kind of mechanics applies if less muscle force is used and the traditional Hill equation applies to movements that are resisted by external force. From the results of the present study it can be seen how these states of motion relate to each other and the findings enable further development of muscle mechanics in this field of modern science. The calculation methods of this study can be applied in research areas of sports and medicine.

6.3 Leg movement

The theory of leg movement is problematic. For instance, the sine-formed equation has no term of friction, but in real sine-formed leg movement there is a force of friction. Therefore the force of friction in real leg movement is canceled by muscular leg force. As a conclusion, muscular leg force is controlled by the nervous system in order to create the sine-formed leg movement. So it is probable that hypothesized models of leg motion are a matter of human ability to learn effective paths of motion. The models of leg movement are good approximations of that motion and they enhance the study of factors involved in these movements.

The Equation (27) fitted well to the jumps on one leg [Hypothesis 3] and therefore the paths of the CoM can be considered damped oscillatory motions (Fig. 22). The equation (39) fitted to the jump on two legs where the path of the CoM represents sine-formed motion [Hypothesis 5] (Fig. 14). The Equation (27) fitted also to the jump on two legs (Fig. 23), but in this case the path of motion was very similar to the sine-form motion and thus it can be considered almost the same as in Figure 14 [Hypothesis 5]. Since the total force exertion in the jump on two legs is greater than in the jump on one leg, it is possible that vertical displacement-time curve becomes a strengthening oscillatory motion (Eq. 34) [Hypothesis 4] as the leg force exertion increases. In Figure 24 there is a typical jump on two legs (CMJ) starting from zero velocity in which the path of the CoM is a strengthening oscillatory motion and in this case Hypothesis 4 receives confirmation. This theory is also supported by the above mentioned change of the model from damped oscillatory motion in the jump on one leg to

sine-formed motion in the jump on two legs. The analysis of the shot put performance yielded paths of motion similar to Equation (34). Therefore it is possible that in the case of elite athletes having strong muscles and producing high pushing forces, the path equation may be equation (34). The analyses of experiments also show that the effect of the leg-pushing force compensate the effect of the force of gravity and the force of friction. The conclusion is that the muscle force controlled by the nervous system directs the leg movement.

Immediately after the ground contact the experimental results of jumps on one leg showed slightly higher vertical displacement values of the center of mass than what were calculated with Equation (27). This may indicate that the braking phase has lower kinetic friction at the instant of impact during the jump on one leg. However, the differences were so small that Equation (27) seemed to be accurate enough for this study. This phenomenon was not observed within the experiments of jumps on two legs.

The above mentioned modeling of leg movement was also applied to the actual shot put performance of a high level athlete. The re-calculated ground reaction forces of the earlier experiment were in good agreement with the measured forces. The calculated parameters of different shot put results (19.47 m and 20.90 m), as drawn on the same figure (25-27), may give some understanding regarding how the effective path of a shot put motion is performed.

Further development of Nigg's equation for decelerated motion

The original model of Nigg (2006) examined the mechanics of the human heel. In this model the motion of the subject's mass m was decelerated by spring force kx and damping force $r\dot{x}$. The equation of motion was then derived $m\ddot{x} + r\dot{x} + k\,x = 0$ and its solution was $x(t) = A\,e^{-c\,t}$. In the case of decelerated motion the roots of the constant c are real. In the case of imaginary roots ($c = a \pm i\,b$) the solution is oscillatory motion, because $e^{-i\,b\,t} = \cos(b\,t) - i\sin(b\,t)$ (Alonso and Finn 1980) and the real part cos*(bt)* is only used. The solution is $x(t) = A\,e^{-c\,t}\cos(b\,t)$, which is the same form of equation as used in the present study.

7 MAIN FINDINGS AND CONCLUSIONS

The main findings and conclusions of the present study can be summarized as follows:

(1) It was hypothesized that movement proceeds at a constant maximum power at a certain range of velocity in arm movement, which means that power P in Equation (12) is constant. For validation of this hypothesis, the Equation (12) was solved for angular velocity-time function. The mass distribution of the arm sectors was determined using an immersion technique and the moments of inertia of the arm rotations were defined.

(2) The most interesting finding of the present study was that the theoretically derived equation with constant maximum power was in good agreement with the experimentally measured results. Another kind of constant power model was a new approach to Hill's equation. Hill's model was transformed into a constant maximum power model consisting of three different components of power: muscle power for external load, internal loss of energy, and friction.

(3) The vertical component of the path of jumping movement was presented as a mathematical model of leg movement. Equations of damped / strengthening and sine-formed oscillatory motions were derived for the path of the body center of mass (CoM) in different jumps. Depending on the type of jumping the different equations fitted the experimental results. Based on these equations, the calculated ground reaction forces (GRFs) of the shot put performance of one athlete were also in agreement with the measured GRFs. It was hypothesized that vertical displacement-time curve of leg movement may become strengthening oscillatory motion as the leg force exertion increases. It is concluded that muscular leg force is controlled by the nervous system and that the hypothesized models of leg motion are a matter of human ability to learn effective paths of motion.

YHTEENVETO (Finnish summary)

Tämän tutkimuksen tarkoituksena oli kehittää uusi mittaustuloksiin perustuva ihmisen käsi- ja jalkaliikkeiden matemaattinen malli. Tutkimuksessa mitattiin kyynärvarren ja olkavarren ojennus/koukistusliikkeitä sagittaalitasossa maksiminopeudella sekä yhden ja kahden jalan hyppyliikkeitä. Lisäksi analyyseissä käytettiin aikaisemmin tehtyjä kuulantyönnön liikemittauksia. Käsi- ja jalkaliikkeiden hypoteesien toimivuutta testattiin liikeanalyysin avulla ja näin saadun tiedon perusteella kehitettiin uusi teoria ihmisen liikkeiden lihasmekaniikasta. Ensin kehitettiin teoreettinen malli käsiliikkeelle, jonka mukaan liike etenee seuraavasti: 1) Liikkeen alku 2) Liike etenee vakiomaksimimomentilla liikkeen ensimmäisessä vaiheessa [Hypoteesi 1] 3) Liike etenee vakiomaksimitehol-la liikkeen toisessa vaiheessa [Hypoteesi 2] 4) liikkeen pysäytys.

Tutkimuksen hypoteesien testaamiseksi tehtiin seuraavat kokeet: kyynärvarren pyöritykset alaspäin (ekstensio) ja ylöspäin (fleksio) maksiminopeudella sekä koko käsivarren pyöritykset alaspäin ja ylöspäin maksiminopeudella. Käsiliikkeet kuvattiin kahdella eri järjestelmällä: 1) Erityinen liikkeen kuvaussysteemi, jossa yksi filmin kuva sisältää sarjan kuvauskohteen kuvia ja määrättyjen pisteiden liikeradat näkyvät katkoviivoina, 2) Kahdeksan kameran liikeanalyysi (Vicon), joka mahdollisti suuremman kuvausnopeuden käytön (300 Hz). Käden eri osien hitausmomentit laskettiin upotustekniikalla. Liikkeellelähdön jälkeen liike etenee hitaan nopeuden ja suuren kiihtyvyyden tilassa ilman ulkoista kuormitusta. Tässä liikkeen vaiheessa liikkeen oletettiin etenevän vakiomaksimimomentilla [Hypoteesi 1]. Mittaustulokset kuitenkin osoittivat, että liike etenee vakiokulmakiihtyvyydellä ja näin ollen pääteltiin, että tämä hypoteesi ei toteutunut. Kuitenkin havainto “liike etenee vakiokiihtyvyydellä” on mielenkiintoinen ja sitä pitäisi tutkia tarkemmin. Vakiokulmakiihtyvyys saattaa johtua hermoston liikkeen ohjauksesta. Vakiokiihtyvyys käsiliikkeen hitaan nopeuden ja suuren kiihtyvyyden vaiheessa voi myös olla oppimisprosessin tulos. Seuraavassa vaiheessa liike etenee suuren nopeuden ja pienen kiihtyvyyden tilassa. Tässä vaiheessa kokeiden analyysit osoittivat, että teoreettisesti johdettu vakiomaksimitehomalli sopi yhteen käsiliikkeiden mittaustuloksien kanssa [Hypoteesi 2].

Tässä tutkimuksessa saatuja tutkimustuloksia verrattiin myös Hillin yhtälöön luurankolihaksen voima-nopeusriippuvuudesta. Yhtälöä kehitettiin edelleen vakiomaksimitehomalliksi, joka muodostui kolmesta eri tehokomponentista (kuva 29). Nämä tehokomponentit ovat suorakaiteiden A, B ja C pinta-alat. Suorakaiteen A pinta-ala, $A = F\,v$, on teho, jolla lihas liikuttaa ulkoista kuormaa (tehokäyrä Kuvassa 1). Jos ulkoista kuormaa ei ole, niin silloin tämä teho kuluu kiihtyvyyteen. Suorakaiteen B pinta-ala, $B = (F + a)\,b$, on lihaksen sisäinen tehohäviö. Tästä tehosta tulee vastavoima liikettä vastustavalle ulkoiselle voimalle. Kun nopeus on nolla, teho B on suurin ja siten se ei liity ulkoiseen liikkeeseen. Suorakaiteen C pinta-ala, $C = v\,a$, on lihas–kuormasysteemin liikettä vastustavan kitkan teho. Lihastyön aikaansaamat kolme eri liiketilaa ovat siis seuraavat: 1) käsiliikkeen alussa liike etenee pienellä nopeudella suurella kiihtyvyydellä

ilman ulkoista kuormaa 2) kun liikkeen nopeus kasvaa se etenee suurella nopeudella pienellä kiihtyvyydellä ilman ulkoista kuormaa 3) maksimiteho ulkoisen kuorman vastustaessa liikettä soveltuu Hillin yhtälöön. Lihaksen tuottamalla teholla on maksimiarvo, koska lihasjännekompleksissa voi siirtyä vain tietty määrä energiaa aikayksikössä. Hillin yhtälössä maksimiteho tekee työtä ulkoista kuormaa vastaan ja tämän tutkimuksen käsiliikkeissä maksimiteho menee kiihdytykseen tai suureen nopeuteen ja kitkaan.

Hyppyliikkeen maakontaktin aikana hyppääjän painopiste liikkuu ensin alaspäin ja sitten ylöspäin tehden tietyn heilahdusliikkeen. Painopisteen liike voidaan esittää jalkaliikkeen matemaattisella mallilla. Tässä tutkimuksessa ensin tehtiin jalkaliikkeelle malli ilman jalan työntövoimaa ja sen jälkeen tehtiin malli, johon jalan työntövoima on lisätty. Tutkimuksen lähtökohdaksi otettiin hypoteesit, että hyppääjän vertikaalinen liike toteuttaa vaimennetun värähdysliikkeen yhtälön $x = Ae^{-\gamma t} \sin(\omega)$ tai voimistuvan värähdysliikkeen yhtälön $x = Ae^{\gamma t} \sin(\omega)$ riittävällä tarkkuudella. Tässä tutkimuksessa johdetun teorian mukainen vaimennetun heilahdusliikkeen liikerata esittää jalkaliikettä ilman jalan lihastyöntövoimaa. Tämä on teoreettinen olettamus, joka ei käytännössä pidä täysin paikkaansa. Kuitenkin oletettiin, että vaimentuvan heilahdusliikkeen yhtälö sopii jalkaliikkeen malliksi, kun liikkeessä käytetään suhteellisen pientä jalan työntövoimaa [Hypoteesi 3]. Kun lihasvoiman käyttö lisääntyy hyppyliikkeessä, niin teorian mukaan oletettiin, että liikeradan käyrä olisi voimistuvan heilahdusliikkeen muotoinen [Hypoteesi 4]. Kolmas vaihtoehto oli se, että vakio γ on nolla ja painopisteen liikeradasta tulee sini-muotoinen heilahdusliike $x = A\sin(\omega t)$ [Hypoteesi 5]. Todellisia kokeita yhden ja kahden jalan hyppyliikkeistä tehtiin ja analysoitiin niin, että tutkimuksen hypoteesien toimivuus voitiin todentaa. Siinä esitettiin seuraavat kysymykset: Onko mahdollista sovittaa riittävällä tarkkuudella vaimenevan heilahdusliikkeen yhtälö [Hypoteesi 3] tai voimistuvan heilahdusliikkeen yhtälö [Hypoteesi 4] tai sini-muotoinen yhtälö [Hypoteesi 5] painopisteen mitattuun vertikaaliseen siirtymä-aika käyrään. Vaimenevan heilahdusliikkeen yhtälö ja sini-muotoisen liikkeen yhtälö [Hypoteesi 3] ja [Hypoteesi 5] sopivat hyvin yhteen yhden ja kahden jalan hypyn painopisteen mitattuun liikerataan. Voimistuvan heilahdusliikkeen yhtälö [Hypoteesi 4] sopi nolla-nopeudesta lähtevään kahden jalan hyppyyn ja myös kuulantyönnön jalkatyöntövaiheeseen. Kokeiden analyysit osoittivat, että jalan lihasvoiman käyttö voi kompensoida painovoiman ja kitkavoiman vaikutuksen. Johtopäätöksenä voidaan todeta, että hermosto ohjaa jalan lihasvoiman käyttöä mahdollisimman tehokkaaseen muotoon. Yllä mainittua mallia sovellettiin myös kuulantyönnön jalkaliikkeeseen.

REFERENCES

Ackermann, M. and van den Bogert, A.J. 2010. Optimality principles for model-based predictions of human gait. Journal of Biomechanics 43: 6: 1055-1060.

Alexander, R.M. 1990. Optimum take-off techniques for high and long jumps. Philosophical Transactions of the Royal Society of London B 329, 3-10.

Alexander, R.M. 1992. Simple models of walking and jumping. Human Movement Science 11: 3-9.

Alexander, R.M. 1995. Simple models of human movement. Applied Mechanics Reviews 48: 461-470.

Alexander, R.M. 1997. Simple models of human locomotion. Journal of Theoretical Medicine 2: 129-135.

Alexander, R.M. 2003. Modelling approaches in biomechanics. Philosophical Transactions of the Royal Society of London B 358, 1429-1435.

Alonso, M. and Finn, E.J. 1980. Damped Oscillations, in Fundamental University Physics I, ed. M. Alonso and E.J. Finn, (Second Edition, Addison-Wesley Publishing Company), pp 352 and 504.

Blum, Y., Lipfer, S. and Seyfarth, A. 2009. Effective leg stiffness in running. Journal of Biomechanics 42: 14: 2400-2405.

Bobbert, M.F., Huijing, P.A. and van Ingen Schenau, G.J. 1986. A model of the human triceps surae muscle-tendon complex applied to jumping. Journal of Biomechanics 19, 887-98.

Caldwell, G.E. 2014. Muscle modeling. pp. 203-233. In: Robertson, D.G.E., Caldwell, G.E., Hamill, J., Kamen, G. and Whittlesey, S.N. (eds.) Research methods in biomechanics. Human kinetics, Champaign, IL.

Challis, J.H. 2000. Muscle-Tendon Architecture and Athletic performance, In: Zatsiorsky, V. (Ed.), Biomechanics in sport, Blackwell Science, University Press, Cambridge, pp. 33-55.

Edman, K.A.P. 1988. Double-hyperbolic force-velocity relation in frog muscle fibres. Journal of Physiology 404, 301-321.

Gacesa, J., Ivancevic, T., Ivancevic, N., Paljic, F. and Grujic, N. 2010. Non-linear dynamics in muscle fatique and strength model during maximal self-perceived elbow extensor training. Journal of Biomechanics 43: 12: 2440-2443.

Glazier, P. and Davids, K. 2009. Constraints on the Complete Optimization of Human Motion. Sports Medicine 39 (1): 15-28.

Günther, M., Schmitt, S. and Wank, V. 2007. High-frequency oscillations as a consequence of neglected serial damping in Hill-type muscle models. Biological Cybernetics, 97, (1), 63–79.

Hatze, H. 1980. A mathematical model for the computational determination of parameter values of anthropometric segments. Journal of Biomechanics 13: 833-843.

Hatze, H. 1981. A comprehensive model for human motion simulation and its application to the take-off phase of the long jump. Journal of Biomechanics 14: 135-42.

Hatze, H. 1983. Computerized optimization of sports motions: an overview of possibilities, methods and developments. Journal of Sports Science 1: 2-12.

Hatze, H. 1984. Quantitative analysis, synthesis and optimization of human motion. Human Movement Science 3: 5-25.

Hatze, H. 1985. Dynamics of the musculoskeletal system, in Biomechanics: current interdisciplinary research, eds. SM. Perren, E. Schneider, (Dordrecht, Marjinus Nijhoff), pp. 15-25.

Haeufle, D.F.B., Günther, M., Bayer, A. and Schmitt, S. 2014. Hill-type muscle model with serial damping and eccentric force–velocity relation. Journal of Biomechanics 47, (6), 1531–1536.

Hill, A.V. 1938. The Heat of Shortening and the Dynamic Constants of Muscle, Proc. Royal Soc. London. 126 (B), pp. 136-195.

Hill, A.V. 1970. First and Last Experiments in Muscle Mechanics, Cambridge University Press, Cambridge.

Herzog, W. 1999. Force-velocity relation. In: Nigg, B. M., Herzog, W. (Eds.), Biomechanics of the Musculo-Skeletal System 2nd ed., John Wiley & Sons Ltd, Chichester, England, pp. 173-180.

Herzog, W. 2000. Mechanical Properties and Performance in Skeletal Muscles. In: Zatsiorsky, V. (Ed.), Biomechanics in sport, Blackwell Science, University Press, Cambridge, pp. 21-32.

Hobara, H., Muraoka, T., Omuro, K., Gomi, K., Sakamoto, M., Inoue, K. and Kanosue, K. 2009. Knee stiffness is major determinant of leg stiffness during maximal hopping. Journal of Biomechanics 42: 11: 1768-1771.

Hobara, H., Inoue, K., Muraoka, T., Omuro, K., Sakamoto, M. and Kanosue, K. 2010. Leg stiffness adjustment for a range of hopping frequencies in humans. Journal of Biomechanics 43: 3: 506-511.

Ivancevic, T., Jain, L. and Pattison, J. 2009. Nonlinear dynamics and chaos methods in neurodynamics and complex data analysis. Nonlinear Dynamics 56: 23–44

Matsumoto, J. 1967. Validity of the Force – Velocity Relation for muscle contraction in the length Region, $l \leq l_O$. The Journal of General Physiology, Volume 50, 1125 – 1137.

McMahon, T. A. 1984. Muscles, Reflexes and Locomotion. Princeton University Press, Princeton New Jersey, p. 8 - 17.

McIntosh, B.R. and Holash, R.J. 2000. Power output and force velocity properties of muscle, In: Nigg, B.M., McIntosh, B.R., Mester, J. (Eds.) Biomechanics and Biology of Movement. Human Kinetics, pp. 193-210.

Morio, C., Lake, M.J., Gueguen, N., Rao, G. and Baly, L. 2009. The influence of footwear on foot motion during walking and running. Journal of Biomechanics 42: 13: 2081-2088.

Ni, J., Hiramatsu, S. and Kato, A. 2003. A Model of Neuro-Musculo-Skeletal System for Human Locomotion Under Position Constraint Condition. Journal of Biomechanical Engineering 125: 4: 499-506.

Nigg, B.M. 2006. "Mathematically determinate systems". In: Nigg, B.M. and Herzog, W. (eds.) Biomechanics of the Musculo-Skeletal System, Third

Edition, John Wiley & Sons Ltd, The Atrium, Southern Gate, Chichester, West Sussex PO19 8SQ, England, pp. 535-608.

Pandy, M.G. 2003. Simple and complex models for studying muscle function in walking. Philosophical Transactions of the Royal Society of London B 358, 1501-1509.

Pandy, M.G. and Zajac, F.E. 1991. Optimal muscular coordination strategies for jumping. Journal of Biomechanics 24, 1-10.

Pop, C., Khajepour, A., Huissoon, J.P. and Patla, A.E. 2003. Experimental /Analytical Analysis of Human Locomotion Using Bondgraphs. Journal of Biomechanical Engineering 125: 4: 490-498.

Popper, K. 2002. Conjectures and Refutations: The Growth of Scientific Knowledge (Routledge Classics)

Rahikainen, A. 1990. Method and apparatus for photographing a movement, United States Patent, Patent Number: 4,927,261.

Rahikainen, A. 2003. The use of rotating disk in the photography of movements, Russian Journal of Biomechanics 7, 1, 47-64.

Rahikainen, A. and Luhtanen, P. 2003. A study of the efficiency of the leg-pushing phase in shot put. Russian Journal of Biomechanics 7: 1: 65-79.

Rahikainen, A. and Luhtanen, P. 2004. A study of the effect of body rotation on the arm push in shot put. Russian Journal of Biomechanics 8, 2, 78-93.

Raikova, R. T. 1996. A model of the flexion – extension motion in the elbow joint – some problems concerning muscle forces modeling and computation, Journal of Biomechanics, 29, 6, 763 – 772.

Raikova, R.T. and Aladjov, H.Ts. 2005. Comparison between two models under dynamic conditions, Computers in Biology and Medicine, 35, pp. 373 – 387.

Raikova. R.T., Aladjov, H., Celichowski, J. and Krutki, P. 2013. An approach for simulation of the muscle force modeling it by summation of motor unit contraction forces. Computational and Mathematical Methods in Medicine, 625427, 10 pages.

Rapoport, S., Mizrahi, J., Kimmel, E., Verbitsky, O. and Isakov E 2003. Constant and Variable Stiffness and Damping of the Leg Joints in Human Hopping. Journal of Biomechanical Engineering 125: 4: 507-514.

Rassier, D.E., McIntosh, B.R. and Herzog, W. 1999. Length dependence of active force production in skeletal muscle, Journal of Applied Physiology 86, 1445-1457.

Selbie, W.S. and Caldwell, G.E. 1996. A simulation study of vertical jumping from different starting postures. Journal of Biomechanics 29, 1137-46.

Sheets. A.L., Corazza, S. and Andriacchi TP 2010. An Automated Image-Based Method of 3D Subject-Specific Body Segment Parameter Estimation for Kinetic Analyses of Rapid Movements. Journal of Biomechanical Engineering, 132:1, 011004 (10 pages).

Umberger, B.R. and Caldwell, G.E. 2014. Musculoskeletal modeling. pp. 247-276. In: Robertson, D.G.E., Caldwell, G.E., Hamill, J., Kamen, G. and Whittlesey, S.N. (eds.) Research methods in biomechanics. Human kinetics, Champaign, IL.

van Soest, A.J., Schwab, A.L., Bobbert, M.F. and van Ingen Schenau, G.J. 1993. The influence of the biarticularity of the gastrocnemius muscle on vertical-jumping achievement. Journal of Biomechanics 26, 1-8.

Winter, D.A. 2004. Biomechanics and Motor Control of Human Movement, 3rd ed. John Wiley & Sons. Inc., Hoboken, New Jersey, pp. 63 and 215 - 222.

ORIGINAL PAPERS

I

CONSTANT POWER MODEL IN ARM MOVEMENT - A NEW APPROACH TO HILL'S EQUATION

by

Ahti Rahikainen & Mikko Virmavirta, 2014

World Journal of Mechanics 4 (6), 157-169

World Journal of Mechanics, 2014, 4, 157-169
Published Online June 2014 in SciRes. http://www.scirp.org/journal/wjm
http://dx.doi.org/10.4236/wjm.2014.46018

Scientific Research

Constant Power Model in Arm Rotation—A New Approach to Hill's Equation

Ahti Rahikainen, Mikko Virmavirta

Neuromuscular Research Center, Department of Biology of Physical Activity, University of Jyväskylä, Jyväskylä, Finland
Email: ahrahik.zz@kolumbus.fi

Received 19 March 2014; revised 18 April 2014; accepted 16 May 2014

Abstract

The purpose of this study was to further develop the constant power model of a previous study and to provide the final solution of Hill's force-velocity equation. Forearm and whole arm rotations of three different subjects were performed downwards (elbow and shoulder extension) and upwards (elbow and shoulder flexion) with maximum velocity. These arm rotations were recorded with a special camera system and the theoretically derived model of constant maximum power was fitted to the experimentally measured data. The moment of inertia of the arm sectors was calculated using immersion technique for determining accurate values of friction coefficients of elbow and whole arm rotations. The experiments of the present study verified the conclusions of a previous study in which theoretically derived equation with constant maximum power was in agreement with experimentally measured results. The results of the present study were compared with the mechanics of Hill's model and a further development of Hill's force-velocity relationship was derived: Hill's model was transformed into a constant maximum power model consisting of three different components of power. It was concluded that there are three different states of motion: 1) the state of low speed, maximal acceleration without external load which applies to the hypothesis of constant moment; 2) the state of high speed, maximal power without external load which applies to the hypothesis of constant power and 3) the state of maximal power with external load which applies to Hill's equation. This is a new approach to Hill's equation.

Keywords

Arm Movement, Force-Velocity Relationship, Muscle Power, Hill's Equation

1. Introduction

Hill's force-velocity relationship of skeletal muscle (**Figure 1**) [1] [2] is one of the most essential equations of

How to cite this paper: Rahikainen, A. and Virmavirta, M. (2014) Constant Power Model in Arm Rotation—A New Approach to Hill's Equation. *World Journal of Mechanics*, **4**, 157-169. http://dx.doi.org/10.4236/wjm.2014.46018

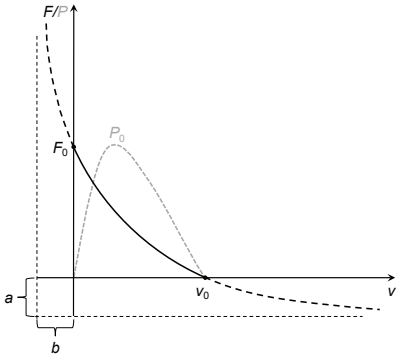

Figure 1. Hill's force-velocity relationship with corresponding power-velocity curve (dashed gray curve), where F_0 is maximum isometric force or force with zero velocity, v_0 is the highest possible velocity, a and b are constant force and constant velocity. Maximum power P_0 is typically found at about 30 % of v_0 [4]. In rotational movement torque M corresponds to force F and angular velocity corresponds to velocity v in Hill's equation.

muscle mechanics and it has been an object of biomechanical studies for years (e.g., [3]-[6]). In muscle mechanics, this relationship is often presented by Hill's equation $(F+a)(v+b)=b(F_0+a)$, where F is current muscle force at current shortening velocity of contraction, a is constant force and b is constant velocity, F_0 is the maximum isometric muscle force, *i.e.*, the maximum force that muscle can develop at a given constant length, and v is velocity [1] [2]. For comparison between different muscles b is best expressed in terms of b/l_0, where l_0 is the standard length of muscle. This equation was based on laboratory measurements with a Levin-Wyman ergometer in which the activated muscle was released at a suitable speed in an isolated muscle condition. The obtained constant velocity was then plotted against the observed tension. Force measured from skeletal muscle during maximum tension depends on several internal and external factors which have been thoroughly reviewed (e.g., [3] [7] [8]). Matsumoto [9] mentioned that because almost all the isotonic data have been restricted to one muscle length l_0, the maximum length with almost no resting tension, and the velocities measured are those initial values when the load begins to move. Examining the length region, $l \le l_0$, for an isotonically contracting muscle, Matsumoto [9] found that the constants a/F_0 and b/l_0 remained fixed throughout the range of lengths over which the shortening takes place. In contrast to Hill's isolated muscle preparations, force (F) of the involved muscles in rotational movement creates a moment ($M = r \times F$) about the joint. The length of the muscle's moment arm (r) changes as the rotational movement proceeds about the joint axis. This rotation movement is the combined effect of the forces of several different muscles. However, it is difficult to determine the contribution of each muscle on force production due to many different factors, and also to determine the torque about the joint. Several extensor and flexor muscles were used by Raikova [10] in her model of the flexion-extension motion in the elbow joint. Furthermore, the force of a skeletal muscle is an accumulation of forces generated by active motor units belonging to this muscle [11]. Raikova *et al*. [12] mentioned that access to each motor unit (MU) is impossible, and the recruitment and force developing properties of all individual MUs cannot be known. In this paper [12] the process of learning fast elbow flexion in the horizontal plane was simulated and the result was compared with experimentally measured data.

Previous experiments of Rahikainen *et al*. [13] were based on the theory of arm rotations including four phases: 1) start of the motion; 2) phase of constant maximum rotational moment; 3) phase of constant maximum muscular power; 4) stopping of the motion. It was assumed that the muscular system is able to transfer only a certain amount of chemical energy during the time of contraction and therefore, arm rotation must have maximum power that cannot be exceeded. It was also assumed that the maximum power acts within a certain range of velocity which was considered as constant maximum power and this is possible only when the velocity is

high enough. The velocity of the motion increases to the point where the maximum power occurs and acting rotational moment is less than the maximum moment. Consequently, power remains constant as the angular velocity increases and the moment decreases.

The present study continues the experiments of Rahikainen *et al.* [13] and further develops its theory of mechanics. The previous study presented a *constant power model* and its validity and accuracy of results were assessed. In the present study new arm rotation experiments of three subjects were captured with two different recording systems. More accurate calculations of moments of inertia and a new more effective determination of the matched range of measured and theoretical angular velocity curves were used. Also a new approach to Hill's equation was presented. In the left side of Hill's equation $(F+a)(v+b)=b(F_0+a)$ the constant a has the dimensions of force and b the dimensions of velocity, otherwise addition is impossible. Therefore, $(F + a)$ is force and $(v + b)$ is velocity, and force multiplied by velocity is power as can be seen in **Figure 1**. The term $(F + a)(v + b)$ is muscles' total power including Fv, which is the power of moving the external load. The right side of the equation, $b(F_0 + a)$, includes only constants in this regard the equation can be considered as a constant power model. However, the constant power of Hill's equation presented in this paper is not the above mentioned power of Hill's original curve as it is usually considered in biomechanics, but it is the sum of three different power components (see Discussion and Conclusions). The constant power model of this study acts during high speed movements with no external load, where Hill's equation does not seem to fit the experimental points ([2] p. 32, **Figure 3**) very well. As an explanation for this mismatch Hill mentioned that "sharp rise at the end of the curve in the region of very low tension was due to the presence of a limited number of fibers of high intrinsic speed and no such equation could fit the observed points below $P/P_0 = 0.05$". The present model is based on the muscular system's ability to transfer chemical energy and, therefore, it is not necessary to know the contribution of the individual muscles involved.

The purpose of the present study was to examine how the theoretical constant power model which was first used in linear motion [14] and later applied to rotational motion [13] fits the measured angular velocity curves of arm rotation experiments. The further purpose of the study was to determine how Hill's equation functions as a constant power model and to compare Hill's equation with the model of the present study.

2. Materials and Methods

In the present study, the measurements of arm rotations (Subjects S1 and S2) were recorded by a special camera system [15] [16]. **Figure 2** shows the principle of the system where angular velocity was calculated with the Formula:

$$\dot{\varphi} = \Delta S / R\Delta T \tag{1}$$

where R is arm length, ΔS is the distance between two successive measuring points and ΔT is time increment. Additional elbow flexion and extensions were performed for one Subject S3 by using Vicon motion analysis system with 8 cameras. This system made it possible to use higher frame rates (300 Hz). Subjects were normal healthy people representing different age and physical activity background (S1: 62 years, 1.80 m, 82 kg; S2: 35 years, 1.69 m, 73 kg, aikido training, weight lifting and S3: 25 years, 1.83 m, 70 kg, high jumping).

The accuracy of the special camera system has been described in references [13] [15]-[17]. The angular velocity-time curves were drawn (with a line thickness of 0.5 mm) on the squared paper, where 1 mm corresponded to an angular velocity of 0.1 rad/s and time of 1 ms giving the accuracy of velocity curves. The theoretical and measured angular velocity curves coincided within the distances of 35 - 70 mm, which was enough for the verification of the constant power model in the arm rotation experiments. Slight oscillations at the beginning of the movement did not exist within the constant power phase and, therefore, the verification of the constant power model was possible in all experiments. The accuracy of the Vicon recording device, verified by calculating the root-mean-square error for each camera, ranged from 0.06 to 0.17 mm during calibration.

2.1. Model of Arm Rotation

The model used in the present study is constructed according to Newton's II law and it was first used in linear motion [14] and then applied to rotational motion [13] by Rahikainen *et al*. The theory of arm rotation is as follows: At the beginning of the movement, angular velocity is naturally zero and it takes some time to generate force. At this early phase of motion, elastic properties of muscle-tendon complex has influence on the motion, but at the state of full tension, these elastic elements have no further dynamic effect. Thereafter it can be

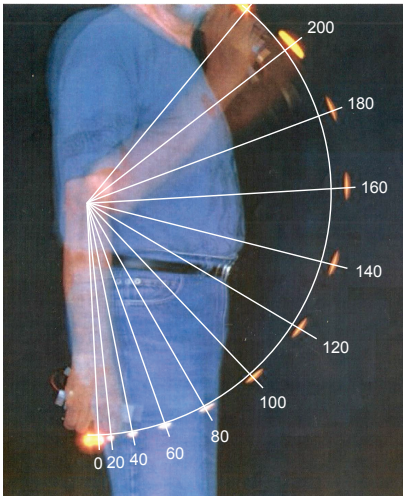

Figure 2. Example of elbow flexion. Rotation angles between two arm images (0 - 200 ms) are given in 20 ms increments according to light marks. It is noteworthy that the moment arm of the muscles involved in elbow flexion changes during the movement and, therefore, the muscles' contribution to power changes as well.

assumed that a maximum muscle force takes action and within rotational motion maximum rotational moment acts as well. At this phase of motion there is a constant value of glide friction acting. Because the muscle system is able to transfer only a certain quantity of chemical energy during the time of contraction, there must be a constant maximum power, which the muscle is able to generate within a certain range of velocity. As the velocity increases the motion reaches the point where the maximum power takes action and acting rotational moment is less than the maximum moment. This way power remains constant as the angular velocity increases and moment decreases. Now, liquid friction, directly proportional to velocity, is acting. The constant glide friction decreases as forces at the joint decrease and it becomes negligible. During the constant power phase of the model rotational moment is moment of inertia multiplied by angular acceleration which equals the moment generated by muscle force minus the moment generated by inner friction of muscle. The effect of gravitational force is added afterwards (see Paragraph 2.3). The model of arm rotation is the equation of motion:

$$I\frac{\mathrm{d}\dot{\varphi}}{\mathrm{d}T}=\frac{P}{\dot{\varphi}}-C\dot{\varphi} \tag{2}$$

where

Moment of inertia in arm rotation	I
Angular velocity	$\dot{\varphi}$
Power generated by arm muscles	P
Time	T
Moment generated by muscle force	$P/\dot{\varphi}$
Moment generated by inner friction of muscle	$C\dot{\varphi}$
Coefficient of friction	C

Inner friction of muscle is liquid friction inside muscle, which is directly proportional to velocity. The same liquid friction was also used in the study of Rahikainen *et al*. [17] which was initially adopted from Alonso and Finn [18]. It was assumed that, initially, movement proceeds at a constant maximum moment and then moment generated by the muscle force ($P/\dot{\varphi}$ in Equation 2) is constant. It was also assumed that, as velocity increases,

movement proceeds at constant maximum power at a certain range of velocity and then the power P in Equation 2 is constant. In order to determine the validity of this hypothesis, Equation 2 was solved for angular velocity-time function and this equation was employed for validity determination.

The solution of Equation 2 from the previous study [13]:

$$\dot{\varphi} = \sqrt{\frac{P}{C}\left(1 - e^{-\frac{2C}{I}T}\right)} \tag{3}$$

2.2. Calculation of Moment of Inertia

The mass distribution of the subject's arm sectors differed from the average values of mass tables in the literature. Therefore, the mass distribution of the arm sectors were determined by sinking the arm sectors into water. The masses of the arm sectors were calculated by multiplying the over flowed water volume with the corresponding arm sector density. The length of the subject's whole arm was measured with fist clenched, and the lengths of arm sectors (hand, forearm and upper arm) were measured. According to Winter [6] the arm sector densities (kg/l) were as follows: hand 1.16, forearm 1.13, upper arm 1.07.

Definition of moment of inertia:

$$I = \int r^2 \mathrm{d}m \tag{4}$$

where dm is rotating mass and r is the distance of rotating mass from the rotational axis. Derivation of the moment of inertia about the end of arm sector assuming even mass distribution:

$$I_1 = \int_0^L r^2 \mathrm{d}m = \int_0^L r^2 \frac{\mathrm{d}m}{\mathrm{d}r}\mathrm{d}r = \frac{m}{L}\int_0^L r^2 \mathrm{d}r = \frac{mL^2}{3} \tag{5}$$

where m is the mass of rotating arm, and L is the length of rotating arm. Derivation of the moment of inertia about the center of the arm sector assuming even mass distribution:

$$I_2 = \int_{-L/2}^{L/2} r^2 \mathrm{d}m = \frac{m}{3L}\left(\frac{L^3}{2^3} + \frac{L^3}{2^3}\right) = \frac{mL^2}{12} \tag{6}$$

Because the distribution of mass in the arm sector is not even, the moment of inertia of an additional mass was calculated with Formula:

$$I_3 = mr^2 \tag{7}$$

where m is additional mass of the arm sector and r is the estimated distance of the center of gravity of additional mass from the rotation axis. Subjects' arm sector distances, lengths and masses are presented in **Table 1**. These values are then substituted in the above mentioned Equations 4-7 to calculate the final moments of inertia of forearm and whole arm rotations about the elbow and shoulder joint (example for S1 summarized in **Table 2**).

Moment of inertia of forearm rotation

Forearm

Moment of inertia of major forearm mass about the elbow joint (m = 1.0 kg, L = 0.28 m):

$$I_{11} = \frac{mL^2}{3} = \frac{1.0 \times 0.28^2}{3} = 0.0261\ \mathrm{kg \cdot m^2}$$

Moment of inertia of additional forearm mass about the elbow joint (m = 0.24 kg, r = 0.07 m):

$$I_{12} = mr^2 = 0.24 \times 0.07^2 = 0.0012\ \mathrm{kg \cdot m^2}$$

Hand

Moment of inertia of the hand sector about the center of mass (m = 0.58 kg, L = 0.11 m):

$$I_{13} = \frac{mL^2}{12} = \frac{0.58 \times 0.11^2}{12} = 0.0006\ \mathrm{kg \cdot m^2}$$

Moment of inertia of the hand sector about the elbow joint (m = 0.58 kg, r = 0.34 m):

$$I_{14} = mr^2 = 0.58 \times 0.34^2 = 0.0670\ \mathrm{kg \cdot m^2}$$

Table 1. The estimated mass distribution of arm sectors. Forearm's additional mass is due to the muscle's mass distribution to the other end of arm sector.

	Distance from elbow joint (m)			Distance from shoulder joint (m)			Length (m)			Mass (kg)		
Subject	S1	S2	S3	S1	S2	S3	S1	S2	S3	S1	S2	S3
Hand							0.11	0.11	0.12	0.58	0.52	0.58
center of mass	0.34	0.32	0.34	0.64	0.60							
Forearm							0.28	0.26	0.27	1.00	0.90	1.00
center of mass				0.44	0.41							
additional mass	0.07	0.06	0.07	0.37	0.34					0.24	0.22	0.24
Upper arm							0.30	0.28	0.33	2.14	2.53	
Battery	0.37	0.35		0.67	0.63					0.26	0.29	0.29

Table 2. Summarized information for calculation of moment of inertia of forearm rotation (upper part) and whole arm rotation (lower part) for one subject. Moment of inertia is calculated about the elbow joint, center of mass (com) and shoulder joint.

Segment	m (kg)	L (m)	r (m)	About	Moment of inertia	I (kg·m^2)
Forearm	1.00	0.28		elbow	$I_{11}=\frac{mL^2}{3}$	0.0261
Forearm (additional mass)	0.24		0.07	elbow	$I_{12}=mr^2$	0.0012
Hand	0.58	0.11		com	$I_{13}=\frac{mL^2}{12}$	0.0006
Hand	0.58		0.34	elbow	$I_{14}=mr^2$	0.0670
Battery	0.26		0.37	elbow	$I_{b1}=mr^2$	0.0356
Total						0.131
Segment	m (kg)	L (m)	r (m)	about	moment of inertia	I (kg·m^2)
Upper arm	2.14	0.30		shoulder	$I_{21}=\frac{mL^2}{3}$	0.0642
Forearm	1.00	0.28		com	$I_{22}=\frac{mL^2}{12}$	0.0065
Forearm	1.00		0.44	shoulder	$I_{23}=mr^2$	0.1936
Forearm (additional mass)	0.24		0.37	shoulder	$I_{24}=mr^2$	0.0329
Hand	0.58	0.11		com	$I_{25}=\frac{mL^2}{12}$	0.0006
Hand	0.58		0.64	shoulder	$I_{26}=mr^2$	0.2376
Battery	0.26		0.67	shoulder	$I_{b2}=mr^2$	0.1167
Total						0.652

Light marker battery

Moment of inertia of the battery about the elbow joint (m = 0.26 kg, r = 0.37 m):

$$I_{b1} = 0.26 \times 0.37^2 = 0.0356 \text{ kg} \cdot \text{m}^2$$

Total moment of inertia of forearm rotation about elbow joint

$$0.0261 + 0.0012 + 0.0006 + 0.0670 + 0.0356 = 0.131 \text{ kg} \cdot \text{m}^2$$

Moment of inertia of whole arm rotation

Upper arm

Moment of inertia about the shoulder joint (m = 2.14 kg, L = 0.30 m):

$$I_{21} = \frac{mL^2}{3} = \frac{2.14 \times 0.30^2}{3} = 0.0642 \text{ kg} \cdot \text{m}^2$$

Forearm

Moment of inertia of the major forearm mass about the center of mass (m = 1.0 kg, L = 0.28 m):

$$I_{22} = \frac{mL^2}{12} = \frac{1.0 \times 0.28^2}{12} = 0.0065 \text{ kg} \cdot \text{m}^2$$

Moment of inertia about the shoulder joint (m = 1.0 kg, r = 0.44 m):

$$I_{23} = mr^2 = 1.0 \times 0.44^2 = 0.1936 \text{ kg} \cdot \text{m}^2$$

Moment of inertia of additional mass about the shoulder joint (m = 0.24 kg, r = 0.37 m):

$$I_{24} = m\,r^2 = 0.24 \cdot 0.37^2 = 0.0329 \text{ kg} \cdot \text{m}^2$$

Hand

Moment of inertia of the hand sector about the center of mass (m = 0.58, L = 0.11 m):

$$I_{25} = \frac{mL^2}{12} = \frac{0.58 \times 0.11^2}{12} = 0.0006 \text{ kg} \cdot \text{m}^2$$

Moment of inertia of the hand sector about the shoulder joint (m = 0.58 kg, r = 0.64 m):

$$I_{26} = mr^2 = 0.58 \times 0.64^2 = 0.2376 \text{ kg} \cdot \text{m}^2$$

Light marker battery

Moment of inertia of the battery about the shoulder joint (m = 0.26 kg, r = 0.67 m):

$$I_{b2} = 0.26 \times 0.67^2 = 0.1167 \text{ kg} \cdot \text{m}^2$$

Total moment of inertia at whole arm rotation about shoulder joint

$$0.0642 + 0.0065 + 0.1936 + 0.0329 + 0.0006 + 0.2376 + 0.1167 = 0.652 \text{ kg} \cdot \text{m}^2$$

According to the above mentioned calculations, the corresponding moments of inertia of forearm rotation and whole arm rotation for S2 were 0.110 and 0.551 kg·m^2, respectively. As the total length of forearm and hand was the same for Subjects S1 and S3, it was assumed that the moments of inertia of these segments were also the same and, therefore, the moment of inertia of forearm rotation about the elbow joint for S3 was 0.131 kg·m^2. The measurements with Vicon camera system for S3 were done with reflective markers and the corresponding moment of inertia without the battery was 0.095 kg·m^2.

2.3. Effect of Gravitational Force on the Movement

In forearm rotation, the effect of gravitational force is minor compared with maximum muscle forces and the moment induced by gravity $\Sigma r \times mg$ was omitted from the motion model (Equation 2). In whole arm rotation, this moment is added to the motion mechanics in the following manner: The power generated by this gravitational moment is $(\Sigma r \times mg)\dot{\varphi}$, where mg is gravitational force of arm segments, r is distance of the center of gravity of segments from the rotation axis and $\dot{\varphi}$ angular velocity of arm rotation. The theoretical angular velocity (Equation 3) and the measured angular velocity match within a very narrow velocity range and the power induced by gravity can be calculated as a constant factor. It is included in the power P according to the previous study [13].

2.4. Determining the Matched Range of Measured and Theoretical Angular Velocity Curves

Figure 3 shows the technique that was used to determine the matched range of measured and theoretical angular

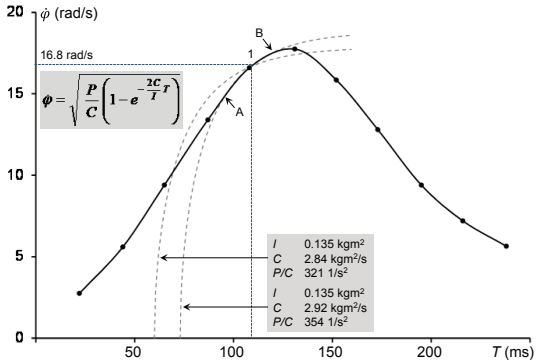

Figure 3. Example of the technique to find the matched range (A - B) of measured and theoretical angular velocity. The zero point of time for the theoretical angular velocity is at the intersection of the time-axis and the broken-line curve (see text for more information). The theoretical angular velocity curve (broken line) coincides with the measured curve (solid line) between A and B.

velocity curves. Friction coefficient values (C) and power values (P) were obtained by fitting the theoretical angular velocity curves to the measured ones. These two curves coincide only if certain C and P values are used in the fitting process. The measured angular velocity values are shown as points on the velocity curve and the theoretical angular velocity (Equation 3) is shown as a broken line. The matched range was found by using the following iteration procedure: based on previous experiments, the randomized initial values (see **Figure 3**) within the matched range were selected for angular velocity at point 1 $\left(\dot{\varphi} = 16.8 \text{ rad/s}\right)$. A zero point on the time axis for the theoretical angular velocity was selected 0.050 s before point 1, which corresponds to 0.060 s on the time axis of the figure. Thereafter, the direction of iteration process was observed and after some iteration, the final theoretical angular velocity was drawn according to Equation 3 to match the measured velocity curve. The correct theoretical angular velocity was obtained with the zero point at 0.073 s on the time axis. The ratio of power and friction coefficient in **Figure 3** is

$$\frac{P}{C} = \frac{\dot{\varphi}^2}{1 - e^{-\frac{2C}{I}T}} \tag{8}$$

The final theoretical angular velocity was drawn with moment of inertia I = 0.135 kg·m^2, friction coefficient value C = 2.92 kg·m^2/s and ratio of power and friction coefficient P/C = 354 1/s^2.

3. Results

Arm rotation experiments recorded by the camera system of Rahikainen [16] are presented in **Figures 4-7** and experiments with Vicon motion analysis system in **Figure 8**. The theoretical angular velocity curves in **Figures 4-8** are marked with broken lines and they coincide with the measured angular velocity curves (solid lines) between the points A - B, where movement proceeds at constant power. Initially, movement proceeds at constant acceleration, then liquid friction becomes influential and acceleration decreases just before the section A - B (constant power), which is finally followed by stopping of the movement. In general, the sections A - B are long enough to verify the existence of the constant power model. The measurements in **Figure 8** with Subject S3, made by the Vicon motion analysis system, did not have a clear section of constant acceleration at the beginning of the movement. High oscillation in that section turned it indefinite. In the elbow extension, the oscillation is weak and the usual constant acceleration section can be distinguished at the movement initiation. It also seems that the constant acceleration section in **Figure 6** has a similar oscillation as in **Figure 8**.

The measured data in **Figures 4-8** have been smoothed by the 6th order polynomial curve fitting. The used friction coefficient values varied between 2.8 - 3.1 kg·m^2/s in forearm rotations and between 3.6 - 3.8 kg·m^2/s in

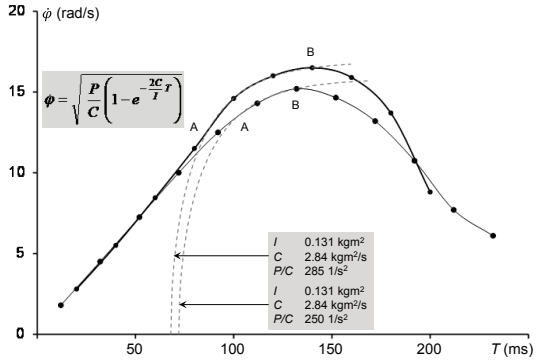

Figure 4. Two elbow extensions (Subject S1). The theoretical angular velocity curve (broken line) coincides with the measured curve (solid line) between A and B.

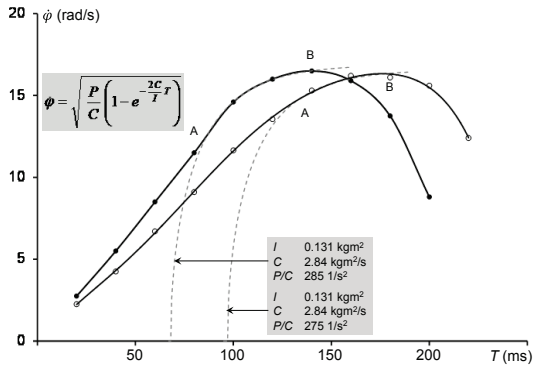

Figure 5. Elbow extension (filled circles) and elbow flexion (open circles) of Subject S1. The theoretical angular velocity curve (broken line) coincides with the measured curve (solid line) between A and B.

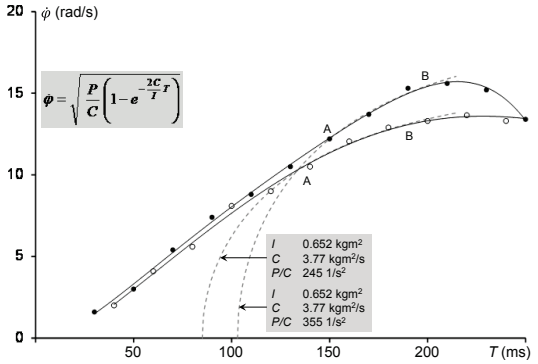

Figure 6. Shoulder extension (filled circles) and shoulder flexion (open circles) of Subject S1. The theoretical angular velocity curve (broken line) coincides with the measured curve (solid line) between A and B.

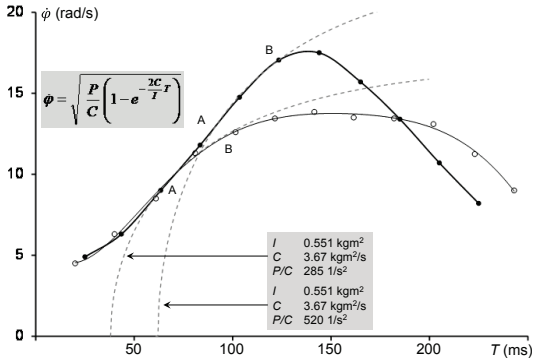

Figure 7. Shoulder extension (filled circles) and shoulder flexion (open circles) of Subject S2. The theoretical angular velocity curve (broken line) coincides with the measured curve (solid line) between A and B.

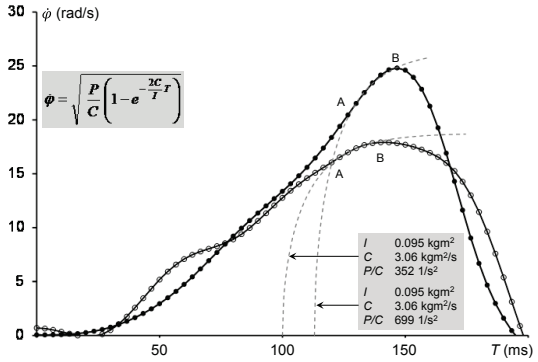

Figure 8. Elbow extension (filled circles) and elbow flexion (open circles) of Subject S3. The theoretical angular velocity curve (broken line) coincides with the measured curve (solid line) between A and B. The elbow joint angles for maximum angular velocity were 123˚ (extension) and 81˚ (flexion).

whole arm rotations. The maximum angular velocities ranged from 13.7 rad/s (shoulder flexion) to 24.8 rad/s (elbow extension). The effect of the ratio of power and friction coefficient P/C on the progress of angular velocity is clearly seen in **Figures 4-8**. In **Figure 4**, the typical variation in consecutive trials of the same subject is seen. The effect of gravity can be seen in **Figure 6** and **Figure 7** as the shoulder extension has larger rotating angular velocity than the shoulder flexion.

4. Discussion and Conclusions

The present study confirmed the existence of constant power model in arm rotations with maximum velocity. The theoretical and measured angular velocity curves showed a short range of coincidence because the arm rotations were made at maximum velocity, but the range was long enough to verify the model. If there were a constant force resisting the arm rotation, the speed of motion would be slower and the velocity-time curve of measured arm rotation would follow the theoretical constant power curve (broken line, **Figures 4-8**) levelling horizontally as time proceeds. Thus a constant force in arm rotation movement corresponds to a constant velocity in the same manner as a force corresponds to a velocity in Hill's equation.

After the initiation of arm rotation, the movement proceeds at a state of low speed, high acceleration without

external load. In this phase of movement it is assumed (hypothesis) that the movement proceeds at a constant maximum muscular moment. Measurements of the rotational movements show that movement proceeds at constant angular acceleration. Therefore, we can conclude that the torque accelerating the movement, or the right side of Equation 2, is constant.

$$I\frac{\mathrm{d}\dot{\varphi}}{\mathrm{d}T}=\frac{P}{\dot{\varphi}}-C\dot{\varphi}$$

Torque generated by the maximum muscular moment is $P/\dot{\varphi}$ and according to the hypothesis it is constant. The moment generated by frictional force $-C\dot{\varphi}$ is not constant (because of the term of velocity) and, therefore, this hypothesis is not fulfilled. However, the finding "movement proceeds at constant acceleration" is interesting and should be studied more closely. In Equation 2 kinetic friction was assumed to be directly proportional to velocity at the beginning of the movement. This is a new hypothesis which is not necessarily true. It is possible that kinetic friction at small velocities is constant and at high velocities is directly proportional to velocity. This leads to a constant torque accelerating the movement at the beginning of movement.

After the phase of constant angular acceleration the movement proceeds at high speed and low acceleration without external load. It is assumed that, within this phase, the movement proceeds at constant maximum muscular power. This hypothesis seems to be true between A and B in **Figures 4-8**. This is the most interesting finding of the present study and further development of Hill's equation provided another kind of model of constant power.

Final solution of Hill's force-velocity equation

The experiments of the present study verified the conclusions of a previous study [13] in which theoretically derived equation with constant maximum power was in agreement with experimentally measured results. As Hill's equation is also a constant power model it can be considered the same as the model of this study in that respect. Hill's force-velocity relationship was created by experiments in which the velocity of muscle contraction was measured against a certain constant force. The experiments of Hill's equation naturally started at zero velocity and continued in the same manner as the experiments of the present study through all the phases. Because of the external load, the experiments of Hill's equation did have slower velocities and, therefore, it was possible to reach maximum velocity within the measuring accuracy. The measurements of the present study were made without external load and none of them reached the maximum theoretical velocity of Equation 3.

The results of Hill's experiments could be transformed into hyperbola equation describing force-velocity dependence of the movement. **Figure 9** represents a further development of Hill's force-velocity relationship. The

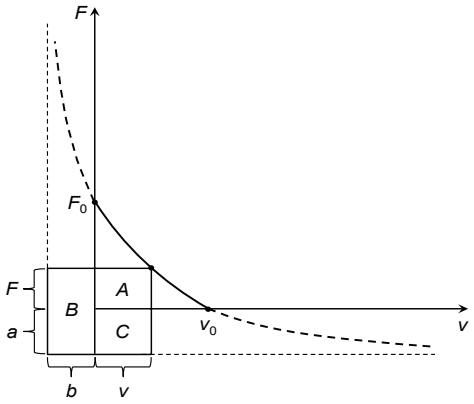

Figure 9. Hill's force-velocity relationship presented with asymptotes (broken lines). In traditional presentation of hyperbola a and b are negative, but here they refer to the positive constant terms of Hill' equation. Hill's equation, $(F + a)\,(v + b)$ = constant, implies that the area of rectangle $A + B + C$ is constant.

Force-velocity axes are shown and also the asymptotes have been drawn as broken lines. Hill's equation, $(F + a)(v + b) =$ constant, implies that the area of the rectangle $(F + a)(v + b)$ is constant. The total power of the muscle is comprised of three different components represented by rectangles A, B and C. The area of rectangle $A = F v$ represents the power needed from muscle against an external load (see the power curve in **Figure 1**). If there is no external load, this power is consumed by acceleration. The area of rectangle $B = (F + a) b$ represents the power of muscle's internal loss of energy. This power creates a counter force against an external load. As the velocity is zero, this power B is highest and, therefore, it is not related to external movement. Thereafter, as velocity increases, this power decreases rapidly initially, then slowly at higher velocities. The area of rectangle $C = va$ represents the power of friction due to the motion of the muscle-load system. Because power is the force multiplied by velocity, the force of friction is a. This is not force directly proportional to velocity, generally known as liquid friction (which is the friction used in the present study), but constant force of friction which is known as glide friction. Now we can see that there are three different states of motion: 1) at the beginning of motion characterized by a state of low speed maximal acceleration without external load; then 2) as the motion continues a state of high speed, maximal power without external load and 3) a state of maximal power with external load, which applies to Hill's equation. The maximum power is due to the fact that the transfer of energy within the muscle system must have a maximum rate and, therefore, muscle's power generation must also have a certain maximum rate. Within Hill's equation maximum power is due to the ability to lift loads and within experiments of the present study due to the high speed of motion.

Muscle mechanics of the present study are based on the experiments which were performed with maximum velocity and therefore the constant power phase became short. If there is a constant force resisting the motion, the motion becomes slower and it can be inferred that the time-velocity curve levels horizontally at the velocity of Hill's equation. Another kind of mechanics applies if less muscle force is used and the traditional Hill equation applies to movements that are resisted by external force. From the results of the present study it can be seen how these states of motion relate to each other and the findings enable further development of muscle mechanics in this field of modern science. The calculation methods of this study can be applied in research areas of sports and medicine.

References

[1] Hill, A.V. (1938) The Heat of Shortening and the Dynamic Constants of Muscle. *Proceedings of the Royal Society B, London*, **126**, 136-195.

[2] Hill, A.V. (1970) First and Last Experiments in Muscle Mechanics. Cambridge University Press, Cambridge.

[3] Herzog, W. (1999) Force-Velocity Relation. In: Nigg, B.M. and Herzog, W., Eds., *Biomechanics of the Musculo-Skeletal System*, John Wiley & Sons Ltd., Chichester, 173-180.

[4] Herzog, W. (2000) Mechanical Properties and Performance in Skeletal Muscles. In: Zatsiorsky, V., Ed., *Biomechanics in Sport*, Blackwell Science, University Press, Cambridge, 21-32.

[5] McIntosh, B.R. and Holash, R.J. (2000) Power Output and Force Velocity Properties of Muscle. In: Nigg, B.M., McIntosh, B.R. and Mester, J., Eds., *Biomechanics and Biology of Movement Human Kinetics*, Human Kinetics, Champaign, 193-210.

[6] Winter, D.A. (2004) Biomechanics and Motor Control of Human Movement, 3rd Edition, John Wiley & Sons Inc., Hoboken, 215-222.

[7] Challis, J.H. (2000) Muscle-Tendon Architecture and Athletic performance. In: Zatsiorsky, V., Ed., *Biomechanics in Sport*, Blackwell Science, University Press, Cambridge, 33-55.

[8] Rassier, D.E., MacIntosh, B.R. and Herzog, W. (1999) Length Dependence of Active Force Production in Skeletal Muscle. *Journal of Applied Physiology*, **86**, 1445-1457.

[9] Matsumoto, J. (1967) Validity of the Force-Velocity Relation for Muscle Contraction in the Length Region, $l \leq l_0$. *The Journal of General Physiology*, **50**, 1125-1137. http://dx.doi.org/10.1085/jgp.50.5.1125

[10] Raikova, R.T. (1996) A Model of the Flexion-Extension Motion in the Elbow Joint—Some Problems Concerning Muscle Forces Modeling and Computation. *Journal of Biomechanics*, **29**, 763-772. http://dx.doi.org/10.1016/0021-9290(95)00072-0

[11] Raikova, R., Aladjov, H., Celichowski, J. and Krutki, P. (2013) An Approach for Simulation of the Muscle Force Modeling It by Summation of Motor Unit Contraction Forces. *Computational and Mathematical Methods in Medicine*, **2013**, Article ID: 625427.

[12] Raikova, R.T., Gabriel, D.A. and Aladjov, H.Ts. (2005) Comparison between Two Muscle Models under Dynamic Conditions. *Computers in Biology and Medicine*, **35**, 373-387.

[13] Rahikainen, A., Avela, J. and Virmavirta, M. (2012) Modeling the Force-Velocity Relationship in Arm Movement. *World Journal of Mechanics*, **2**, 90-97. http://dx.doi.org/10.4236/wjm.2012.22011

[14] Rahikainen, A. and Luhtanen, P. (2004) A Study of the Effect of Body Rotation on the Arm Push in Shot Put. *Russian Journal of Biomechanics*, **8**, 78-93.

[15] Rahikainen, A. (1990) Method and Apparatus for Photographing a Movement. US Patent No. 4 (927), 261.

[16] Rahikainen, A. (2003) The Use of Rotating Disk in the Photography of Movements. *Russian Journal of Biomechanics*, **7**, 47-64.

[17] Rahikainen, A., Avela, J. and Virmavirta, M. (2012) Study of Leg Movement in One and Two Legged Hopping. *International Journal of Applied Mechanics*, **4**, 16 p.

[18] Alonso, M. and Finn, E.J. (1980) Damped Oscillations. In: Alonso, M. and Finn, E.J., Eds., *Fundamental University Physics I*, 2nd Edition, Addison-Wesley Publishing Company, Boston, 352, 504.

II

STUDY OF LEG MOVEMENT IN ONE- AND TWO-LEGGED HOPPING

by

Ahti Rahikainen, Janne Avela & Mikko Virmavirta, 2012

International Journal of Applied Mechanics 4, (1) 16 pages

III

MODELING THE FORCE-VELOCITY RELATIONSHIP IN ARM MOVEMENT

by

Ahti Rahikainen, Janne Avela & Mikko Virmavirta, 2012

World Journal of Mechanics vol 2, 90-97

World Journal of Mechanics, **2012, 2, 90-97**
doi:10.4236/wjm.2012.22011 Published Online April 2012 (http://www.SciRP.org/journal/wjm)

Modeling the Force-Velocity Relationship in Arm Movement

Ahti Rahikainen, Janne Avela, Mikko Virmavirta
Department of Biology of Physical Activity, University of Jyväskylä, Neuromuscular Research Center, Jyväskylä, Finland
Email: ahrahik.zz@kolumbus.fi

Received February 1, 2012; revised March 2, 2012; accepted March 17, 2012

ABSTRACT

Modeling the force-velocity dependence of a muscle-tendon unit has been one of the most interesting objectives in the field of muscle mechanics. The so-called Hill's equation [1,2] is widely used to describe the force-velocity relationship of muscle fibers. Hill's equation was based on the laboratory measurements of muscle fibers and its application to the practical measurements in muscle mechanics has been problematic. Therefore, the purpose of this study was to develop a new explicit calculation method to determine the force-velocity relationship, and test its function in experimental measurements. The model was based on the motion analysis of arm movements. Experiments on forearm rotations and whole arm rotations were performed downwards and upwards at maximum velocity. According to the present theory the movement proceeds as follows: start of motion, movement proceeds at constant maximum rotational moment (Hypothesis 1), movement proceeds at constant maximum power (Hypothesis 2), and stopping of motion. Theoretically derived equation, in which the motion proceeds at constant maximum power, fitted well the experimentally measured results. The constant maximum rotational moment hypothesis did not seem to fit the measured results and therefore a new equation which would better fit the measured results is needed for this hypothesis.

Keywords: Muscle Mechanics; Muscle Power; Force-Velocity Relationship; Arm Movement

1. Introduction

Modeling the force-velocity relationship of muscle-tendon unit involves many different factors. In muscle mechanics force-velocity relationship of skeletal muscle is often presented by so-called Hill's equation $(F + a)(v + b) = b(F_0 + a)$, where F is the maximum force within muscle contraction, a and b are constants, F_0 the isometric force of muscle or the constant maximum force generated by muscle with zero velocity and v is velocity, (**Figure 1**) [1,2]. This equation was based on the laboratory measurements in which force (F) of the activated muscle lifted different loads ($F = mg$) and speed of the load (v) was then measured. In Hill's equation F is force, a is constants force, v is velocity, b is constant velocity and F_0 is constant force. In the equation the vectors of forces and velocities have the same direction and therefore Hill's equation can be presented in a scalar form. The left side of Hill's equation is the product of force and velocity and that is power. As the right side of the equation is constant it can be seen that Hill's equation is a constant power model. Hill's force-velocity relationship is one of the most essential equations of muscle mechanics and it has often been principle object in biomechanical studies for about 50 years, e.g. [3-6]. Force measured from skeletal muscle during maximum tension depends on several internal and external factors. Internal factors are e.g. anatomical structure of muscle (cross sectional area, pennation etc.), fiber type distribution (fast and slow twitch muscle fibers have different force-velocity equations), condition of the muscle (fatigue, training) and muscle length. External factors are e.g. contraction type (isometric, concentric and eccentric) and contraction velocity (rate of change of muscle length). Good reviews of the above mentioned factors have been presented, e.g. [4,7,8]. Force (F) creates a moment about the joint which is moment arm multiplied by force ($M = r \times F$). Length of muscle's moment arm depends on joint angle and it changes as the rotation movement proceeds about the joint axis. The combined effect of the forces of several different muscles produces the rotation movement about the joint axis.

Due to all the above mentioned factors it is difficult to determine the force production [9, 10], and also to determine the torque about the joint. The purpose of this study was to develop a new explicit calculation method to determine the force-velocity relationship and test its function in experimental measurements. This method is based on the assumption that in muscle mechanics there exists a constant maximum power which the muscle is

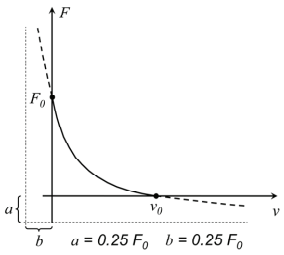

Figure 1. Hill's equation $(F + a)(v + b) = b(F_0 + a)$ where F_0 is so-called isometric force or force with zero velocity, v_0 is the highest possible velocity, a and b are constant force and constant velocity. In rotational movement torque M corresponds to force F and angular velocity φ corresponds to velocity v.

able to generate within a certain range of velocity. The principle of constant maximum power is the same as in Hill's equation except that the constant maximum power in the present study is a characteristic of whole muscle group instead of separate muscle fibers as in the Hill's equation. This study continues the development of the earlier findings [11-13].

2. Methods

The experiments in the present study consisted of three different maximum velocity arm movements: 1) forearm rotation downwards, 2) whole arm rotation downwards and 3) upwards. The selection of these movements was based on the earlier findings of Rahikainen and Luhtanen [11] where so called "constant power theory" seemed to work at the last phase of the arm push in shot put. In order to study this finding more extensively it was reasonable to choose a simple procedure as represented by arm rotations in the present study. The photographs of arm movements in this study were generated by a special motion camera system [14,15] which represents the movement as a series of object images. The paths of the mark lights attached to the moving object can be seen as broken light-lines. The principle of the method is to photograph the moving object through a rotating disc which consists of one transparent opening and nine filter openings serving as the shutter apertures. As the exposure disc rotates in front of the camera lens (film camera Canon T70) and the camera aperture is open, the disc serves as the shutter. This way several overlapping exposures are generated on the same frame. The transparent opening generates images of the moving object, and the filter openings generate the light-lines indicating the paths of mark lights attached to the moving object (**Figure 2**). In this study the speed of rotation of the exposure disc was 300 rotations per minute, exposing five (300/60) object images per second and giving the time interval of 20 ms

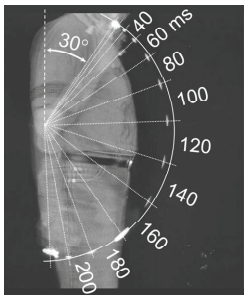

Figure 2. Forearm rotation downwards with maximum force. Angle of rotation φ and its corresponding time T (ms) are presented on the subject image.

for nine light-lines between consecutive object images (for more detail, see [14,15]). **Figure 2** represents a forearm rotation downwards. As seen in the figure the radius of the rotation circle is not exactly the same as the radius of forearm rotation. This is because of a slight motion of the elbow joint. Actually the radius of forearm rotation is slightly larger than the radius of circle on the figure and it can be measured from the forearm image before the start of the rotation movement. Angular velocity measurements are calculated with the formula

$$\dot{\phi} = \Delta S / R \Delta T \tag{1}$$

in which the length of forearm is the radius of rotation R and the distance measured between two successive measured points on the path of light-lines is the distance increment ΔS.

2.1. Measurement of Rotation Arc

For convenience the arc ΔS_1 was measured as a straight line ΔS_2 (**Figure 3**) and the error between these two values was estimated. The arc ΔS_1 can be calculated from the straight line ΔS_2 from the formula:

$$\Delta S_1 = R \arccos\left(1 - \frac{1}{2}\left(\frac{\Delta S_2}{R}\right)^2\right)$$

Formula derivation from the right-angled triangle in **Figure 3**.

$$\Delta S_2^2 = R^2 \sin^2 \Delta\varphi + R^2 \left(1 - \cos \Delta\varphi\right)^2 \tag{2}$$

$$\left(\frac{\Delta S_2}{R}\right)^2 = \sin^2 \Delta\varphi + \cos^2 \Delta\varphi + 1 - 2\cos \Delta\varphi \tag{3}$$

$$\sin^2 \Delta\varphi + \cos^2 \Delta\varphi = 1 \tag{4}$$

$$\left(\frac{\Delta S_2}{R}\right)^2 = 2 - 2\cos \Delta\varphi \tag{5}$$

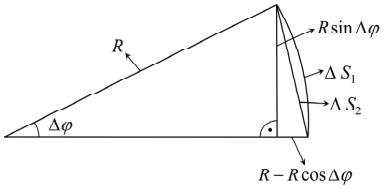

Figure 3. Measurement of the rotation arc. φ = angle of rotation, R = length of forearm, arc ΔS_1 = distance the mark light travels during the time interval Δt and ΔS_2 = the arc $\Delta S1$ measured as a straight line.

$$\cos\Delta\varphi = 1 - \frac{1}{2}\left(\frac{\Delta S_2}{R}\right)^2 \quad (6)$$

$$\Delta S_1 = R \arccos\left(1 - \frac{1}{2}\left(\frac{\Delta S_2}{R}\right)^2\right) \quad (7)$$

The maximum value measured from **Figure 2** (corresponding time 140 ms) is $\Delta S/R = \Delta S_2/R = 0.356$. Substituting this value in the formula above (7) the arc of rotation is obtained as ratio form $\Delta S_1/R = 0.358$. It can be seen that ΔS_2 fits with adequate accuracy to the distance ΔS_1.

2.2. Progress of Research

The present study continues the earlier study [11] and it is a new round in the diagram of **Figure 4** presenting the progress of research (testing the hypotheses): 1) Equation of arm movement was derived and test predictions were made. 2) Experiments were performed in arm rotations. 3) Equation of arm rotation was fitted to the experimental results and their compatibility was observed. 4) If the present equation of motion did not fit at all the measuring results, the hypothesis would be disproved. If the present equation of motion fitted the measuring results in some definite accuracy, the hypothesis would receive confirmation. 5) In the future, by making additional experiment (a new round in the diagram) the hypothesis will receive more confirmation.

2.3. Arm Rotation

Because the muscle system is able to transfer only a certain quantity of chemical energy during the time of contraction, it is obvious that arm rotation must have maximum power that cannot be exceeded. It can also be assumed that the maximum power acts within a certain range of velocity and it is a constant maximum power. At the beginning of the movement angular velocity is naturally zero and it takes some time to generate force. After the start of the movement it is possible that a maximum muscle force takes action and within rotational motion maximum rotational moment acts as well. The constant

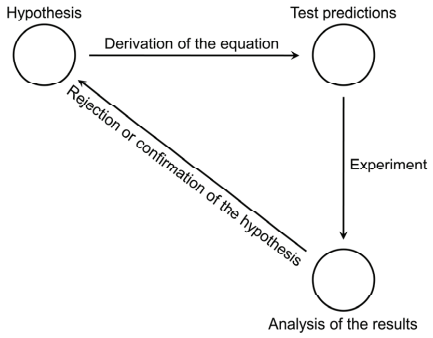

Figure 4. Diagram of the progress of testing the hypotheses of arm rotations.

maximum power acts within a certain range of velocity which cannot be at the beginning of the rotational movement because power is the product of moment and angular velocity. Therefore, a constant power "theory" is possible only when the velocity is high enough. As the velocity increases the motion reaches the point where the maximum power takes action and acting rotational moment is less than the maximum moment. This way power remains constant as the angular velocity increases and moment decreases.

2.4. Research Hypotheses

According to the present theory and above mentioned facts the movement proceeds as follows: 1) start of motion, 2) movement proceeds at constant maximum rotational moment during the first part of the movement [**Hypothesis 1**], 3) movement proceeds at constant maximum muscular power during the second part of the movement [**Hypothesis 2**], 4) stopping of motion. In order to test the research hypotheses, the following experiments were conducted: forearm rotation downwards at maximum velocity (1), whole arm rotation downwards at maximum velocity (2), whole arm rotation upwards at maximum velocity (3). The maximum power hypothesis was tested so that the theoretical angular velocity-time values from Equation (15) were fitted into the measured angular velocity-time curves of arm rotations. It was assumed that if the measured angular velocity-time values matched the theoretical values within a certain velocity range then the Hypothesis 2 would be fulfilled. The maximum rotational moment hypothesis was tested by Equation (8).

2.5. A Model of Arm Rotation

It was assumed (hypothesis) that in muscle mechanics there exists the maximum power (P) which the muscle is able to generate within a certain range of velocity. The

Model of arm rotation was constructed according to Newton's II law which was applied to rotational motion where moment of inertia multiplied by angular acceleration equals rotational moment. Rotational moment equals moment generated by muscle force subtracted moment generated by inner friction of muscle. The effect of gravitational force is minor and it is added to the motion mechanics afterwards in Section 2.6. The model of arm rotation is the equation of motion:

$$I\frac{\mathrm{d}\dot{\varphi}}{\mathrm{d}T}=\frac{P}{\dot{\varphi}}-C\dot{\varphi} \tag{8}$$

where I is moment of inertia in arm rotation, $\dot{\varphi}$ is angular velocity, P is power generated by arm muscles, T is time, $P/\dot{\varphi}$ is moment generated by muscle force, $C\dot{\varphi}$ is moment generated by inner friction of muscle and C is constant coefficient of friction.

The mass distribution of the subject's arm sectors differed from the average values in subject mass tables. Therefore the mass distribution of the arm sectors were defined by sinking the arm sectors into water, and weighing the over flowed water. The masses of the arm sectors were calculated by means of water volume and arm sector density ($V*\rho$). The length of subject's whole arm was 0.64 m and the arm sectors, hand, forearm 1, forearm 2, upper arm 1, upper arm 2 were 0.128 m each. Arm sector densities were 1.16, 1.13, 1.07 for hand, forearm and upper arm, respectively [6]. Moment of inertia for the forearm rotation was I = 0.11 kgm^2 and for the whole arm rotation I = 0.52 kg·m^2.

Hypothesis 1 implies that movement proceeds at a constant maximum rotational moment. In that case the moment generated by muscle force $P/\dot{\varphi}$ in Equation 8 is a constant maximum moment. Hypothesis 2 implies that movement proceeds at a constant maximum muscular power. In that case the power P in Equation (8) is a constant maximum power. In order to determine the validity of Hypothesis 2, Equation (8) was solved for angular velocity-time function and this equation was employed for validity determination:

$$\text{Equation of power}\quad I\dot{\varphi}\frac{\mathrm{d}\dot{\varphi}}{\mathrm{d}T}=P-C\dot{\varphi}^2 \tag{9}$$

Where $I\dot{\varphi}\dfrac{\mathrm{d}\dot{\varphi}}{\mathrm{d}T}$ is power in arm rotation, P is power generated by arm muscles and $C\dot{\varphi}^2$ is power consumed by friction.

Solution

$$I\frac{\dot{\varphi}}{P-C\dot{\varphi}^2}\mathrm{d}\dot{\varphi}=\mathrm{d}T \tag{10}$$

$$-\frac{I}{2C}\int_0^{\dot{\varphi}}-2C\dot{\varphi}\frac{1}{P-C\dot{\varphi}^2}\mathrm{d}\dot{\varphi}=\int_0^T\mathrm{d}T \tag{11}$$

$$\ln\left(P-C\dot{\varphi}^2\right)-\ln\left(P\right)=-\frac{2C}{I}T \tag{12}$$

$$\ln\left(\frac{P-C\dot{\varphi}^2}{P}\right)=-\frac{2C}{I}T \tag{13}$$

$$1-\frac{C}{P}\dot{\varphi}^2=e^{-\frac{2C}{I}T} \tag{14}$$

$$\dot{\varphi}=\sqrt{\frac{P}{C}\left(1-e^{-\frac{2C}{I}T}\right)} \tag{15}$$

2.6. Effect of Gravitational Force on the Movement

The moment which is induced by gravity $\sum r\times mg$ was omitted from the motion model. The power generated by this moment is $\left(\sum r\times mg\right)\dot{\varphi}$, where mg is gravitational force of arm segments, r is distance of the center of gravity of segments from the rotation axis and $\dot{\varphi}$ angular velocity of arm rotation. The theoretical angular velocity function, Equation (15), and the measured angular velocity function coincide within so narrow velocity range that the power induced by gravity can be calculated as a constant factor. In this case it is included in the power P as follows: P of rotation downwards = power generated by muscular force + power generated by gravitational force and P of rotation upwards: P = power generated by muscular force-power generated by gravitational force.

2.7. Finding the Matched Range of Measured and Theoretical Angular Velocity Functions

There are two unknown variables in Equation (15), power P and kinetic friction coefficient C. In order to determine these two unknown variables, two equations were required. These two equations were obtained from the hypothesis according to which the movement proceeds at constant maximum power within certain velocity range. By substituting two angular velocity-time value pairs from the measured angular velocity-time curve in Equation (15) the two required equations were obtained. The zero point of time (**Figure 5**) is at the intersection point of the time-axis and the broken-line curve and in order to find that some iteration was done. From these two equations P and C could be solved. Then the constant maximum power hypothesis was tested by comparing the calculated theoretical values from Equation (15) with the values of measured angular velocity-time curve.

3. Results

In **Figure 5** the line (A-E) is connecting the experimental data points of **Figure 2**. **Figure 6** shows the whole arm

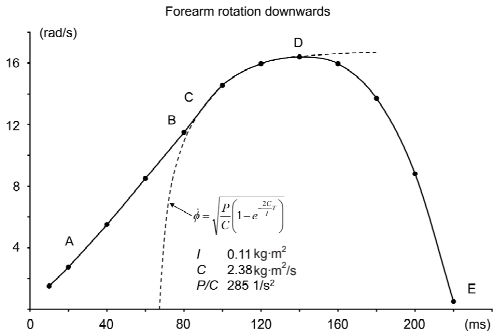

Figure 5. The measured angular velocities from forearm rotation downwards (points on the curve A-E) and the theoretical angular velocity values calculated from Equation 15 (broken line). The zero point of time for the theoretical angular velocity curve is at the intersection of the time-axis and the broken-line curve (the same time scaling is same for both curves).

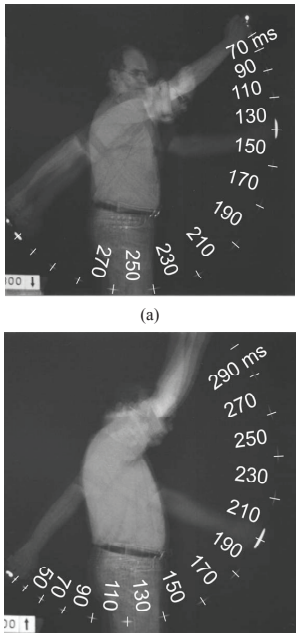

(a)

(b)

Figure 6. Whole arm rotation downwards (a) and upwards (b). Time of rotation is seen with the increment of 20 ms.

rotations upwards and downwards. In **Figures 5** and **7** the solid line is the curve fitting to the points representing the technique to filter small digitizing errors in traditional motion analysis. This way the complicated analysis of the series of the object images in the present study

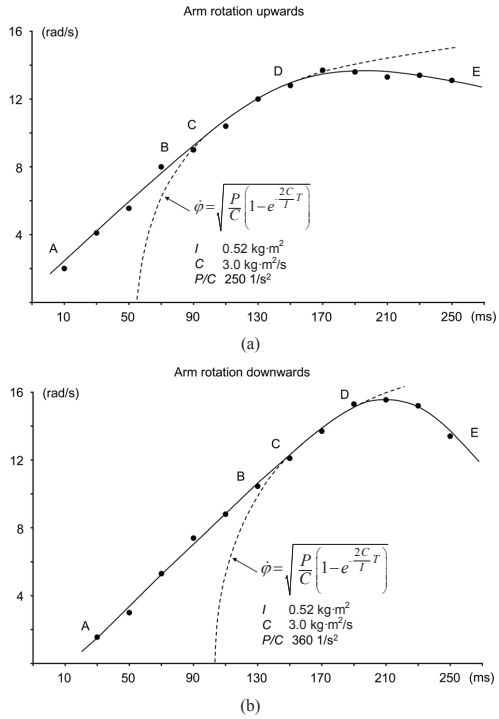

Figure 7. The measured angular velocities (points on the curve fitting A-E) from the whole arm rotation downwards (a) and upwards (b) and the theoretical angular velocity values calculated from Equation 15 (broken lines). The zero point of time for the theoretical angular velocity curve is at the intersection of the time-axis and the broken-line curve.

could be facilitated without losing a sufficient accuracy.

Hypothesis 1 states that the rotational movement proceeds at a constant maximum rotational moment within a certain range of velocity. This statement implies that rotational moment is about constant or $P/\dot{\varphi}$ is constant. By observing **Figures 5** and **7** it can be seen that movement proceeds at constant acceleration or $\mathrm{d}\dot{\varphi}/\mathrm{d}T$ is constant approximately between the points A-B on the velocity-time curve. The kinetic friction $C\dot{\varphi}$ is not constant. By substituting these terms in Equation (8)

$$I\frac{\mathrm{d}\dot{\varphi}}{\mathrm{d}T}=\frac{P}{\dot{\varphi}}-C\dot{\varphi}$$

it can be seen that the left side of the equation is constant and the right side of the equation is not constant. Therefore, we can conclude, that Hypothesis 1 is not fulfilled.

The measured values of the **forearm rotation downwards** are presented in **Table 1**. Angular velocities of the forearm rotation are shown in **Figure 5** as points on the

Table 1. Measured values of the forearm rotation downwards. Angular velocity is calculated with the Equation 1 and the angular acceleration according to Figure 7. A-B and C-D represent the estimated phases where the movement proceeds at constant acceleration and constant power, respectively.

T (ms)		$\Delta\varphi(rad)$	$\Sigma\Delta\varphi(rad)$	$\dot{\varphi}(rad/s)$	$\ddot{\varphi}(rad/s^2)$
20		0.055	0.06	2.75	114
40	A	0.110	0.17	5.50	155
60		0.170	0.35	8.52	155
80	B	0.231	0.59	11.54	155
	C				
100		0.291	0.89	14.56	128
120		0.319	1.22	15.93	72.5
140	D	0.329	1.56	16.48	12
160		0.319	1.89	15.93	-56

curve A-E. The theoretical angular velocity function with maximum power hypothesis (Equation 15) was fitted into the curve of the measured angular velocity-time values. Moment of inertia of forearm rotation was calculated I = 0.11 kg·m^2 (see 2.5). The values of friction coefficient C and power and friction coefficient ratio P/C were obtained within the curve fitting, C = 2.38 kg·m/s^2 and P/C =285 1/s^2. In **Figure 5** the movement proceeds at a constant acceleration between the phases A and B (~ 40 - 80 ms) until the liquid friction begins to influence and acceleration decreases between B-C. According to the Hypothesis 2 the movement proceeds at a constant power between C-D which is followed by stopping of the movement (D-E). The theoretical angular velocity curve (broken line) coincides with the measured angular velocity curve within section C-D. Therefore, we conclude that Hypothesis 2 is fulfilled within this range of velocity.

Figure 7 represents the curves of the measured points of angular velocity-time values from the **whole arm rotations downwards** and **upwards** (**Figure 6**). The theoretical angular velocity functions with maximum power hypothesis (Equation 15) were fitted into the measured point curves. Moment of inertia of forearm rotation was calculated I = 0.52 kg·m^2 (see 2.5). The values of friction coefficient C and power and friction coefficient ratio P/C were obtained within the curve fitting, whole arm rotation downwards C = 3.0 kg·m/s^2 , P/C =360 1/s^2 and whole arm rotation upwards C = 3.0 kg·m/s^2, P/C =250 1/s^2. The movement follows the hypothesized movement pattern described in the forearm rotation above. The theoretical angular velocity curves (broken lines) coincide with the measured angular velocity curves in section C-D (~ 150 - 190 ms and 90 - 150 ms in downward and upward rotation, respectively, **Figure 7**).

Validity and Accuracy of Results

In order to confirm the accuracy of results, power P was calculated by comparing two independent calculation methods. Equation (9)

$$I\dot{\varphi}\frac{\mathrm{d}\dot{\varphi}}{\mathrm{d}T} = P - C\dot{\varphi}^2 \Rightarrow P = I\,\dot{\varphi}\frac{\mathrm{d}\dot{\varphi}}{\mathrm{d}T} + C\dot{\varphi}^2 \qquad (16)$$

yields one power value ($\boldsymbol{P_1}$) and the other one ($\boldsymbol{P_2}$) comes from the curve fitting used in **Figures 5** and **7** (P/C).

In *forearm rotation downwards* the angular acceleration at point T = 0.10 s, $\dot{\varphi}$ = 14.5 rad/s was calculated by using the tangent of the angular velocity curve (**Figure 8**). The tangent point can be found because the tangent has only one point on the curve, otherwise there are two intersection points. The value of angular acceleration in **Figure 8** was calculated according to

$$\frac{\mathrm{d}\dot{\varphi}}{\mathrm{d}T} = 14.5/0.12 \text{ 1/s}^2 = 121 \text{ 1/s}^2.$$

This value of angular velocity derivative can also be calculated using Equation (15). The time and angular velocity of this equation corresponding to the measured angular velocity curve time 0.10 s and velocity 14.5 rad/s was calculated with Equation 13. Substitution of velocity 14.5 rad/s into Equation 13 gives time 0.031 s. The derivative of Equation (15)

$$\dot{\varphi} = \sqrt{\frac{P}{C}\left(1 - e^{-\frac{2C}{I}T}\right)},$$

$$X_1 = 1 - e^{\frac{-2C}{I}T}, \quad X_2 = \frac{-2C}{I}T$$

$$\frac{\mathrm{d}\dot{\varphi}}{\mathrm{d}T} = \frac{\mathrm{d}\dot{\varphi}}{\mathrm{d}X_1}\cdot\frac{\mathrm{d}X_1}{\mathrm{d}X_2}\cdot\frac{\mathrm{d}X_2}{\mathrm{d}T} = \frac{\sqrt{\frac{PC}{I^2}}\,e^{\frac{-2C}{I}T}}{\sqrt{1 - e^{\frac{-2C}{I}T}}} \qquad (17)$$

Substituting in this equation T = 0.031 s, I = 0.11 kg·m^2, C = 2.38 kg·m^2/s and P = 693 W, the value of angular acceleration of 112 1/s^2 was obtained. Moment arm of gravitational force is so short at forearm rotation that the power generation of gravitational force has no significance. In *whole arm rotation downwards* and *whole arm rotation upwards* the effect of gravitational force is within power P. The accuracy of results is presented in **Table 2**.

4. Conclusions

Hypothesis 1: Movement proceeds at a *constant maximal rotational moment*. Measurements of the rotation movements show that movement proceeds at a *constant angular acceleration* between A-B. Therefore, it can be concluded that the torque accelerating the movement or the

Table 2. Determination of accuracy of the results. The accuracy was obtained as a difference between the power values P_1 (from Equation 16) and P_2 (from the curve fitting in Figures 5 and 7).

	Forearm rotation	Whole arm rotation	
	Down (**Figure 4**)	Down (**Figure 6**)	Up (**Figure 6**)
Time (T)	0.100 s	0.160 s	0.114 s
Angular velocity $\left(\dot{\varphi}\right)$	14.5 rad/s	13.3 rad/s	11 rad/s
Angular acceleration $\left(\frac{\mathrm{d}\dot{\varphi}}{\mathrm{d}T}\right)$	14.5 / 0.12 1/s^2	13 / 0.16 1/s^2	11 / 0.17 1/s^2
Moment of inertia (I)	0.11 kg·m^2	0.52 kg·m^2	0.52 kg·m^2
Power into acceleration $\left(I\dot{\varphi}\frac{\mathrm{d}\dot{\varphi}}{\mathrm{d}T}\right)$	193 W	562 W	370 W
Coefficient of friction (C)	2.38 kg·m^2/s	3.0 kg·m^2/s	3.0 kg·m^2/s
Power into friction $\left(C\dot{\varphi}^2\right)$	500 W	531 W	363 W
Muscle Power (P_1)	**693 W**	**1093 W**	**733 W**
Power/Coefficient of friction (P/C)	285 1/s^2	360 1/s^2	250 1/s^2
Muscle Power (P_2)	**678 W**	**1080 W**	**750 W**
Error $\frac{P_1 - P_2}{0.5\left(P_1 + P_2\right)}100$	2.2%	1.2%	2.3%

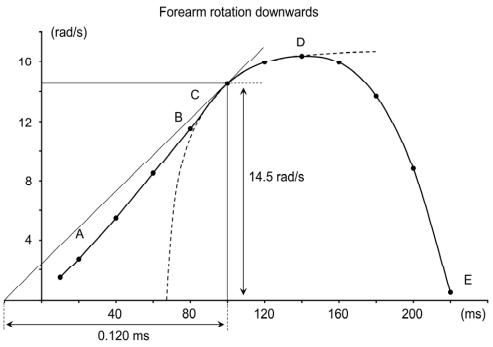

Figure 8. Calculation of angular acceleration at point (T = 0.10 s, $\dot{\varphi}$ = 14.5 rad/s), where the theoretical angular velocity curve (broken line) coincides with the measured angular velocity curve (points) between C-D.

left side of Equation (8) is constant.

$$I\frac{\mathrm{d}\dot{\varphi}}{\mathrm{d}T} = \frac{P}{\dot{\varphi}} - C\dot{\varphi}$$

Torque accelerating the movement is not the same as muscle force which is included in the term $P/\dot{\varphi}$. Therefore, we can conclude that Hypothesis 1 is not fulfilled. However, "*movement proceeds at a constant acceleration*" is an interesting finding which should be studied more closely. In Equation (8) kinetic friction was assumed to be directly proportional to velocity between A-B. This is a third hypothesis included into this study, which is not necessarily true. It is possible that kinetic friction is constant at small velocities and at large velocities directly proportional to velocity. Then there is a *constant torque value* accelerating the movement between A-B. The constant acceleration of the velocity curve may be related to the evolution of the human beings. For example the smooth acceleration may be essential for the accuracy of javelin throwing and targeting in fighting and hunting. As mentioned in [10] when modeling the control of the human limb motions, the final aim is to estimate the force production of individual muscles involved. Therefore the constant acceleration theory may play important role in human movements.

Hypothesis 2: movement proceeds at *a constant maximal muscle power*. Since the matched range (C-D) of the theoretical and measured velocity curves of arm rotation was long enough, it can be clearly seen that the curves did not intersect each other. Therefore it can be inferred that the constant maximum power hypothesis is true between C-D. In addition to the present study of three different type of arm rotation experiments the model of constant maximum power was also fulfilled in the previous experiments of shot put [11]. The different arm movements used in these experiments helped to achieve a greater certainty for the functioning ability of the present model. This model can be considered the most interesting finding of the present study.

REFERENCES

[1] A. V. Hill, "The Heat of Shortening and the Dynamic Constants of Muscle," *Proceedings of the Royal Society of London*, Vol. 126, No. 843, 1938, pp. 136-195.

[2] A. V. Hill, "First and Last Experiments in Muscle Mechanics," Cambridge University Press, Cambridge, 1970.

[3] W. Herzog, "Force-Velocity Relation," In: B. M. Nigg and W. Herzog, Eds., *Biomechanics of the Musculo-Skeletal System*, 2nd Edition, John Wiley & Sons Ltd, Chichester, 1999, pp. 173-180.

[4] W. Herzog, "Mechanical Properties and Performance in Skeletal Muscles," In: V. Zatsiorsky, Ed., *Biomechanics in sport*, Blackwell Science University Press, Cambridge, 2000, pp. 21-32. doi:10.1002/9780470693797.ch2

[5] B. R. MacIntosh and R. J. Holash, "Power Output and Force Velocity Properties of Muscle," In: B. M. Nigg, B. R. MacIntosh and J. Mester, Eds., *Biomechanics and Biology of Movement*, Human Kinetics, Champaign, 2000, pp. 193-210.

[6] D. A. Winter, "Biomechanics and Motor Control of Human Movement," 3rd Edition, John Wiley & Sons Inc., Hoboken, 2004, pp. 215-222.

[7] J. H. Challis, "Muscle-Tendon Architecture and Athletic performance," In: V. Zatsiorsky, Ed., *Biomechanics in sport*, Blackwell Science University Press, Cambridge, 2000, pp. 33-55. doi:10.1002/9780470693797.ch3

[8] D. E. Rassier, B. R. MacIntosh and W. Herzog, "Length Dependence of Active Force Production in Skeletal Muscle," *Journal of Applied Physiology*, Vol. 86, No. 5, 1999, pp. 1445-1457.

[9] R. T. Raikova, "A Model of the Flexion – Extension Motion in the Elbow Joint—Some Problems Concerning Muscle Forces Modeling and Computation," *Journal of Biomechanics*, Vol. 29, No. 6, 1996, pp. 763-772. doi:10.1016/0021-9290(95)00072-0

[10] R. T. Raikova and H. Ts. Aladjov, "Comparison between Two Models under Dynamic Conditions," *Computers in Biology and Medicine*, Vol. 35, No. 5, 2005, pp. 373-387. doi:10.1016/S0010-4825(04)00041-1

[11] A. Rahikainen and P. Luhtanen, "A Study of the Effect of Body Rotation on the Arm Push in Shot Put," *Russian Journal of Biomechanics*, Vol. 8, No. 2, 2004, pp. 78-93.

[12] A. Rahikainen, "Biomechanics in Shot Put," Helsinki University, Helsinki, 2008.

[13] A. Rahikainen, J. Avela and M. Virmavirta, "Modeling the Force—Velocity Relationship in Arm Movement," *Proceedings of the* 14*th ECSS Congress*, Oslo, 24-27 June 2009, p. 570.

[14] A. Rahikainen, "Method and Apparatus for Photographing a Movement," US Patent No. 4927261, 1990.

[15] A. Rahikainen, "The Use of Rotating Disk in the Photography of Movements," *Russian Journal of Biomechanics*, Vol. 7, No. 1, 2003, pp. 47-64.

IV

A STUDY OF THE EFFICIENCY OF THE LEG-PUSHING PHASE IN SHOT PUT

by

Ahti Rahikainen & Pekka Luhtanen, 2003

Russian Journal of Biomechanics 7, 65-79

Russian Journal of Biomechanics, Vol. 7, № 1: 65-79, 2003

Russian Journal of Biomechanics
www.biomech.ac.ru

A STUDY OF THE EFFICIENCY OF THE LEG-PUSHING PHASE IN SHOT PUT

A. Rahikainen*, P. Luhtanen**

*Helsinki University of Technology, Department of Engineering Physics and Mathematics, Institute of Mathematics, Helsinki University of Technology, PL 1000, 02015 TKK, Otakaari 1, Espoo, Finland, E-mail: ahti.rahikainen@hut.fi
**KIHU – Research Institute for Olympic Sports

Abstract. The aim of this paper is to study the mechanics of the leg-pushing phase in shot put, and to evaluate its efficiency. The length of a shot put may vary during the same competition by as much as 1 meter. The technique of a shot put usually cannot be controlled so well that with a certain technique the best possible distance corresponding to the shot putter's condition is obtained. The purpose of this work is to find causes of insufficient shot put technique.

In this paper two shot puts by Arsi Harju (20.90 m and 19.47 m) in "Kyroskoski Shot Put Carnivals" were analyzed. A mathematical analysis was made by employing an equation of the path of shot based on the kinematic data observed in a research report by KIHU. Using this equation, the rate of increase of the shot putter's velocity during the leg-pushing phase and the force acting on the center of the shot putter's mass were computed. The efficiencies of the leg-pushing phases of the two shot puts were determined by two different means: first, by employing the speed values at the end of the leg-pushing phase in the "speed of shot"- curves of KIHU, and second, by using the shot putter's velocity values and their changes.

It was found that the speed of shot of the 20.90 m put (7.1 m/s) was noticeably higher than that of the 19.47 m put (6.5 m/s). The speed of shot as a velocity vector comprises the velocity produced by the leg-pushing phase and the velocity of the shot putter's rotation. The rotational velocities of these two shot puts were almost the same, and therefore, the velocity increase produced by the leg-pushing phase was the cause for the velocity variation at the end of the leg-pushing phase, and it actually determined the outcome of the put. The rate of speed of the shot at the end of the leg-pushing phase indicates the efficiency of the leg-pushing phase. The better shot put produced a 0.6 m/s higher speed of shot than the poorer put. This speed increase could yield a 1.6 m increase to the length of the put. The calculations indicated that if the leg-pushing technique is correct, it is possible to get really long puts.

The jump on one leg was studied in order to find out how the mechanics of the leg-pushing phase works without a pushing force, and thereby to find the natural flexibility of the muscles and tendons. In the effective leg-pushing phase the leg's natural flexibility matches the leg-pushing force in the best possible way.

The better shot put had a higher downward velocity before the leg-pushing phase, which increased the pressure in the leg. The muscle's ability to produce force increases as the pressure in the muscle increases (to a certain degree) and due to this fact the efficiency of the leg-pushing phase also increases. To find the optimum technique for the leg-pushing phase in shot put, the jump and the fall that is after the jump should be studied.

Key words: motion analysis, sports research, biomechanics, muscle mechanics, shot put.

Introduction

This study was made from the basis of Reference [6]. Together with the studies in References [5] and [4], it contains an entire sequence of the movements of shot put in the form of mathematical equations. KIHU - Research Institute for Olympic Sports provided the subject matter for the measured data in this work, (References [1] and [2]). The measuring method applied to measure the three dimensional coordinate-data for the movements of shot put has been presented in Reference [13]. This study covers the leg-pushing phase before the arm push begins. This theme has conventionally been treated in sport research that gives guidance for coaching, References [8] – [14].

In Reference [13] the entire sequence of shot put is divided into five phases: the first double support phase, the first single support phase, the flight phase, the second single support phase, and the second double support phase. The conclusion of Reference [13] states as follows: "The results of the present study have several implications: 1) The speed of the release was the most influential determinant of the distance of the throw. In practice, therefore, the attainment of a high speed of the shot at release should be the main aim. 2) Most of the shot velocity at release was generated during the second double support phase (79 - 83%). 3) These findings suggest, therefore, that performance can be improved by increasing the acceleration of the shot during the second double support phase." In this study, the two most important phases of shot put are studied, that is the leg-pushing phase and arm-pushing phase. Together they comprise "the second single support phase and the second double support phase" as mentioned above. The time of arm push proved to be the most important factor in determining the course of shot put. By counting from the film frames taken above, the time of arm push was evaluated to be 0.11 seconds. However, this accuracy was not enough, and a more precise value was inferred to be 0.112 seconds.

This study yielded much knowledge, making the previous conception of the mechanics of shot put more complete. Reference [9] states about the jump preceding the leg-pushing phase as follows: "the flat direction of the take-off from the left must be supported decisively by a well-timed and well-dispensed kicking action of the right leg. Otherwise the take-off must be a distinct jumping movement with a too-steep ascent and also a so steep fall of the right foot." However, calculations of this work indicate that "the distinct jumping movement" produces 1.6 m more length to the put than the above-mentioned doctrine. This is because the jumping movement produces a higher pressure in the muscles of the pushing leg at the moment of ground contact, and due to this pressure the leg produces a higher pushing force, and the acceleration of the shot putter's center of gravity increases. Another example of Reference [9]: "The conclusion of Palm (1990), that the activity of the right leg is the decisive element in the acceleration of rotationists is to specify: during the delivery an effective acceleration of the center of gravity can come from the right leg only in an *indispensable interaction* with the work of the left. The function of the legs during the delivery is to manage the straightening of the body with a heave-up push to give the base for the powerful trunk turn." However, according to this study the conclusion of Palm seems to be right. "An *indispensable interaction* with the work of the left leg" means that the brace of the left leg is needed in order to get more speed for the body rotation. However, this study indicates that the major factor to accelerate the body is the work of the right leg because the powerful acceleration of the body begins before the left leg comes to the ground. When the arm push begins, the brace of the left leg is needed so that the reaction torque of the arm push does not retard the powerful trunk turn. Therefore, the end of the previous passage should be "The function of the legs during *the arm push* is to give the base for the powerful trunk turn". At the end of Reference [9] it is written as follows: " 3. Reverse Phase. The aim of this phase: after release the thrower has to completely decelerate the remaining horizontal velocity and rotatory energy of the body." However, the thrower cannot have any horizontal velocity at the

end of the delivery because both legs are up in the air and they are not able to decelerate any horizontal velocity. Therefore, the powerful push of the right leg must be straight upwards, and the brace of the left leg is not needed.

Methods

The length of a shot put may vary during the same competition by as much as 1 m. The technique of a shot put is not always controlled so well that with a certain technique the best possible length, corresponding to the shot putter's condition, is obtained. In order to be able to improve the technique of a shot put, we should study why sometimes surprisingly good results are obtained, whereas other times the results are poorer than usually. It is possible that some of the phases of the put are poorly done, and for this reason the length of the put is worse than in general. By using the «Speed of shot»- curves (Figure 1 and Figure 2),

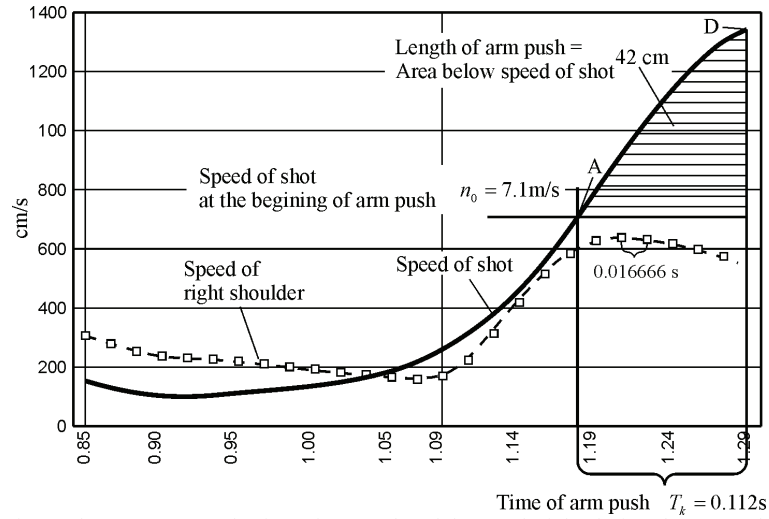

Fig. 1. The 20.90 m put. The time of arm push and the speed of shot before the arm push.

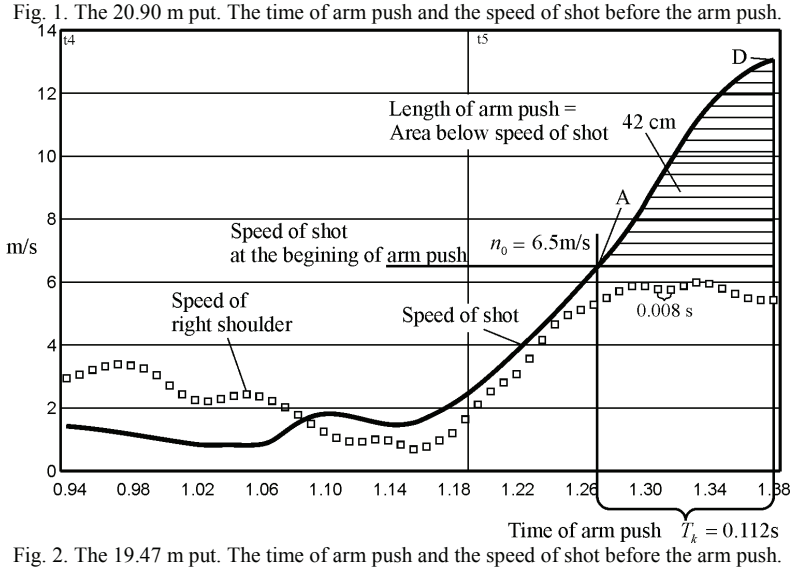

Fig. 2. The 19.47 m put. The time of arm push and the speed of shot before the arm push.

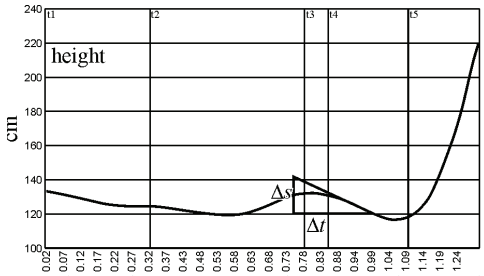

Fig. 3. The 20.90 m put. Shot putter's downward velocity at the beginning of the leg-pushing phase. From Figure 15 the minimum velocity $V = \Delta s/\Delta t$ = - 1.1 m/s.

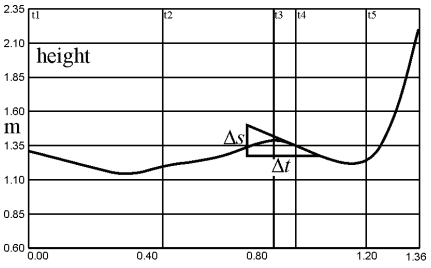

Fig. 4. The 19.47 m put. Shot putter's downward velocity at the beginning of the leg-pushing phase. From Figure 19 the minimum velocity $V = \Delta s/\Delta t$ = - 0.88 m/s.

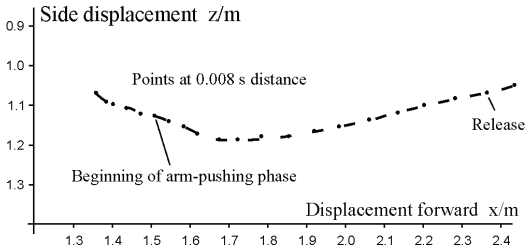

Fig. 5. The path of the shot during the arm push seen from above in the 19.47 m put.

it is possible to find out in which phase and for what reason the result of the put has become worse. When the time of the arm-pushing phase is known, it can be separated from the end of the "Speed of shot"- curve. By this means the "Speed of shot"-curve is decomposed into two sections: a leg-pushing phase and an arm-pushing phase. The speed of shot at the end of the leg-pushing phase, which is here called the carrying speed n_0, can be seen in Figures 1 and 2. Then the progress of the speed of shot in the better shot put can be compared with that of the poorer one, and we find out in which of the two phases the weakening of the outcome of the put has occurred. When the two above-mentioned shot puts are compared by this means, it is discovered that the carrying speed n_0 = 7.1 m/s of the 20.90 m put (Figure 1) is plainly higher than that of the 19.47 m put n_0 = 6.5 m/s (Figure 2). The carrying speed or carrying velocity is comprised of the velocity produced by the leg-pushing phase and the velocity of body rotation. The rotational velocities in these two shot puts have almost the same value, and therefore, the velocity produced by the leg-pushing phase determines the outcome of the put.

The course of the leg-pushing phase can be studied with the curves of the reports by KIHU "Rate of change in velocity and height of shot ", Figure 3, Reference [1] and Figure 4, Reference [2]. When we compare the "height of shot" curves of the two above-mentioned shot puts, it can be seen that when the motion of shot during the leg-pushing phase changes from the downward to the upward direction, the shot putter comes into the turning point with a smaller downward velocity in the poorer put (Figure 4) than in the better one (Figure 3). This means that at the beginning of the leg-pushing phase the shot putter has a higher downward velocity in the better put than in the poorer one. The beginning of the leg-pushing phase is a decisive factor for the success of the total leg-pushing phase. A high pushing force at the beginning of the leg-pushing phase increases the force acting on the proper leg-pushing phase. High pressure in the leg at the beginning of the put seems to be the fact that most effectively increases the force of the actual leg-pushing phase. To find the optimal technique for the leg-pushing phase, the jump and the fall that is after the jump should be studied.

A more accurate motion analysis of the leg-pushing technique and the efficiency of the put was accomplished by using an equation of the path of the shot putter's center of mass during the leg-pushing phase. First, the jump on one leg was studied in order to find out how the mechanics of the leg-pushing phase works without a pushing force. The study of the jump on one leg might not seem necessary, however, it is impossible to get into the equations of shot put without a simpler case of jump on one leg. On the other hand, theoretical derivation of equations in cases like jump on one leg and shot put is not possible without measurements, and fitting the equations into the measurements, because there is no other way to be certain that the equations really work. Therefore, measurements of jump on one leg are also needed.

An equation of the *theoretical* path of motion during the leg-pushing phase in *the jump on one leg* was derived by mathematical means, and it was *fitted* to the corresponding measured path of motion in *the real jump on one leg,* Reference [3], Figures 8 and 9. By this means the equation of the real path of motion during the leg-pushing phase (before muscular force accelerates motion) was obtained, and thereby the natural flexibility of muscles and tendons was solved. *In the effective leg-pushing phase the leg's natural flexibility matches the leg-pushing force in the best possible way.*

After this the efficiencies of the leg-pushing phases for *the two above-mentioned shot puts* were determined. Then, an equation of the *theoretical* path of motion during the leg-pushing phase in *shot put* was solved by using mathematical means, and it was *fitted* to the corresponding measured paths of motion in *the real shot puts*, obtained from the curves of the reports of KIHU, References [1] and [2], Figure 13 and 17. By this means the equations of the paths of motion in the real shot puts were obtained. When the equation of the path of motion is known, we obtain velocity and acceleration by computing the time derivative. By this means we discover the two most important factors influencing the efficiency of put: the increase of the velocity of shot, and the force accelerating the shot putter.

Estimation of the efficiency of the leg-pushing phase using "speed of shot"-curves

Speed of shot at the end of the leg-pushing phase in the 19.47 m put. In Figure 2, the speed of the right shoulder is marked by box images indicating the position of film frames. The speed of film is 125 frames per second, in which case the boxes are at 0.008 second intervals from each other. The time of arm push is computed from "The path of shot from above"- curve in Figure 5. The departure of the shot from the shot putter's cheek and moving farther away is about four frame intervals, and the time of the straight part of arm push is about ten frame intervals. In this case, about fourteen frame intervals are obtained for the time of arm push, the speed of which is 125 frames per second or the intervals between the frames are 0.008 seconds. The time of arm push is then 0.112 seconds. Then the beginning and end points of the arm push can be marked on the "Speed of shot"-curve in Figure 2. As the release of the shot occurs immediately after the last box, the time of arm push, 0.112 seconds, is separated from there, and we get into the beginning of arm push. At this point the speed of shot, or the carrying speed, is n_0 = 6.5 m/s. Using these beginning and end points, the displacement of the shot during the arm push or the length of arm push can be computed. As the speed of shot is in the vertical axis and the time in the horizontal axis, the displacement of shot during the arm push is the area between the speed of shot and the carrying speed n_0 = 6.5 m/s. The length of arm push is calculated to be about 42 cm. The force acting on the arm push can be computed by the angle of inclination of the speed of shot. The average acceleration is equal to the change of speed per elapsed time $a = \Delta V / \Delta t$, and the average force is equal to the mass of shot multiplied by the average acceleration $F = m\, \Delta V / \Delta t$. The maximum force is 580 N, which corresponds to the force of gravity of a mass of 59 kg.

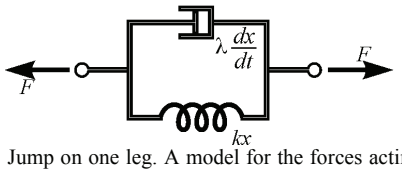

Fig. 6. Jump on one leg. A model for the forces acting during the leg-pushing phase. The total leg-pushing force is composed of the elastic force of leg tendons *kx* and the force of leg's internal friction $\lambda\, dx/dt$, which is associated with the viscosity of the leg's medium where the motion takes place. The force *F* acts on the ankle and pelvis joints. Adapted from Reference [8].

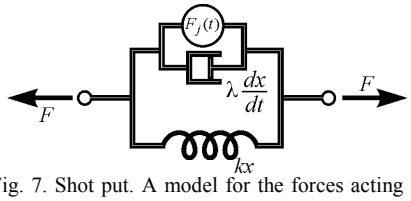

Fig. 7. Shot put. A model for the forces acting during the leg-pushing phase. The total leg-pushing force *F* is composed of the accelerating leg-pushing force $F_j(t)$, the elastic force of leg tendons *kx* and the force of leg's internal friction $\lambda\, dx/dt$. The force *F* acts on the ankle and pelvis joints. Adapted from Reference [8].

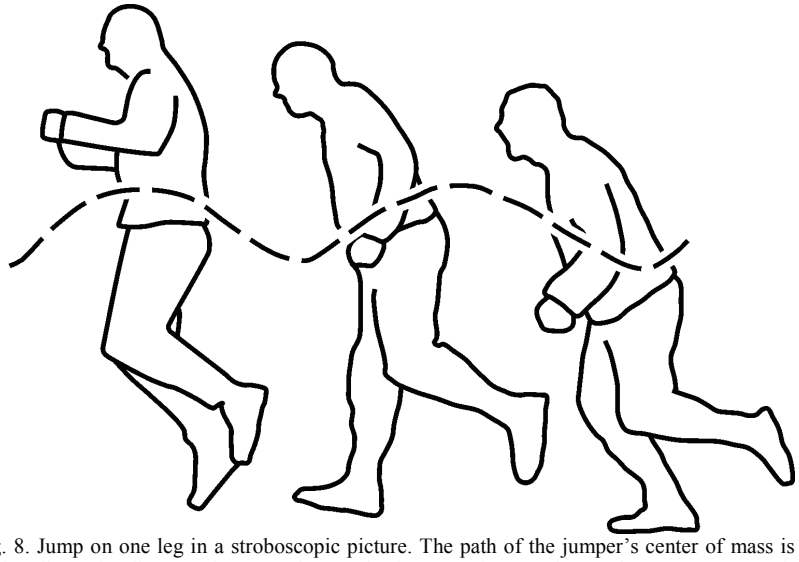

Fig. 8. Jump on one leg in a stroboscopic picture. The path of the jumper's center of mass is the broken-line. The distances between the streaks from one interruption to the next correspond to a time interval of 0.04 s. Lines on the walkway are at 0.5 meter's distance.

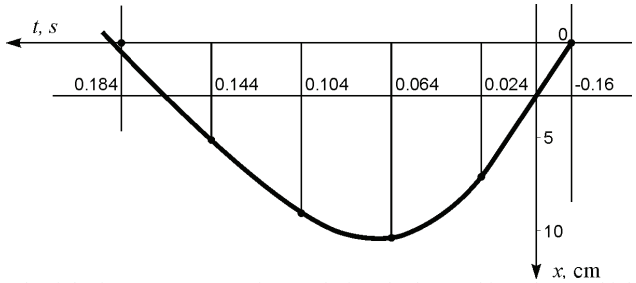

Fig. 9. The path of the jumper's center of mass during the leg-pushing phase, which is measured from the broken-line of Fig. 8. The time axis increases to the left.

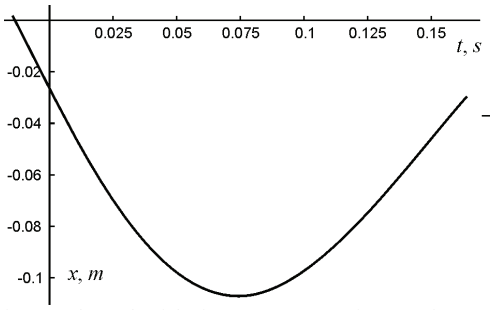

Fig. 10. The path of the jumper's center of mass x from Figure 9. For better perception the path of motion has been multiplied by -1. The time axis increases to the right. The leg-pushing force begins to increase the jumper's velocity at the time $t = 0.164$.

$$x = -A\mathrm{e}^{-\gamma t}\sin(\omega t) - \frac{g}{\omega_0^2}$$

$A = 0.105$ m, $\gamma = 3.5\ \mathrm{s}^{-1}$,

$\omega = 18.9\ \mathrm{s}^{-1}$, $\dfrac{g}{\omega_0^2} = 0.027$ m.

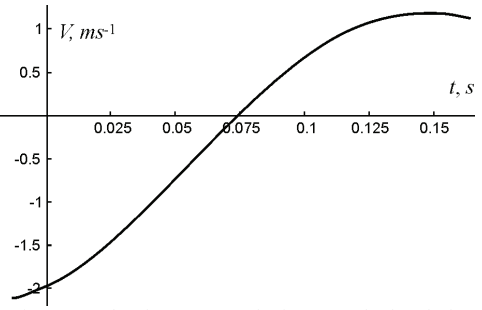

Fig. 11. The jumper's velocity V calculated from Eq. (5) and multiplied by -1.

$$V = -Ae^{-\gamma t}[-\gamma\sin(\omega t) + \omega\cos(\omega t)]$$

$A = 0.105\,\mathrm{m}$, $\gamma = 3.5\,s^{-1}$, $\omega = 18.9\,s^{-1}$.

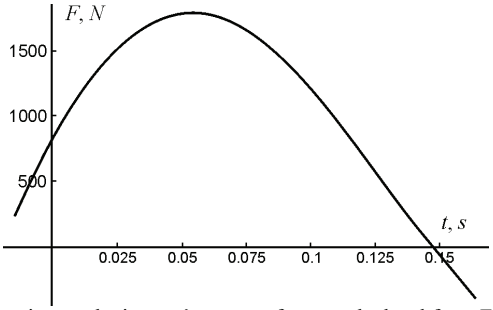

Fig. 12. The force F acting on the jumper's center of mass calculated from Eq. (7) and multiplied by -1. The moving mass m is 2/3 of the jumper's mass 85 kg.

$$F = -mAe^{-\gamma t}[(\gamma^2 - \omega^2)\sin(\omega t) - 2\gamma\omega\cos(\omega t)]$$

$A = 0.105\,\mathrm{m}$, $\gamma = 3.5\,s^{-1}$, $\omega = 18.9\,s^{-1}$, $m = 56.7\ \mathrm{kg}$.

Speed of shot at the end of the leg-pushing phase in the 20.90 m put. In the research report of KIHU (Figure 1), the right shoulder has been marked by box images. These boxes indicate the position of film frames. Pictures from the side and behind are taken with a camera, the speed of which is 60 frames per second, and pictures from above at 50 frames per second. The speed of film corresponding to the box images in Figure 1 is 60 frames per second, in which case the time intervals between boxes are 0.01666 seconds. The time of arm push can be computed from the above-taken film. The departure of the shot from the shot putter's cheek and moving farther away takes about one and a half frame intervals, and the time of the straight part of arm push is about four frame intervals. Therefore, the time of arm push is about five and a half frame intervals, which taken from above are at 50 frames per second, or the intervals between frames are 0.02 seconds. The time of arm push is then $5.5 \cdot 0.02 = 0.11$ seconds. The measuring system of the 19.47 m put was better, and therefore for the time of arm push is taken 0.112 seconds. The beginning and end points of the arm push can now be marked on the "Speed of shot"- curve. As the release of the shot occurs immediately after the

last box, the time of arm push, 0.112 seconds, is separated from there, and we get into the beginning of arm push. In this point the speed of shot is the carrying speed n_0, and its value is n_0 = 7.1 m/s. Using these beginning and end points, the displacement of shot during the arm push or the length of arm push can be computed. The length of arm push is the area between the speed of shot and the carrying velocity. The length of arm push is calculated to be about 42 cm. As both puts, the 19.47 m and 20.90 m put, have a very similar form of the path of shot and they are performed by the same shot putter with a certain length of arm, the length of arm push of both puts must be the same. The maximum force, calculated as above, is 540 N, which corresponds to the force of gravity of a mass of 55 kg.

Estimation of the efficiency of the leg-pushing phase using mathematical means

Mathematical model for the leg-pushing phase in the jump on one leg. In order to find out how the mechanics of the leg-pushing phase works in shot put, the mechanics of jump on one leg is first studied. The mechanics of the leg-pushing phase in jump on one leg is similar to the mechanics of the leg-pushing phase in shot put. The rotational movement in shot put corresponds to the advancing movement in jump on one leg; the mechanics of the leg-pushing phase is the same. Experiments were made in jumps on one leg, in which the photographic motion analysis technique of Reference [3] and Figure 8 was employed. The path of the jumper's center of mass was measured from the stroboscopic photograph depicted in Figure 8, and the curve of the path of motion in Figure 9 was obtained. During the leg - ground contact, the curve of the path of motion is such that the beginning of movement seems to be a damped oscillatory motion without muscular force. In the leg-pushing phase of movement, just before the jump, the jumper uses muscular force, accelerating the movement into advancing velocity. In the movement, the elastic force of leg tendons $F = -k\,x$, where x is the displacement and k is a constant, changes the direction of motion from downwards into upwards. The leg's internal friction produces a force *F?*, which is associated with the viscosity of the leg's medium in which the motion takes place. This force may be written as $F' = -\lambda v$, where λ is a constant and v is the velocity, Figure 6, Reference [8]. The gravitational force produces a downward force mg, where m is the mass of the jumper and g is the acceleration of gravity. The mass m is not the same as the mass of the moving subject because the free leg does not become involved in the accelerated motion at all, and the acceleration of the exerting leg is varying, being zero at the lower end of the foot and the same as the upper part of the body at the upper end of the foot. So, in this case it is sufficient to use a rough estimate of the mass m as approximately 2/3 of the mass of the moving subject. The equation of the leg-pushing phase in jump on one leg is then obtained as

$$m\frac{d^2x}{dt^2} + \lambda\frac{dx}{dt} + kx = mg\,. \tag{1}$$

This equation can be written as

$$\frac{d^2x}{dt^2} + 2\gamma\frac{dx}{dt} + {\omega_0}^2 x - g = 0\,, \tag{2}$$

where $2\gamma = \lambda/m$ and $\omega_0^2 = k/m$ is the natural angular frequency without damping. The solution of this equation suitable for the jump on one leg is of the form

$$x = -Ae^{-\gamma t}\sin(\omega t) + \frac{g}{\omega_0^2}\,, \tag{3}$$

in which

$$\omega = \sqrt{\omega_0^{\,2} - \gamma^2} = \sqrt{\frac{k}{m} - \frac{\lambda^2}{4m^2}}\,. \tag{4}$$

Taking the time derivative of the path of motion Eq. (3) we obtained the velocity

$$V = \frac{dx}{dt} = A\,\mathrm{e}^{-\gamma t}\left[-\gamma\,\sin(\omega t) + \omega\,\cos(\omega t)\right]. \tag{5}$$

Taking the time derivative of the velocity Eq. (5), we obtain the acceleration, and multiplying it by the moving mass we obtain the force acting on the center of mass

$$\frac{d^2x}{dt^2} = A\,\mathrm{e}^{-\gamma t}\left[\left(\gamma^2 - \omega^2\right)\sin(\omega t) - 2\gamma\,\omega\,\cos(\omega t)\right], \tag{6}$$

$$F = m\,A\,\mathrm{e}^{-\gamma t}\left[\left(\gamma^2 - \omega^2\right)\sin(\omega t) - 2\gamma\,\omega\,\cos(\omega t)\right]. \tag{7}$$

Making the substitutions: the path of motion Eq. (3), the velocity Eq. (5) and the acceleration Eq. (6) into the differential equation Eq. (2), it can be seen that Eq. (3) is the solution of Eq. (2).

Fitting the equations to the measurements in jump on one leg. Figure 9 represents the measured path of the jumper's center of mass during the leg-pushing phase, which has been obtained from the broken-line of Figure 8. The jumping leg comes to the ground at the point marked with 0. At that point the value in vertical axis of displacement *x*, cm is 0, and in the horizontal axis of time *t*, s is –0.016 seconds. The mathematical fitting is the continuous line, and the measured path is the points. The mathematical fitting for the measured path is Equation 3

$$x = -Ae^{-\gamma t}\sin(\omega t) + \frac{g}{\omega_0^2},$$

$$A = 0.105\ \mathrm{m},\ \gamma = 3.5\ \mathrm{s}^{-1},\ \omega = 18.9\ \mathrm{s}^{-1},\ \frac{g}{\omega_0^2} = 0.027\ \mathrm{m},\ \omega = \sqrt{\omega_0^2 - \gamma^2} = 18.9\,s^{-1}.$$

Mathematical model for the leg-pushing phase in shot put. The swinging motion of the shot putter's center of mass during the leg-pushing phase is described by a differential equation, which differs from Eq. (1) for the jump on one leg in that it contains an additional term of the accelerating leg-pushing force $F_j(t)$ (Figures 6 and 7). In the movement, the elastic force of leg tendons $F = -k\,x$, where *x* is the displacement and *k* is a constant, changes the direction of motion from downwards into upwards. The leg's internal friction produces a force *F?*, which is associated with the viscosity of the leg's medium in which the motion takes place. This force may be written as $F' = -\lambda v$, where λ is a constant and *v* is the velocity (Figure 7, Reference [8]). The gravitational force produces a downward force *mg*, where *m* is 2/3 of the mass of the shot putter and *g* is the acceleration of gravity. The equation of the leg-pushing phase in shot put is obtained as

$$m\frac{d^2x}{dt^2} + \lambda\frac{dx}{dt} + k\,x = mg - F_j(t). \tag{8}$$

If we make $2\gamma = \lambda/m$ and $\omega_0^{\,2} = k/m$, the equation may be written in the form

$$\frac{d^2x}{dt^2} + 2\gamma\frac{dx}{dt} + \omega_0^{\,2}x - g + \frac{F_j(t)}{m} = 0. \tag{9}$$

To solve the force $F_j(t)$ let us use our physical intuition for guidance and just write an attempt for the path of the shot putter's center of mass as

$$x = A\,\mathrm{e}^{\gamma t}\,\sin(\omega t) + \frac{g}{\omega_0^{\,2}}. \tag{10}$$

Taking the time derivative of Eq. (10), we get the velocity

$$V = \frac{d\,x}{d\,t} = A\,\mathrm{e}^{\gamma t}\left[\omega\cos(\omega t) + \gamma\sin(\omega t)\right]. \tag{11}$$

Taking the time derivative of Eq. (11), we get the acceleration, and multiplying it by the shot putter's mass we get the force acting on the shot putter's center of mass

$$\frac{d^2x}{d\,t^2} = A\,\mathrm{e}^{\gamma t}\left[\left(\gamma^2 - \omega^2\right)\sin(\omega t) + 2\,\gamma\,\omega\cos(\omega t)\right], \tag{12}$$

$$F = m\,A\,\mathrm{e}^{\gamma t}\left[\left(\gamma^2 - \omega^2\right)\sin(\omega t) + 2\,\gamma\,\omega\cos(\omega t)\right]. \tag{13}$$

Making the substitutions: Eq. (10), (11) and (12) into the differential equation Eq. (9), we obtain the leg pushing force

$$F_j(t) = -\,m\,A\,\mathrm{e}^{\gamma t}\left[\left(3\,\gamma^2 - \omega^2 + {\omega_0}^2\right)\sin(\omega t) + 4\,\gamma\,\omega\cos(\omega t)\right]. \tag{14}$$

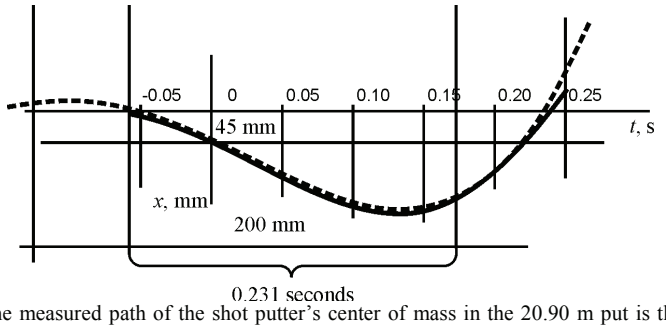

Fig. 13. The measured path of the shot putter's center of mass in the 20.90 m put is the broken-line, and its mathematical fitting is the continuous line. At the time t_4 the right leg comes to the ground after the jump. At the time t_5 the left leg comes to the ground. The left leg's pushing force begins to increase the shot putter's velocity at the time t = 0.23 s. Accuracy is the breadth of line.

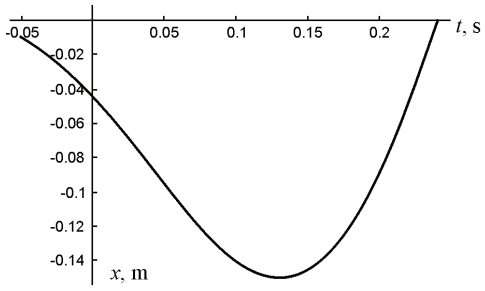

Fig. 14. The path of the shot putter's center of mass x from Figure 13, which for better perception has been multiplied by -1. The left leg's pushing force begins to increase the velocity at the time t = 0.23 s.

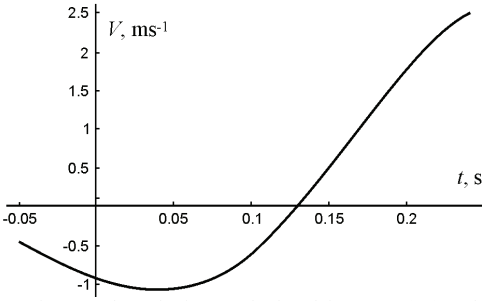

Fig. 15. The velocity V calculated from Eq. (11) and multiplied by -1.

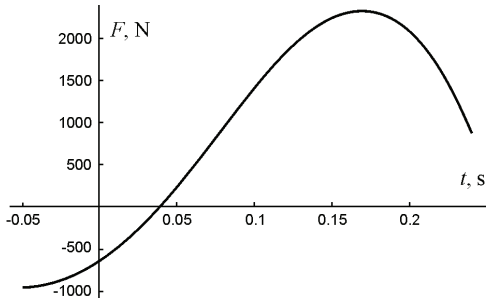

Fig. 16. The force F acting on the shot putter's center of mass calculated from Eq. (13) and multiplied by -1. The moving mass m is 2/3 of the shot putter's mass 131.6 kg.

$$F = -mAe^{\gamma t}[(\gamma^2 - \omega^2)\sin(\omega t) + 2\gamma\omega\cos(\omega t)],$$

$$A = 0.065\,\text{m},\ \gamma = 4\,\text{s}^{-1},\ \omega = 14.2\,\text{s}^{-1},\ m = 87.7\,\text{kg}$$

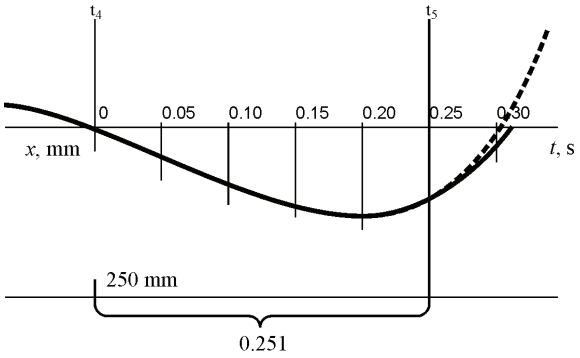

Fig. 17. The measured path of the shot putter's center of mass x in the 19.47 m put is the broken-line, and its mathematical fitting is the continuous line. At the time t_4 the right leg comes to the ground and at the time t_5 the left leg comes to the ground.

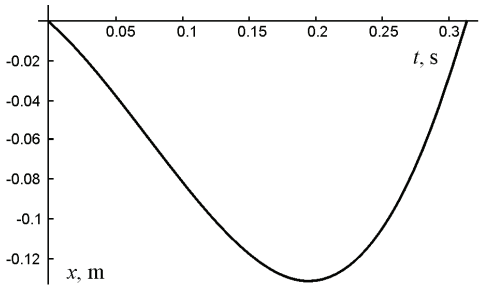

Fig. 18. The path of the shot putter's center of mass x from Figure 17, which for better perception has been multiplied by -1. The left leg's pushing force begins to increase the velocity at the time $t = 0.28$ s.

$$x = -A\,e^{\gamma t}\sin(\omega t),$$

$$A = 0.065\,\text{m},\ \gamma = 4\,\text{s}^{-1},\ \omega = 10\,\text{s}^{-1}.$$

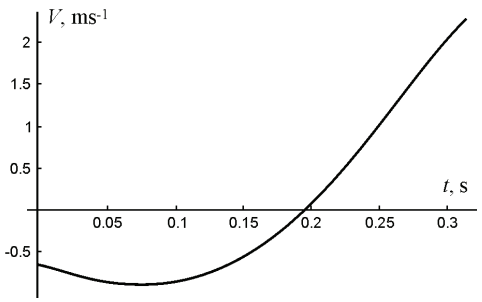

Fig. 19. The velocity V calculated from Eq. (11) and multiplied by -1.

$$V = -Ae^{\gamma t}[\omega\cos(\omega t) + \gamma\sin(\omega t)]$$

$$A = 0.065\,\text{m},\ \gamma = 4\,\text{s}^{-1},\ \omega = 10\,\text{s}^{-1}.$$

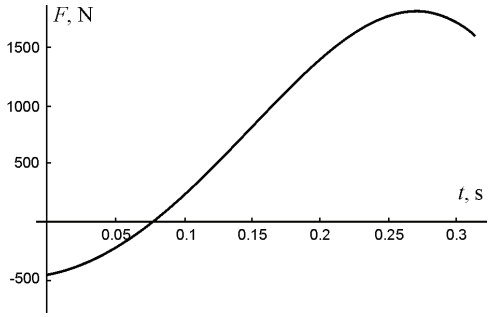

Fig. 20. The force F acting on the shot putter's center of mass calculated from Eq. (13) and multiplied by -1. The moving mass m is 2/3 of the shot putter's mass 131.6 kg.

$$F = -\,m\,A\,\mathrm{e}^{\gamma t}\left[\left(\gamma^2-\omega^2\right)\sin\left(\omega\,t\right)+2\,\gamma\,\omega\,\cos\left(\omega\,t\right)\right],$$

$$A = 0.065\ \mathrm{m},\quad \gamma = 4\ \mathrm{s}^{-1},\quad \omega = 10\ \mathrm{s}^{-1},\quad m = 87.7\ \mathrm{kg}.$$

Fitting the equations to the measurements in the 20.90 m put. Figure 13 represents the measured distance of the shot from the ground (broken-line) during the leg-pushing phase of the 20.90 m put (Reference [1]). As the distance between the shot and the shot putter's center of mass remains constant during the leg-pushing phase, the curve in Figure 13 also represents the path of the shot putter's center of mass in the vertical direction. The jumping leg (right leg) comes to the ground at the point of intersection of the broken-line and t_4 –line. At that point the value in vertical axis of displacement x, mm is 0, and in the horizontal axis of time t, s is –0.05 seconds. The first horizontal line below the time axis is at the distance of 45 mm, and the second horizontal line is at the distance of 200 mm. The mathematical fitting is the continuous line and the measured path is the broken-line. The mathematical fitting for the measured path is Equation (10)

$$x = A\,\mathrm{e}^{\gamma t}\,\sin\left(\omega\,t\right) + \frac{g}{\omega_0^{\,2}},$$

$$A = 0.065\,\mathrm{m},\ \gamma = 4\,\mathrm{s}^{-1},\ \omega = 14.2\,\mathrm{s}^{-1},\ \frac{g}{\omega_0^2} = 0.045\,\mathrm{m},\ \omega = \sqrt{\omega_0^2-\gamma^2} = 14.2\,\mathrm{s}^{-1}.$$

Fitting the equations to the measurements in the 19.47 m put. Figure 17 represents the measured distance of the shot from the ground (broken-line) during the leg-pushing phase of the 19.47 m put (Reference [2]). As the distance between the shot and the shot putter's center of mass remains constant during the leg-pushing phase, the curve in Figure 17 also represents the path of the shot putter's center of mass in the vertical direction. The displacement of the shot putter's center of mass x is in the vertical axis (lines are 250 mm apart), and the time t(s) is in the horizontal axis. The jumping leg comes to the ground at the point 0, which is the 0 point of the both axes. The mathematical fitting is the continuous line and the measured path is the broken-line. The mathematical fitting for the measured path is

$$\begin{aligned} &x = A\,e^{\gamma t}\sin\left(\omega\,t\right)\\ &A = 0.065\ \mathrm{m},\quad \gamma = 4\ \mathrm{s}^{-1},\quad \omega = 10\ \mathrm{s}^{-1} \end{aligned} \tag{15}$$

The leg pushing force can be computed by substituting Eq. (15), (11) and (12) into differential equation Eq. (9), in which case the pushing force is

$$F_j\left(t\right) = -\,m\,A\,\mathrm{e}^{\gamma t}\left[\ \left(3\,\gamma^2-\omega^2+\omega_0^{\,2}\right)\sin\left(\omega\,t\right)+4\,\gamma\,\omega\,\cos\left(\omega\,t\right)\ \right]-mg\,. \tag{16}$$

Results

Jump on one leg. Estimation of the rate of velocity increase and pushing force during the leg-pushing phase by using mathematical means. In order to be able to compare the pushing forces that are exerted during leg-pushing phases, the efficiency of the leg-pushing force is calculated by the ratio "maximum leg-pushing force / force of gravity of subject's mass", which is here called the pushing force ratio. Before the jumper's foot comes into contact with the ground, the only force acting on the jumper is the force of gravity. In the jump on one leg in Figure 12, the force of gravity is negative, and it is below the zero level of the curve of force. At the beginning of the leg-pushing phase in Figure 12, the force curve yields the force 350 N. To this the force of gravity of the jumper's mass, $85\ \text{kg} \cdot 9.82\ \text{m/s}^2 = 830\ \text{N}$ must be added, to obtain the leg-pushing force of 1180 N. The force curve yields the maximum force of 1800 N. This is added by the force of gravity 830 N to obtain the maximum leg-pushing force of 2630 N. The pushing force ratio is 2630/830 = 3.2. Therefore, in this case the jumper's leg-pushing force is 3.2 times the weight of the jumper.

In Figure 11, the velocity increase in the leg-pushing phase is calculated from the minimum value of the downward velocity to the point 0.15 seconds after the minimum value. The velocity curve yields the velocity increase of 3.0 m/s. During the time 0.1 s $\rightarrow$ 0.15 s the velocity increases hardly at all because there is no pushing force accelerating the motion.

Shot put. Estimation of the rate of velocity increase and pushing force during the leg-pushing phase using mathematical means. The 20.90 m put. Figure 16, at the beginning of the leg-pushing phase the force curve yields the force of -1000 N. To this the force of gravity of the shot putter's mass, 131.6 kg · 9.82 m/s^2 = 1300 N must be added, and the leg-pushing force at the beginning of the leg-pushing phase, 300 N, is obtained.

The maximum leg-pushing force is calculated as follows: The force curve yields the maximum force of 2300 N, to which the force of gravity of the shot putter's mass, 131.6 kg · 9.82 m/s^2 = 1290 N is added, to obtain the maximum leg-pushing force of 3590 N. In this case the pushing force ratio is 3590 / 1290 = 2.8.

In Figure 15, the velocity increase in the leg-pushing phase is calculated from the minimum value of the downward velocity to the point that is 0.15 seconds after the minimum value. The velocity curve yields the velocity increase of 2.6 m/s.

The 19.47 m put. In Figure 20, at the beginning of the leg-pushing phase the force curve yields the force of -700 N. To this the force of gravity of the shot putter's mass, 131.6 kg · 9.82 m/s^2 = 1300 N must be added, and the leg-pushing force at the beginning of the leg-pushing phase 600 N is obtained.

The maximum leg-pushing force. The force curve yields the maximum force of 1800 N, to which the force of gravity of the shot putter's mass, 131.6 kg · 9.82 m/s^2 = 1300 N is added, and the maximum leg-pushing force is 3100 N. In this case, the pushing force ratio is 3100 / 1290 = 2.4.

In Figure 19, the velocity curve yields the velocity increase of 1.4 m/s calculated from the minimum value of the downward-directed velocity to the point that is 0.15 seconds after the minimum value.

Conclusions

The better put had the pushing force ratio of 2.8 and the velocity increase of 2.6 m/s. The poorer put had the corresponding pushing force ratio of 2.4 and the velocity increase of 1.4 m/s. In Reference [5], page 56, there are two measurements of Arsi Harju's leg-pushing forces, yielding the maximum leg-pushing force of 2610 N for the 19.85 m put and 2400 N for the 18.79 m put. The force of gravity of the subject's mass is 1290 N. The pushing force

ratios are 2.0 and 1.86 correspondingly. The difference in values may be caused by many reasons, but in any case they are about the same order of magnitude. One possible reason is that the distance between the shot and the shot putter's center of mass is not sufficiently near to a constant, but elasticity has some effect on that. For the sake of comparison, the corresponding values for the jump on one leg were also calculated. The pushing force ratio was 3.2 and the increase of velocity 3 m/s.

The jump on one leg was studied in order to find out how the leg-pushing phase works without a pushing force. In the effective leg-pushing phase, the leg's natural flexibility fits the exerted pushing force in the best possible way.

The speed of shot at the end of the leg-pushing phase or the carrying speed for the two puts was determined by using "Speed of shot"-curves. The carrying speed of the 20.90 m put was n_0 = 7.1 m/s and that of the 19.47 m put was n_0 = 6.5 m/s. The rate of carrying speed indicates the efficiency of the leg-pushing phase. The better put produced a 0.6 m/s higher carrying speed than the poorer put. The effect of speed increase on the length of the put can be calculated with Equation (6) in Reference [14]. The effect is a 1.6 m increase in length. However, the poorer put had a more effective arm push, and for this reason the difference in the lengths of the puts was only 1.43 m. By combining the leg-pushing phase of the better put and the arm push of the poorer put the length of the put could have been 21.07 m. Therefore, if the leg-pushing technique is right, it is possible to get really long puts.

The calculations indicate that the better put had the maximum leg-pushing force of 3590 N and the poorer put 3090 N. In this case, the leg-pushing force of the better put was 500 N higher, which increases the length of the put by 1.6 m. Therefore, the better put had a noticeably more effective pushing technique than the poorer put. The better put had a higher downward velocity before the leg-pushing phase (Figures 3 and 4), which increased the pressure in the leg. Muscle's ability to produce force increases as the pressure in the muscle increases (to a certain degree), and as a result, the efficiency of the leg-pushing phase increases.

References

1. *Vanttinen T.*, *Blomqvist M.*, *Luhtanen P.*, *Auvinen M.*, *Palo-Kangas J.*, *Tuominiemi J.*, *Yrjola M.*, *Ranta M.*, *von Hertzen R.*, *Holmlund U.* Rotational shot put technique V, Research Institute for Olympic Sports, Research Report, Jyvaskyla, Finland, 1998 (in Finnish).
2. *Vanttinen T.*, *Blomqvist M.*, *Luhtanen P.*, *Auvinen M.*, *Palo-Kangas J.*, *Tuominiemi J.*, *Yrjola M.*, *Ranta M.*, *von Hertzen R.*, *Holmlund U.* Rotational shot put technique VII, Research Institute for Olympic Sports, Research Report, Jyvaskyla, Finland, 2000 (in Finnish).
3. *Rahikainen A.* United States Patent, Patent Number: 4,927,261, Date of Patent: May 22, 1990.
4. *Rahikainen A.*, *Luhtanen P.* A new method to estimate the effect of shot putter's rotational velocity on the length of put. Helsinki University of Technology, Laboratory of Mechanics, Research Report No 60, 2001, 15 p (in Finnish).
5. *Rahikainen A.*, *von Hertzen R.*, *Ranta M.A.*, *Luhtanen P.* About the optimum shot put technique. Helsinki University of Technology, Laboratory of Mechanics, Research Report No 58, 2000, 30 p (in Finnish).
6. *Rahikainen A.*, *Luhtanen P.* A new method to estimate the efficiency of the leg-pushing phase in shot put. Helsinki University of Technology, Laboratory of Mechanics, *Research Report* No 59, 2001, 21 p (in Finnish).
7. *Luhtanen P.*, *Auvinen M.*, *Yrjola M.*, *Rahikainen A.* (editorial staff), Finnish Shot Put, Lahden Kirjapaino ja Sanomalehti Oy LahtiPrint, Lahti, 2000.
8. *McMahon Th.* A. Muscles, Reflexes and Locomotion. Princeton University Press, Princeton New Jersey 1984. P. 8-17.
9. *Bartonietz K.E.* Rotational Shot Put Technique: Biomechanical Findings and Recommendations for training. Track and Field Quarterly Review 94 (3), 1994. P. 18-29.
10. *Pyka I.*, *Otrando B.* Rotational shot put. National Strength and Conditioning Association Journal, Volume 13, Number 1, 1991.

11. *Palm V.* Some Biomechanical Observations of the Rotational Shot Put. Modern Athlete and Coach 28 (3), July 1990. P. 15-18.
12. *Stepanek J.* Comparison of the Glide and the Rotational Technique in the Shot Put. Biomechanics in Sports V, Proceedings of the Fifth International Symposium of Biomechanics in Sports, held in 1987 Athens, Greece. Publisher: Hellenic Sports Research Center of Athens.
13. *Luhtanen P.*, *Blomqvist M.*, *Vanttinen T.* A Comparison of two elite shot putters using the rotational shot put technique, IAAF quarterly, New Studies in Athletics, no. 4/1997. P. 25-33.
14. *Lichtenberg D.*, *Wills J.* Maximizing the range of the shot put. Am. J. Phys., Vol. 46, No. 5, May 1978. P. 546-549.

ИССЛЕДОВАНИЕ ЭФФЕКТИВНОСТИ ФАЗЫ ДЕЙСТВИЯ ТОЛЧКОВОЙ НОГИ ПРИ ТОЛКАНИИ ЯДРА

А. Рахикайнен, П. Лухтанен (Хельсинки, Финляндия)

Аннотация. Целью данной работы является изучение механических аспектов толкания ядра в фазе действия толчковой ноги и оценка его эффективности. Исследования проводились на основе анализа двух выступлений Арси Харью (Arsi Harju) в Кирёскоски (Kyroskoski), результаты которых различались на 1,43м: 4 июля 1998г., 6 попыток, результат–20,90м; 22 июля 2000г., 6 попыток, результат–19,47м. На основе проведенных измерений [1-2] определены эффективность фазы действия толчковой ноги и определяющие её факторы. В работе проведён более точный анализ такого спортивного движения на основе полученного математическими методами уравнения траектории центра масс толкателя ядра. Вычисления, выполненные с помощью этого уравнения, показали увеличение как скорости движения центра масс, так и силы, действующей на него, в фазе отталкивания опорной ноги. Эффективность этой фазы оценивалась величинами скорости и силы. В основу исследований положены данные, опубликованные в отчетах [5, 7, 8].

Ключевые слова: толкание ядра, фаза действия толчковой ноги, механика, движение центра масс, скорость, сила.

Received 15 November 2002